MB-R-65/40

N65-24359 (ACCESSION NUMBER) (THRU) 1
82 (PAGES) (CODE)
CR 62826 (NASA CR OR TMX OR AD NUMBER) (CATEGORY) 11
FACILITY FORM 602

Hard copy (HC) 3.00
Microfiche (MF) .75

FINAL REPORT

FEASIBILITY STUDY FOR DEVELOPMENT OF A HYPERVELOCITY GUN

by

D. E. Brast and D. R. Sawle

prepared for

NATIONAL AERONAUTICS AND SPACE ADMINISTRATION

CONTRACT NAS 8-11204

May 1965

MB ASSOCIATES
San Ramon
(near San Francisco)
California

TABLE OF CONTENTS

LIST OF FIGURES

LIST OF FIGURES (cont)

LIST OF FIGURES (cont)

LIST OF TABLES

I. INTRODUCTION

The defining features of a rail gun are (See Figure 1) a pair of conducting rails and across them a conducting armature. Electric current is passed through the rails and armature so that the magnetic field produced by the current in the rails (and possibly in auxiliary field coils) interacts with the current in the armature. The resulting Lorentz force (jxB) tends to accelerate the armature away from the end of the rails at which the current is introduced.

Practically, two kinds of armature have been used, electric arc plasma[1,2] and solid conductors[3-7]. In most projectile accelerators, the projectile is itself conductive and serves as the armature. In our gun, the projectile is nonconductive (usually nylon) and the armature that drives it is an arc plasma[8]. This circumvents the problem of ohmic heating in the projectile.

In our experiments, the gun itself is anywhere from three to eight inches or so in length and consists of a pair of metal rails, usually copper, sandwiched between two insulating slabs. The resulting barrel can be made to have either a square or circular cross section.

With guns of this kind and no auxiliary field, we have accelerated nylon projectiles to the velocities listed below:

Weight of Projectile	Shape	Velocity
0.01 mg	Roughly Spherical	10.3 km/sec
0.6 mg	Cubic	3.7 km/sec
2.4 mg	Spherical	6.0 km/sec
5 mg	Cube	5.8 km/sec
31 mg	Cube	5 to 6 km/sec
37 mg	Spherical	4.8 km/sec

In each case except the first, the projectiles were single and fitted snugly in the barrel. The 10.3 km/sec was achieved by a drag technique.

The system used consists of a 28 k joule, 142 μfd condenser bank, which is discharged by a triggered spark gap either directly into the gun or into an impedance matching pulse transformer giving peak currents up to 700 k amp at ringing frequencies as high as 25 k c. The arc is initiated by a small bit of aluminum foil behind the projectile and travels the entire length of the gun during the first half-cycle of the discharge. When a pulse transformer is used, about three fourths of the bank energy

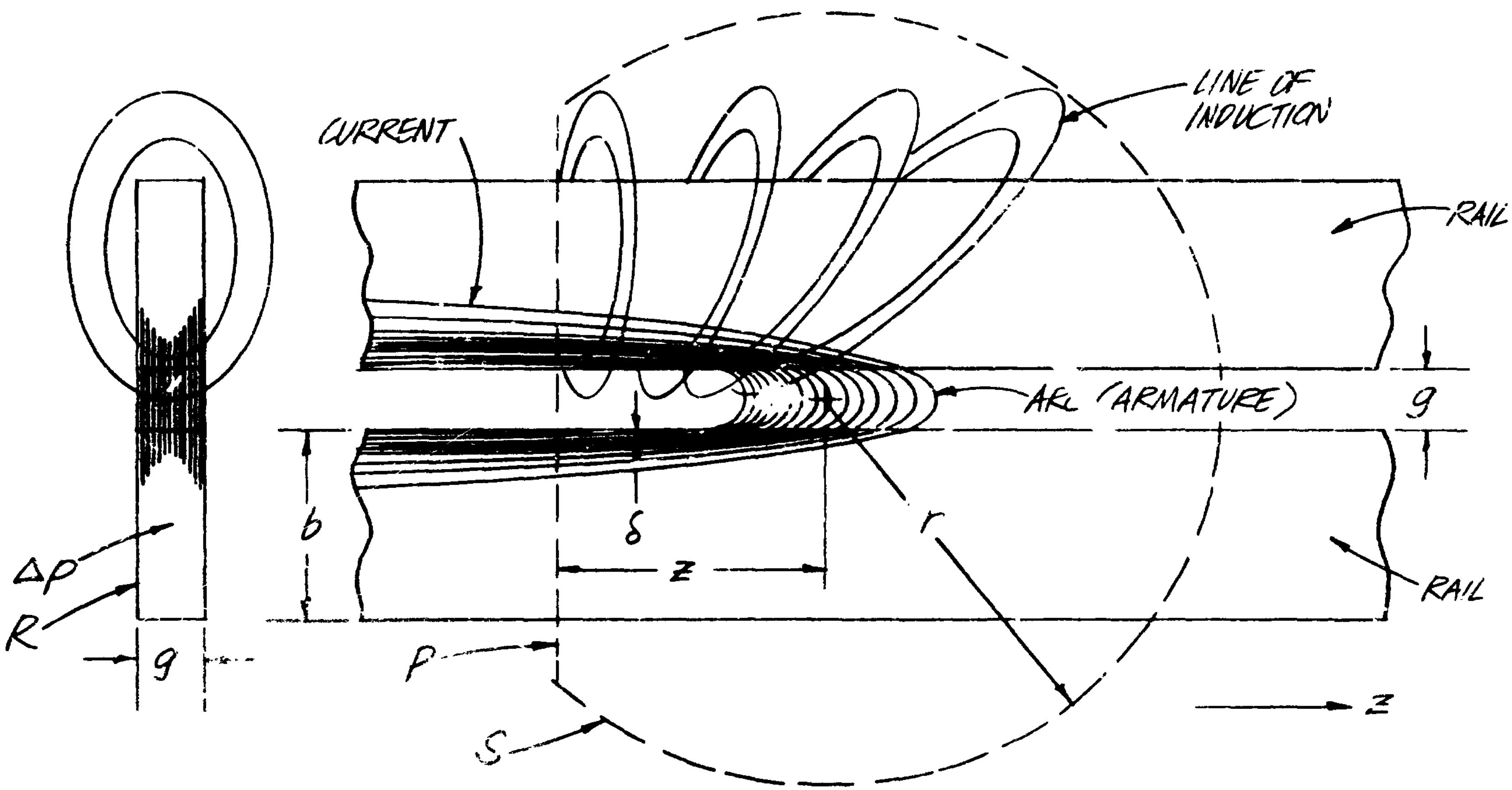

Figure 1. The Arc Discharge Between Parallel Rails

is dissipated in that time. Of the total bank energy, however, at most about 3% goes into the kinetic energy of the projectile.

Besides this simple system, we have also tried two-stage and auxiliary field systems, for which we have a second independent, 28 k joule, 144 μ fd condeser bank and a second pulse transformer. Although high velocities were achieved by these means, in no case did they equal those quoted above.

Routine diagnostics included magnetic flux loops very close to the barrel to record the progress of the arc, a photoelectric muzzle-watcher to record the appearance of the luminous arc plasma at the muzzle (this always coincides with the current front as determined by the flux loop at the muzzle as has been observed by other researchers[9]), a flux loop to record the total instantaneous current, and transit time and crater depth measurements to determine velocity. In a few experiments, we measured directly the voltage across the muzzle and breech of the gun to determine the resistive voltage of the arc and the rate of change of flux in the gun.

In the rail gun acceleration of plasmas, velocities upwards of 100 km/sec have been achieved[1,2]. Offhand, one would, with some modesty, hope to use the same techniques and more energy to achieve somewhat lower velocities for small projectiles. However, because even a 1 mg nylon sphere has an areal mass density 10^6 times that of the usual rail gun plasma bodies (10 gm/cm^2 versus 10 μgm/cm^2) the magnetic pressure required to produce the same acceleration in the projectiles as in the plasmas is correspondingly higher.

The magnetic fields needed for such large accelerations are of the order of a megagauss. The ohmic heat per unit volume produced by such high fields (turned on fast enough to be contained by good conductors) is sufficient to melt the current carrying portion of the rails[4], and momentum then goes into the molten rail material. Also the pressures are so high that the rails suffer plastic flow.

Smaller accelerations of longer duration over greater distance leads to: (1) greater loss of energy into mass sputtered off the rails by current carrying ions, and (2) heating of even a nonconducting projectile by the arc through thermal conduction.

The auxiliary field systems was an attempt to solve this dilemma.

Another limitation is that, for high magnetic pressures, current begins to flow in front of the projectile as well as behind. The forward arc runs away from the projectile and at the same time grows at the expense of the one behind. The force on the rear arc is therefore diminished with the net effect of a lower projectile velocity.

There have been two general approaches to this problem. One has been to try to understand and control this phenomenon, the other to concede its inevitability and to accelerate the projectile by drag.

In the following sections, we present the theory behind both approaches, the relevant experimental results, and, based upon these, our recommendations for future work. Appended to this is a detailed description of the novel equipment and techniques developed in the course of these experiments.

SYMBOLS

$\sim$	is of the order of
$\mathcal{O}$	something of the order of
$b, g, r, z, \rho, \Delta\rho, R, \mathcal{S}$	see Figure 1
B	magnetic induction
I	instantaneous current
I_p	peak current
j	current density
L'	inductance per unit length
M	mass of the projectile
m_I	mass-input per unit charge
r_{outer}	radius of the outer electrode of a coaxial rail gun
S	surface of integration
t	time
v	velocity of the arc
V	volume of integration
$\mathbb{1}$	unit tensor
δ	skin depth
σ	electrical conductivity
ω	angular frequency

II. OPERATION OF THE RAIL GUN

A. THE LORENTZ FORCE ON THE ARC

The Lorentz force on an arc in a rail gun without an auxiliary field can always be written as $\frac{1}{2}L'I^2$, where I is the instantaneous total current in the rails, and L' is some inductance per unit length. The total momentum produced by this force will then be $\int \frac{1}{2}L'I^2 dt$. If L' is nearly constant in time, and if we know its value, we have a very useful expression for the momentum in terms of an easily measured quantity, I . In general this will not be the case, because L' is dependent on the current distribution in the rails, and, except in special cases, for example, the case of infinitely thin wire rails, this current distribution will vary with time in an unknown way.

Fortunately, the rail gun considered here falls under one of those special cases, at least to an approximation, and we can get an estimate of L' by means of the Maxwell stress tensor, $BB - \frac{1}{2}|B|^2\mathbf{1}$ ($\mathbf{1}$ is the unit tensor) in the following way.

The Lorentz force on an arbitrary volume, V , is given by

$$
\begin{aligned}
F &= \int j \times B \, dV \\
&= \oint_S \frac{1}{\mu_0} \left(BB - \tfrac{1}{2}|B|^2 \mathbf{1}\right) \cdot dS
\end{aligned}
\qquad (1)
$$

where S is the surface enclosing V , and dS is outward. For S (See Figure 1) we take the truncated spherical surface $\mathcal{S}$ of radius r centered about the arc and the disc P perpendicular to the axis of symmetry at a distance z from the arc. The integral over S is the Lorentz force on the portion of the rails enclosed by S and upon the arc.

We now let $\mathcal{S}$ go to infinity. On $\mathcal{S}$, B is proportional to $1/r^2$. Therefore, the integral on $\mathcal{S}$ is proportional to $1/r^2$ and goes to zero. P is now the entire plane. For $z^2 \gg g^2$, the forward component of the Lorentz force will be given by the integral of $\frac{1}{2\mu_0}|B|^2$ over this plane. The integral of $B_z B \cdot dS$ will be negligible for the following reasons. B_z is due solely to the current in and near the arc, so that

$$
\begin{aligned}
B_z|_P &\sim \mu_0 I g / z^2 \\
\frac{1}{\mu_0} B_z B \cdot dS &\sim \mu_0 I^2 g^2 / z^4 \\
\int_P \frac{1}{\mu_0} B_z B \cdot dS &\sim \mu_0 I^2 g^2 / z^2
\end{aligned}
\qquad (2)
$$

On the other hand, in the gap

$$|B| \sim \mu_0 I/g \qquad \text{so that} \qquad \int_P \frac{1}{2\mu_0}|B|^2|dS| \sim \mu_0 I^2 \tag{3}$$

If one compares the approximate expressions in (2) and (3), one sees that for $z^2 \gg g^2$, $\int_P \frac{1}{\mu_0} B_z B \cdot dS$ can be ignored, and that the total forward force on the rails and arc is given by

$$F_{total} = \int_{P(z^2 \gg g^2)} \frac{1}{2\mu_0}|B|^2|dS|$$

The forward force on the rails alone is given by

$$F_{rail} = \int_{LP} \frac{1}{2\mu_0}|B|^2|dS| + \int_R \frac{1}{\mu_0} B_z B \cdot dS \tag{4}$$

where LP is the cross section of the rails, R is the surface of the rails, and dS is now outward from the rails. The forward force on the arc, F_{arc} is just $F_{total} - F_{rails}$ or,

$$F_{arc} = \int_{P-LP} \frac{1}{2\mu_0}|B|^2|dS| - \int_R \frac{1}{\mu_0} B_z B \cdot dS \tag{5}$$

The first integral in Equation (5) is the external magnetic energy per unit length behind the arc.

In the case of an azimuthally symmetrical discharge in a coaxial-cylinder rail gun, the first integral is just $\frac{\mu_0}{4\pi} I^2 \ln \frac{r_{outer}}{r_{inner}}$, which is just $\frac{1}{2} I^2$ times the geometric external inductance. The second integral is zero in this case, because both B_z and $B \cdot dS_R$ are zero. Therefore, for azimuthal symmetry, L' is just the geometrical external inductance per unit length, independent of the radial distribution of the current in the electrodes.

The same result holds for the previously mentioned special case of infinitely thin wire rails and for the case of infinite conductivity. This can be derived from Equation (4) or from the conservation of energy and Faraday's Law. Both of these derivations depend on the fact that, in these special cases, the volume of the current carrying region of the rails is zero. In one case we have a line current, in the other a surface current distribution. This means that B will be parallel to R ($B \cdot dS_R = 0$). ΔR will be zero, and, therefore, both integrals in Equation (4) will be zero. From the point of view of Faraday's Law, it means that we can speak of the magnetic flux through the circuit, which is not possible if flux penetrates a current carrying volume of finite extent.

In the case of interest, the discharge is not azimuthally symmetrical, the cross sectional size of the rails is comparable to the size of the gap so that the rails cannot be considered infinitely thin, and the electrical skin depth in the rails for typical transit times is considerable compared to the other dimensions so that the rails cannot offhand be considered of infinite conductivity. Near the arc, lines of induction which cut the rails because of their finite conductivity have components both normal to the surface of the rails and along the z-direction. Therefore, the second integral in Equation (5) may no longer be negligible.

In order to estimate this integral, we again make use of the fact that, away from the arc, only the current in the arc and not the current in the rails contributes to B_z. B_z will, therefore, be roughly proportional to the inverse square distance from the arc, $1/z^2$, and to the sine of the angle between the rail-surface normal and the radius vector from the surface to the center of the arc. This sine is approximately g/z so that B_z is proportional to $1/z^3$. At a given distance, z, from the arc, the width of the area on the rails cut by B will be the skin depth, δ, corresponding to the time for the arc to travel that distance. Letting v be the velocity of the arc and σ the conductivity of the rails, we have

$$\delta \sim \sqrt{t/\mu_0 \sigma} \qquad t \sim z/v$$

$$\int_R \frac{1}{\mu_0} B_z B \cdot dS$$

$$\sim \int_0^g \frac{1}{\mu_0} |B|^2 \sqrt{\frac{g}{\mu_0 \sigma v}}\, dz + \int_g^\infty \frac{1}{\mu_0} |B|^2 \frac{g^2}{z^2} \frac{g}{z} \sqrt{\frac{z}{\mu_0 \sigma v}}\, dz \qquad (6)$$

$$\sim \frac{1}{\mu_0} |B|^2 g \sqrt{\frac{g}{\mu_0 \sigma v}}$$

If we let the first integral in Equation (5) be $\frac{1}{2} L' I^2$ and the second integral a correction to it, then, whatever the exact value of L' is, it will be roughly true that $L' \sim \mu_0$, and near the gap, $|B| \sim L' I/g$.

Substituting these expressions into Equation (6), we have

$$\frac{1}{\mu_0} \int_R B_z B \cdot dS \sim \left(\frac{1}{2} L' I^2\right) / \sqrt{\mu_0 \sigma v g}$$

Putting in the typical values

$$g = 1.5 \text{ mm}$$

$$v = 5 \text{ km/sec}$$

$$\sigma = 5.8 \times 10^7 \text{ mho/m for copper}$$

we have $1/\sqrt{\mu_0 \sigma v g} \sim 0.04$.

This is the order of magnitude of the fractional correction that will have to be made in the expression for the Lorentz force derived from the first integral of Equation (5). From the above calculation, we see that, for copper, it is perhaps small enough to be neglected. For steel with a conductivity of, say, 5.8×10^6 mho/m, the correction is about 0.12, perhaps large enough to be considerable. (See Table 1 for electrical resistivities of rail materials).

As long as this correction is not too large, the skin depth at P will be small enough so that we can get a fair approximation to L' from the high frequency inductance per unit length. Even for $\delta \ll g$, this may still be somewhat inaccurate because the surface current distribution in this problem is not exactly that of the steady state alternating current problem. However, when it is accurate enough, the high frequency inductance per unit length can be measured directly in a ringing circuit or indirectly by means of a two-dimensional electrical analog.

To summarize, the Lorentz force on the arc is given by

$$F_{arc} = \frac{1}{2} L' I^2 \left[1 - \mathcal{O}\left(\frac{1}{\sqrt{\mu_0 \sigma v g}}\right)\right] \tag{7}$$

where L' is roughly the high-frequency inductance per unit length and $\mathcal{O}\left(\frac{1}{\sqrt{\mu_0 \sigma v g}}\right)$ is a correction of the order of the ratio between the skin depth near the arc to the width of the gap.

B. MASS-INPUT LIMITATION ON THE PROJECTILE VELOCITY

The momentum as calculated from Equation (7) using the measured values of L' and I is actually about three times greater than the mass of the projectile times its measured velocity, even when only a single arc filament is observed. As a tentative explanation for this we proposed a mass-input to the arc proportional to the total charge through the arc. This is the sort of thing one would expect if ion sputtering were taking place[11].

Table 1

IMPORTANT PHYSICAL CHARACTERISTICS OF ELEMENTAL RAIL MATERIALS

Element	Atomic Number	Total heat content 20°C through M. P. $\frac{\text{k joule}}{\text{cm}^3}$	Self sputtering yield at 200 ev* $\frac{\text{a m u}}{\text{ion}}$	Electrical Resistivity $\mu\Omega$ cm	Tensile Strength 10^3 psi
Be	4	6.9	11	4.3	50
C	6	>15.0	0.4	800	-
Mg	12	1.9	8	4.6	30
Al	13	2.7	8	2.8	40
Ti	22	> 6.0	11	3.2	100
V	23	> 6.7	17	25	100
Cr	24	>12.0	37	13	60
Fe	26	9.2	34	10	100
Co	27	10.5	39	9.8	100
Ni	28	9.2	43	7.8	160
Cu	29	5.6	61	1.7	70
Zn	30	2.1	35	5.8	30
Y	39	> 3.5	24	65	20
Zr	40	> 5.1	20	39	100
Nb	41	>10.0	20	14	50
Mo	42	>11.0	31	5.7	60
Ru	44	>10.0	38	7.6	-
Rh	45	> 8.5	52	4.5	100
Pd	46	6.8	98	10.8	40
Ag	47	> 3.3	127	1.59	40
Hf	72	> 5.0	33	36	100
Ta	73	11.0	33	12.4	150
W	74	>12.0	28	5.5	200
Re	75	15.0	46	19.1	150
Os	76	11.0	54	9.5	150
Ir	77	11.0	88	5.3	-
Pt	78	8.2	97	9.8	50
Au	79	5.4	171	2.2	20

*Not much data exists on the sputtering of cathodes by ions of the same element; therefore, the self-sputtering yields listed here have been based on data for sputtering by noble gases(10). Since sputtering at those energies is thought to be predominantly a momentum transfer process, the yield for each element has been taken from the data for the noble gas of most nearly same atomic weight(11).

For experiments without an impedance matching transformer, the current had the form of a slightly damped sine wave. Putting $I_p \sin \omega t$ for the current, M for the mass of the projectile, and m_I for the mass-input per unit charge, we get the following expression for velocity

$$V = \frac{L' I_p}{4 m_I} \frac{\omega t - \frac{1}{2} \sin 2\omega t}{\frac{\omega M}{I_p m_I} + 1 - \cos \omega t} \tag{8}$$

by equating the momentum of the projectile and arc plasma to the momentum calculated from Equation (7).

Figure 2 shows a plot of position versus time based on Equation (8). The curve was made to fit through a set of experimental points by setting m_I = 4.6 Cu atoms/ion. In order to show the seriousness of including mass input, another curve with $m_I = 0$ was arbitrarily made to fit through the experimental point at 30 μsec by setting L' equal to about one-third its measured value. It is very unlikely that the measurement of L' could be so much in error, but, even if it were, the curve for $m_I = 0$ still has the wrong shape. It, therefore, seems that phenomenologically, at least, a charge proportional mass-input describes the situation. The following section indicates how the description may be more than phenomenological.

1. Ion Sputtering

According to Thom, Norwood, and Jalufka, the current in a plasma rail gun is carried equally by ions and electrons[12]. When the ions impinge on the cathode, they dislodge atoms of the cathode metal (this process is called sputtering), some of which are ionized near the anode and then serve as charge carriers. Therefore, regardless of what kind of atoms were initially present in the arc, it eventually becomes loaded up with atoms of cathode material.

The number of atoms sputtered per ion impact is roughly proportional to the translational energy of the impacting ion. An estimate can be made from the total resistive voltage across the arc. This has an average value of about 200 v by actual measurement. Current carrying copper ions impinging on the copper cathode with the corresponding energy of 200 ev would sputter roughly 0.9 copper atoms/ion (61 atomic mass units; see Table 1).

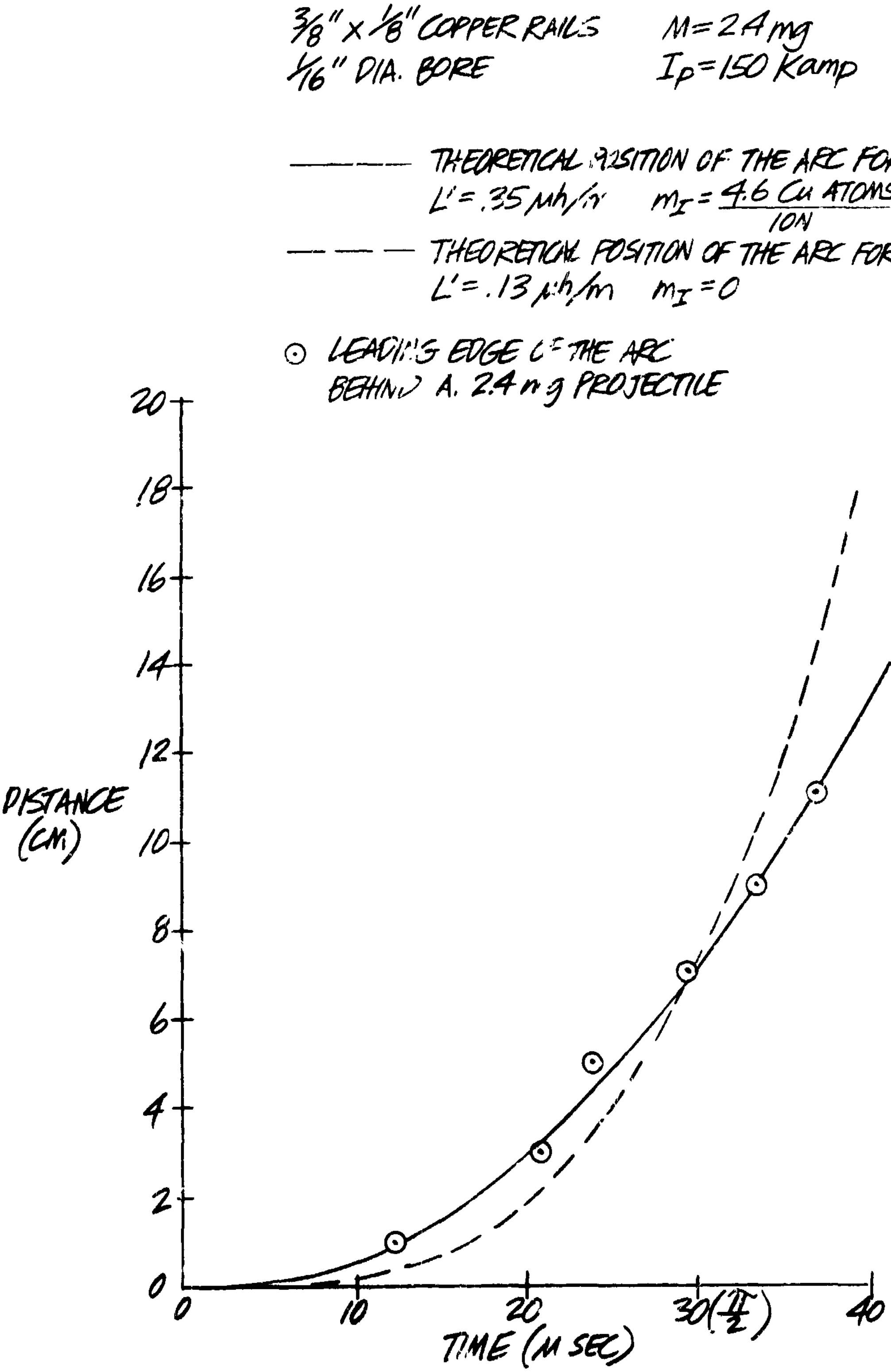

Figure 2. Distance vs Time For the Projectile Theoretical and Experimental

2. Ohmic Skin Heating

During the transit of the arc down the rail, current and magnetic field diffuse into the rail due to the finite conductivity of the rail material. As we will show, the average energy density deposited by ohmic heating in the region of the arc is approximately the magnetic energy density in the gap. If this energy density is greater than the heat content of the rail material from its initial temperature, say, room temperature, to just above its melting point, then rail material will be melted in that region(4). Since there is a forward component of the Lorentz force on the rails near the arc, this molten material will be carried forward and will, therefore, contribute to the mass of the arc-projectile system. (Although heating continues in the rails behind the arc, the Lorentz force is outward, and the molten material there will only be pressed against the rails, not carried forward.)

The heating in the region of the arc is determined as follows. The average power per unit volume is j^2/σ where j is the average current density and σ the conductivity. The volume under consideration has the thickness of the rails, g, and an average depth $\sqrt{2t/\mu_0\sigma}$, the electrical skin depth corresponding to the length of time, t, for the arc to travel its own length. The current density is, therefore $(I/g)\sqrt{\mu_0\sigma/2t}$, where I is the total current. The average power is $\mu_0 I^2/2g^2 t$, which is roughly the magnetic energy density in the gap, as stated. For

$$I = 200 \text{ k amp and}$$

$$g = 1.5 \text{ mm},$$

$$\frac{\mu_0 I^2}{2g^2} \sim 10 \text{ k joule/cm}^3$$

The averages above are very loosely defined, and the consequent results are only good to an order of magnitude. The actual heating will depend upon the details of the current distribution in the rails. Even so, one can see from Table 1, that this is the right order of magnitude to melt the current carrying part of the rail.

From flux loop data, we have a typical value for t of 10 μsec. The corresponding electrical skin depth is 0.7 mm, and the thermal depth is 0.03 mm. It would, therefore, be impossible for the heat generated to dissipate by conduction during the passage of the arc. The appearance of the rails after the shot bears this out. In fact, for a steel rail with 8 mil copper cladding, the entire copper face was melted in the region of highest current. The total amount of copper melted over a 6 cm length has a mass of from 0.1 to 1 gm. Ten or so milligrams of this carried forward against the projectile would account for the mass-input effect.

For a given energy density the amount of material melted will increase in direct proportion to the skin depth and hence the square root of the resistivity in the rail material. In addition to the decrease in inductance, this may have contributed to the poorer performance of steel compared to copper even though the steel rails showed less deformation.

C. MECHANICAL EFFECTS

1. Lorentz Force On The Rails

In the region behind the arc, the Lorentz force density is outward from the gap in the plane of the rails. The equivalent pressure at the gap surface of the rails is just the magnetic energy density in the gap For the case described in the last section, this is a pressure of about 10^6 psi, enough to cause plastic flow in the solid rail material.

In addition to plastic flow at the gap surface, the Lorentz force causes gross motion of the rails in the lateral direction. Since the rails are restrained in this direction by bolts or steel dowel pins, this motion causes plastic flow of the rail around the bolts.

The appearance of the rails after the shot shows that considerable plastic flow and gross motion of the rails do occur. Depending upon the rail material, the peak current, and upon the insulator, which serves to prevent relief perpendicular to the plane of the rails, the gap may be enlarged by a factor of 2 or 3. The effect of this spreading is to lower the Lorentz force on the arc. This can be seen either as a decrease in inductance or, equivalently, a drop in magnetic pressure due to expansion.

2. The Pressure And Length Of The Arc

The arc is contained at the front by the inertial forces of the projectile and of its own mass, from the sides by the rails and insulator, and from behind by what may be thought of as a magnetic pressure, (typically 10^6 psi). In the steady state, the ordinary kinetic pressure in the arc will just balance this magnetic pressure. For temperatures of 10 to 100 ev this corresponds to the following:

10^{22} to 10^{21} atoms/cm^3 particle density

1 to .1 gm/cm^3 mass density

Given the mass of the arc and the cross section of the barrel, the arc length is completely specified by this density. Flux loop measurements give this length as very roughly 1 cm. The corresponding mass range is 2 to 20 mg, consistent with the observed mass-input limitation.

The mechanical effect of the arc pressure is to stress the insulator over the arc. This stress is followed by another due to the plastic deformation of the rails, as described above. One-half inch thick cloth-phenolic insulators have been broken into two pieces along the barrel by this shock. Melamine-glass cloth laminate blocks, which we now use, show some separation of the laminations but seem to be more than strong enough to withstand the pressures in the present current regime. This sort of failure helps to lower the Lorentz force on the arc by allowing the rails to spread.

D. SPLITTING OF THE ARC

In the ideal operation of the rail gun, as we first imagined it, the projectile would fit tightly in the barrel, the arc would be confined behind the projectile, and, therefore, the projectile would have to move at least as fast as the center of mass of the whole arc-projectile system. By increasing the current, the velocity of the center of mass and, consequently, of the projectile would have to increase.

Early in the last contract, it became apparent that even as little as a 3% looseness of fit could reduce the velocity by one-half. All projectiles were thereafter made to fit tightly, with the result of velocities as high as 6.0 km/sec. The position of the arc versus time as determined from magnetic flux loop data showed that the arc was remaining behind the projectile.

On the basis of these results, an impedance matching transformer was built to increase the current and, we expected, the velocity. Instead, what happened was that, after a point, an increase in current led to a decrease in velocity (See Figures 3 and 4).

An improved magnetic flux loop technique (See Appendix A) has revealed a phenomena which may explain this. Figures 5 through 20 are plots of the position of the arc versus time, the flux loop data from which they were taken, and the corresponding projectile-velocity data. They show, in every case except experiment 2.10-1 (Figures 13 and 14), that two arcs were present, one moving faster than the projectile and the other, behind it, moving at the same speed as the projectile or slightly slower. The velocity data is consistent with the interpretation that the projectile is somewhat in front of the slower arc.

In all but experiment 3-1 (Figures 19 and 20), the projectile was initially some few centimeters in front of the aluminum foil used to start the arc. This was done

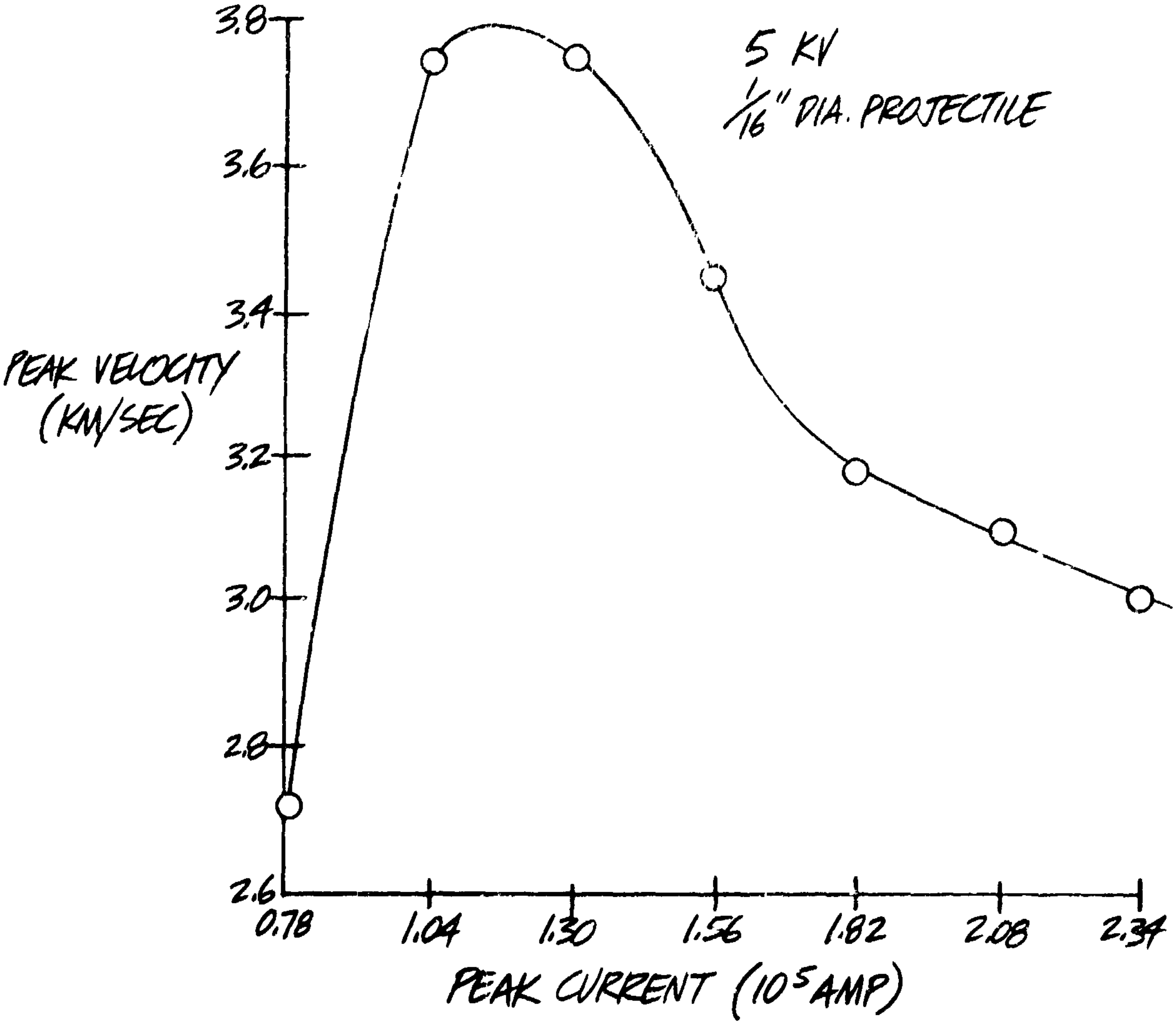

Figure 3. Projectile Velocity vs Peak Current

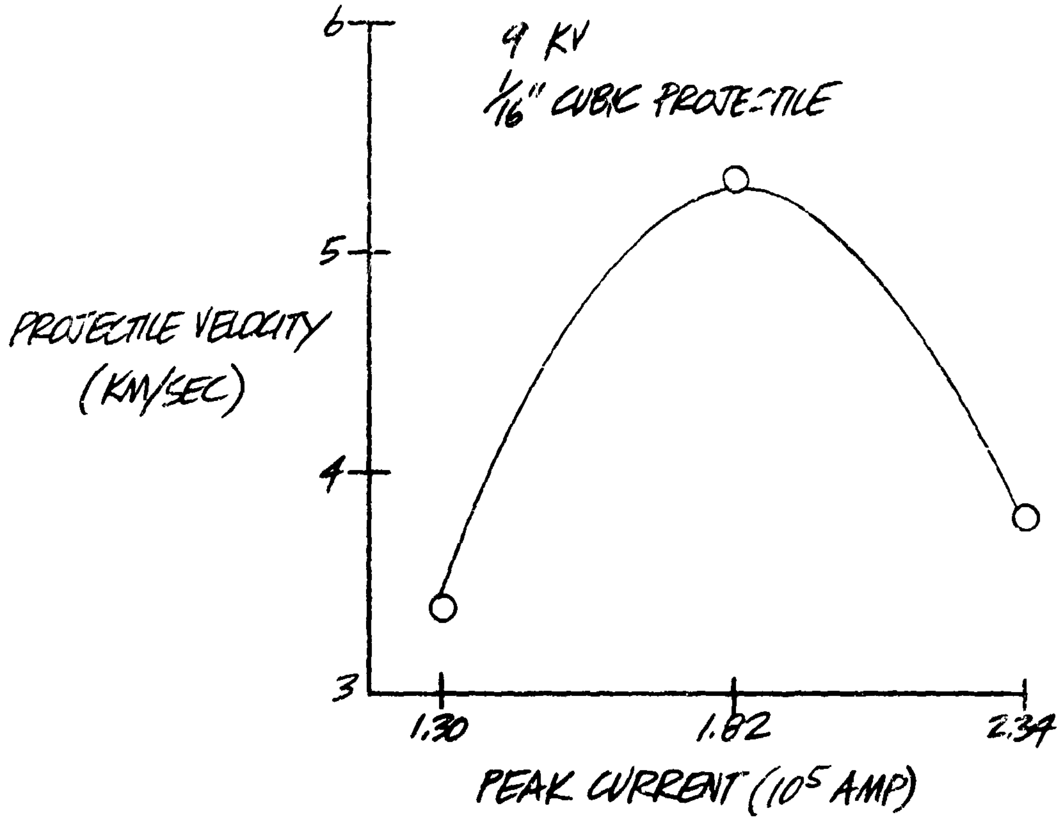

Figure 4. Projectile Velocity vs Peak Current

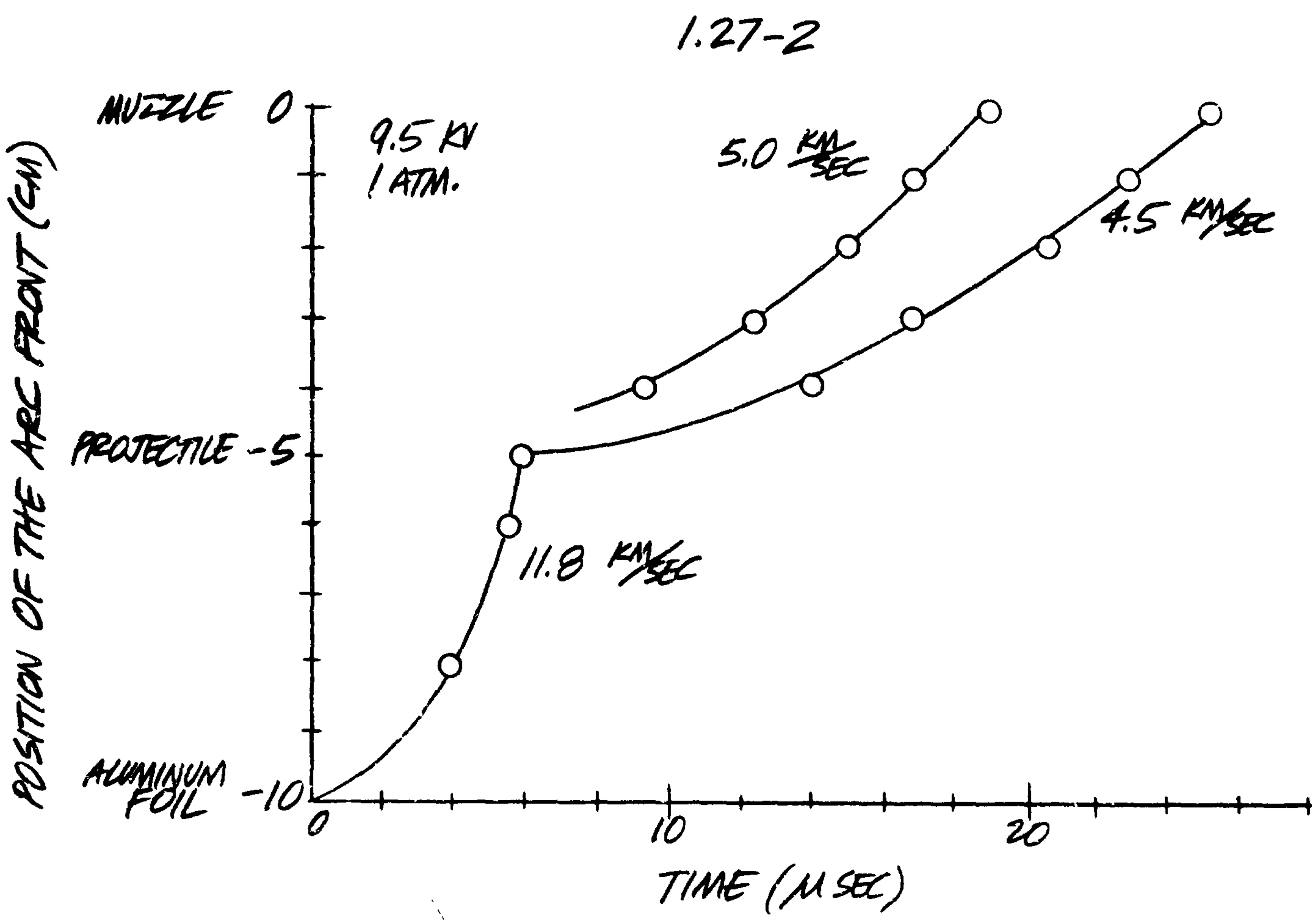

Figure 5. Position of the Arc Front versus Time
(As determined from the following magnetic flux data)

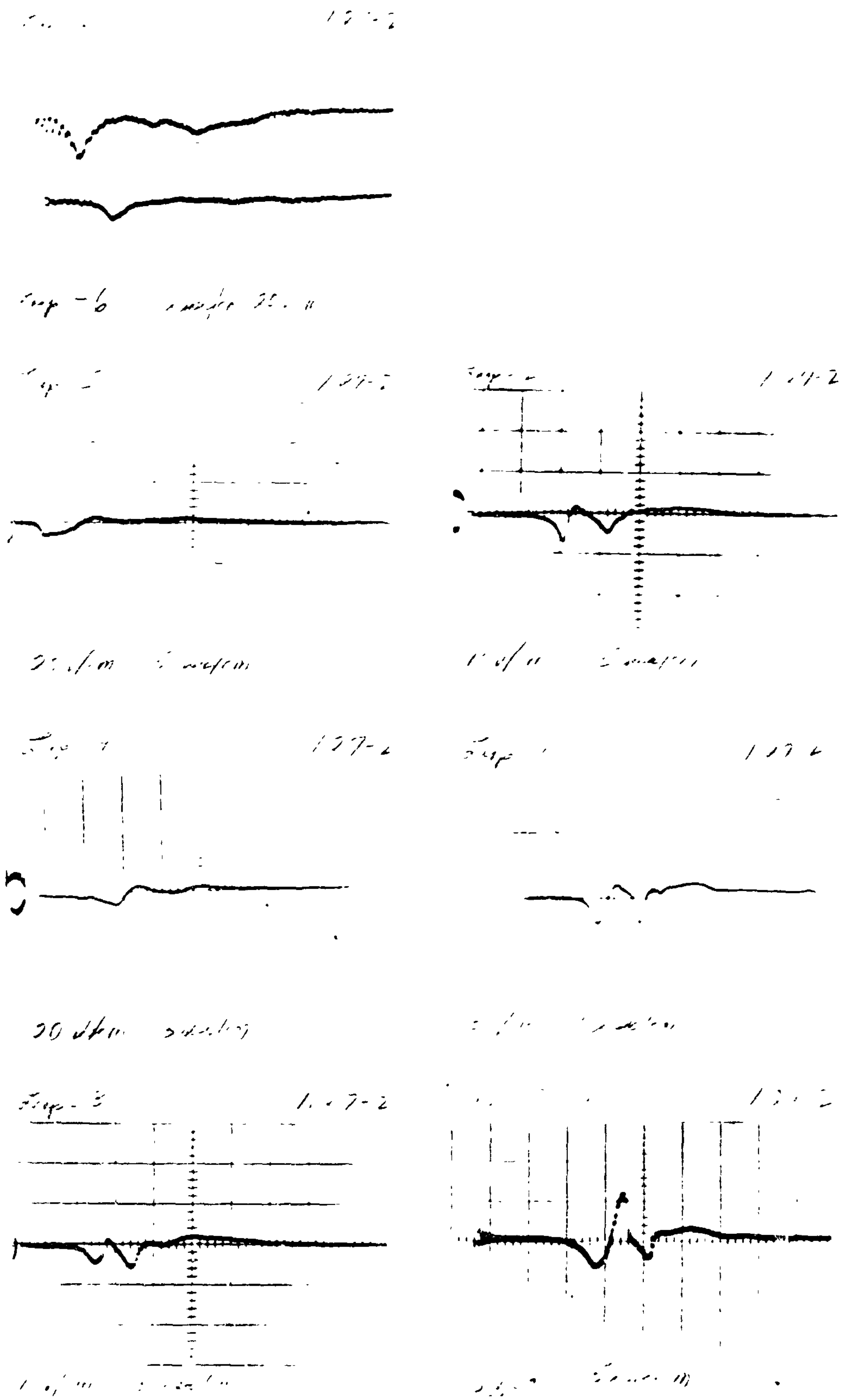

Figure 6. Magnetic Flux Data

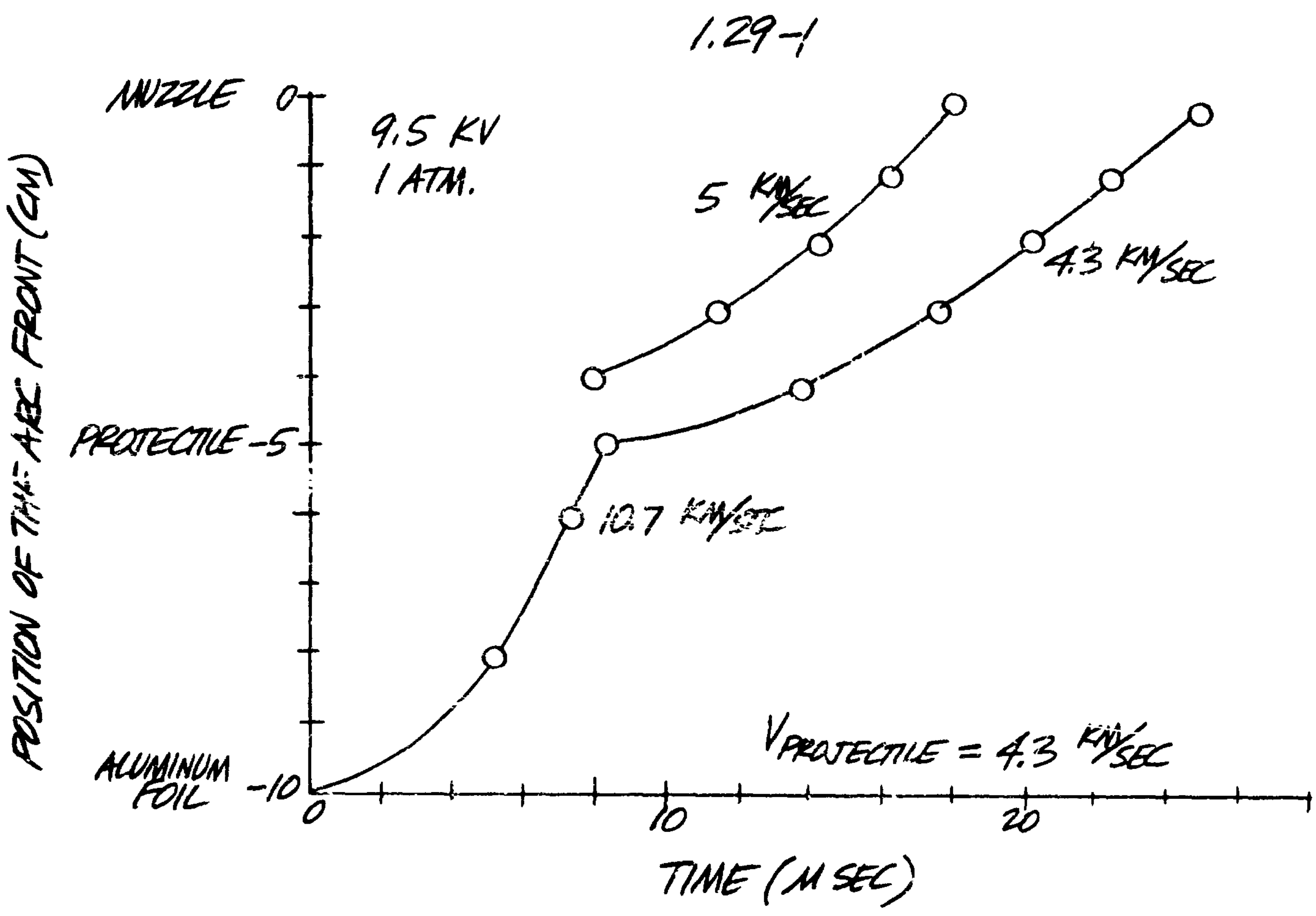

Figure 7. Position of the Arc Front versus Time
(As determined from the following magnetic flux data)

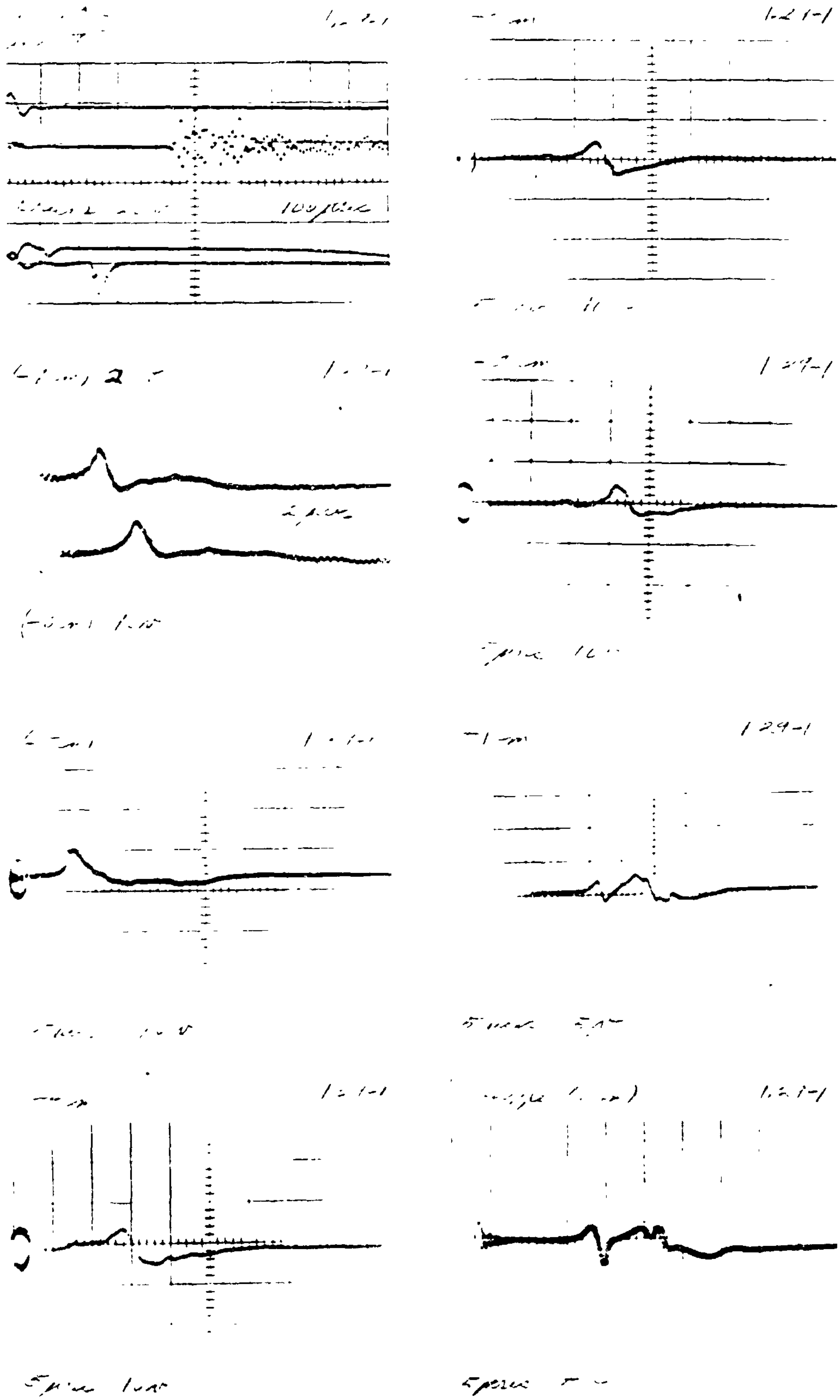

Figure 8. Magnetic Flux and Projectile Velocity Data

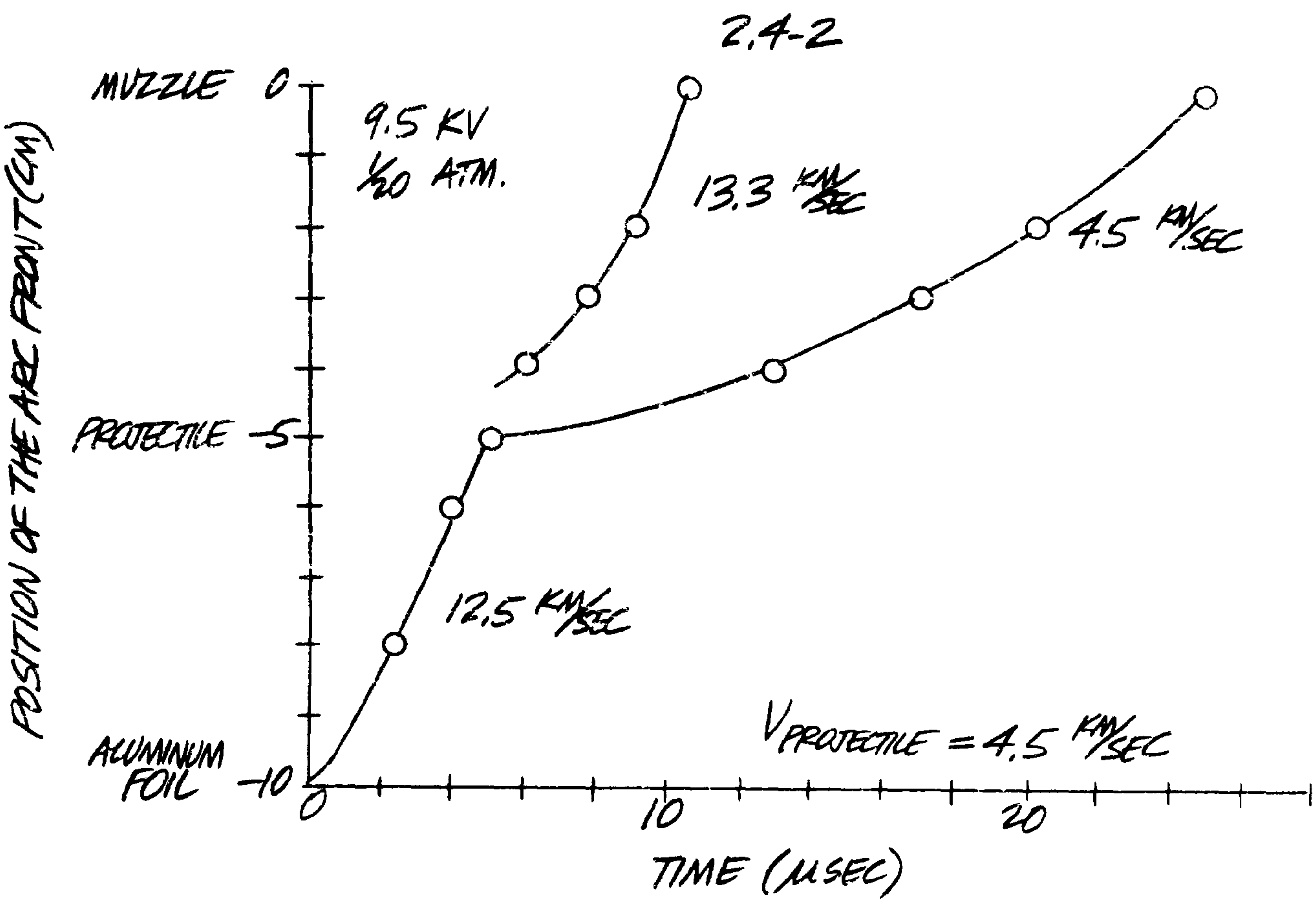

Figure 9. Position of the Arc Front versus Time
(As determined from the following magnetic flux data)

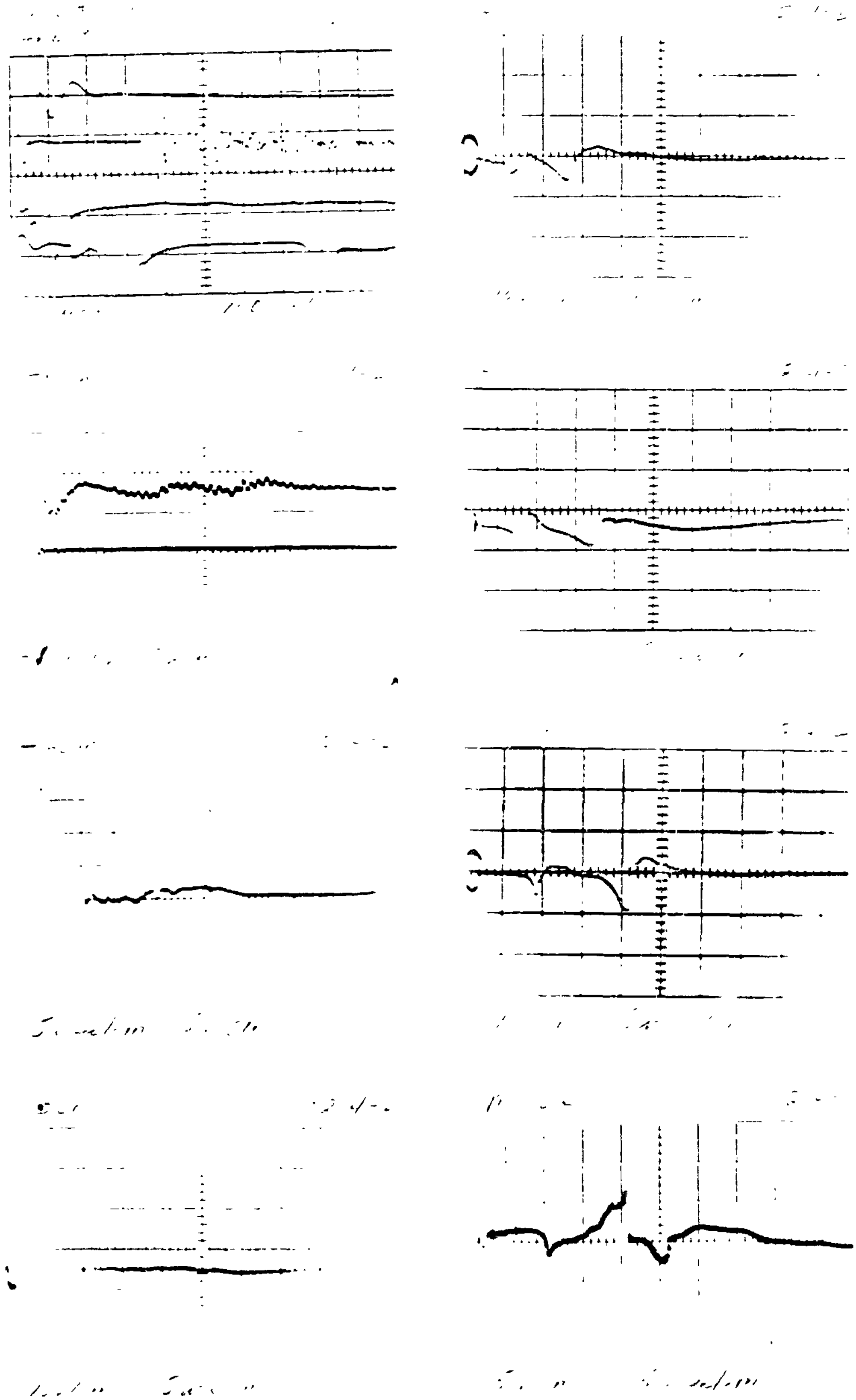

Figure 10. Magnetic Flux and Projectile Velocity Data

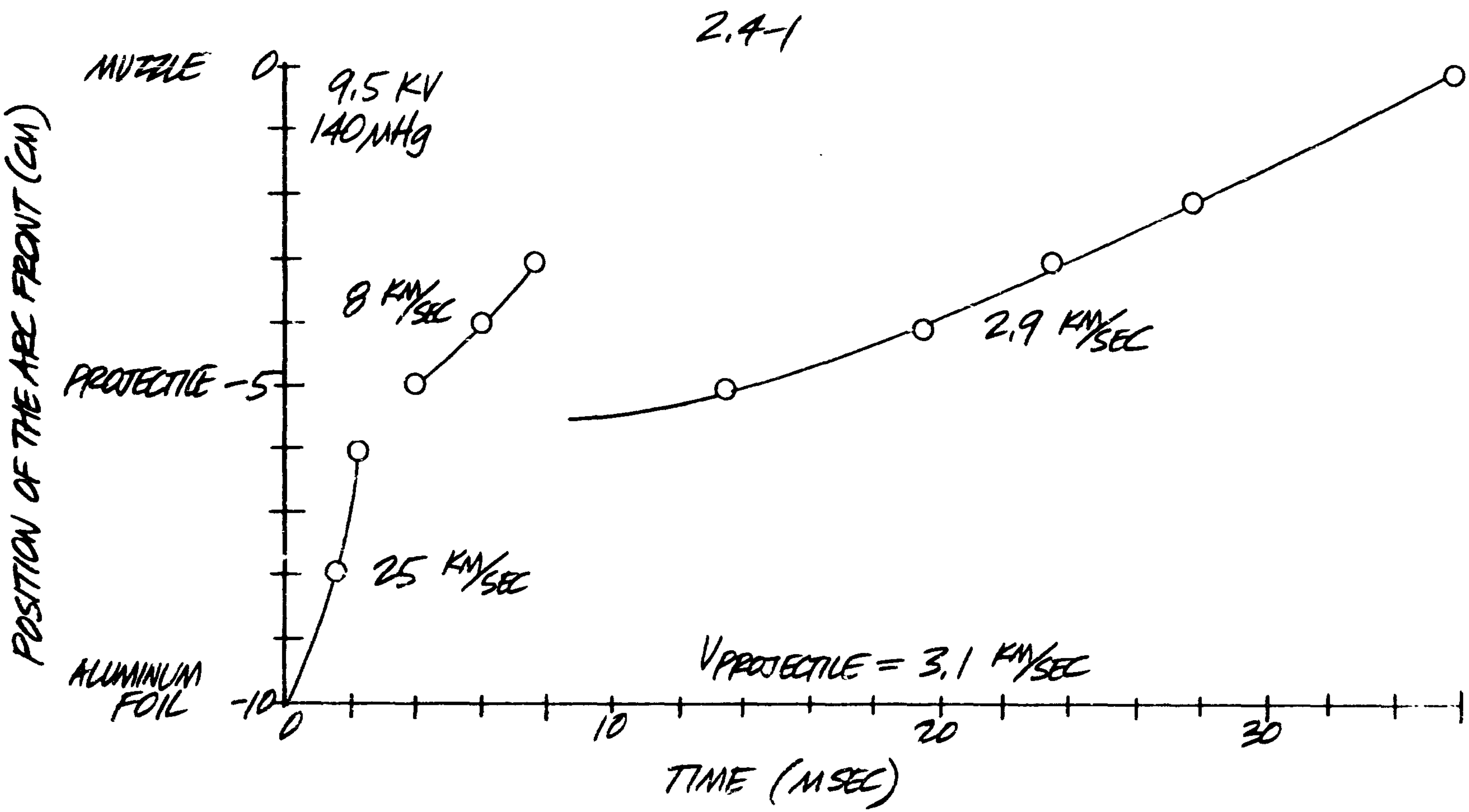

Figure 11. Position of the Arc Front versus Time
(As determined from the following magnetic flux data)

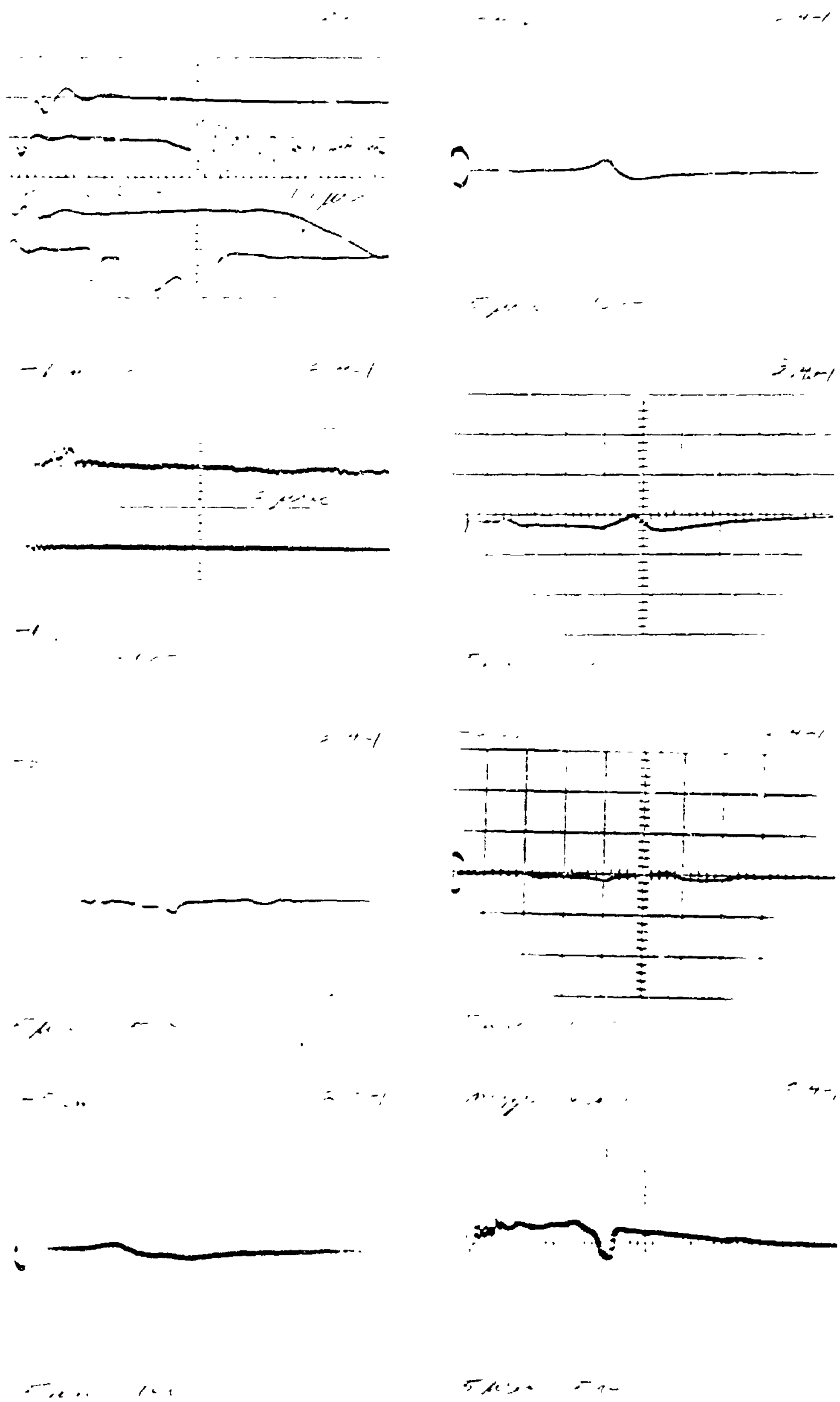

Figure 12. Magnetic Flux and Projectile Velocity Data

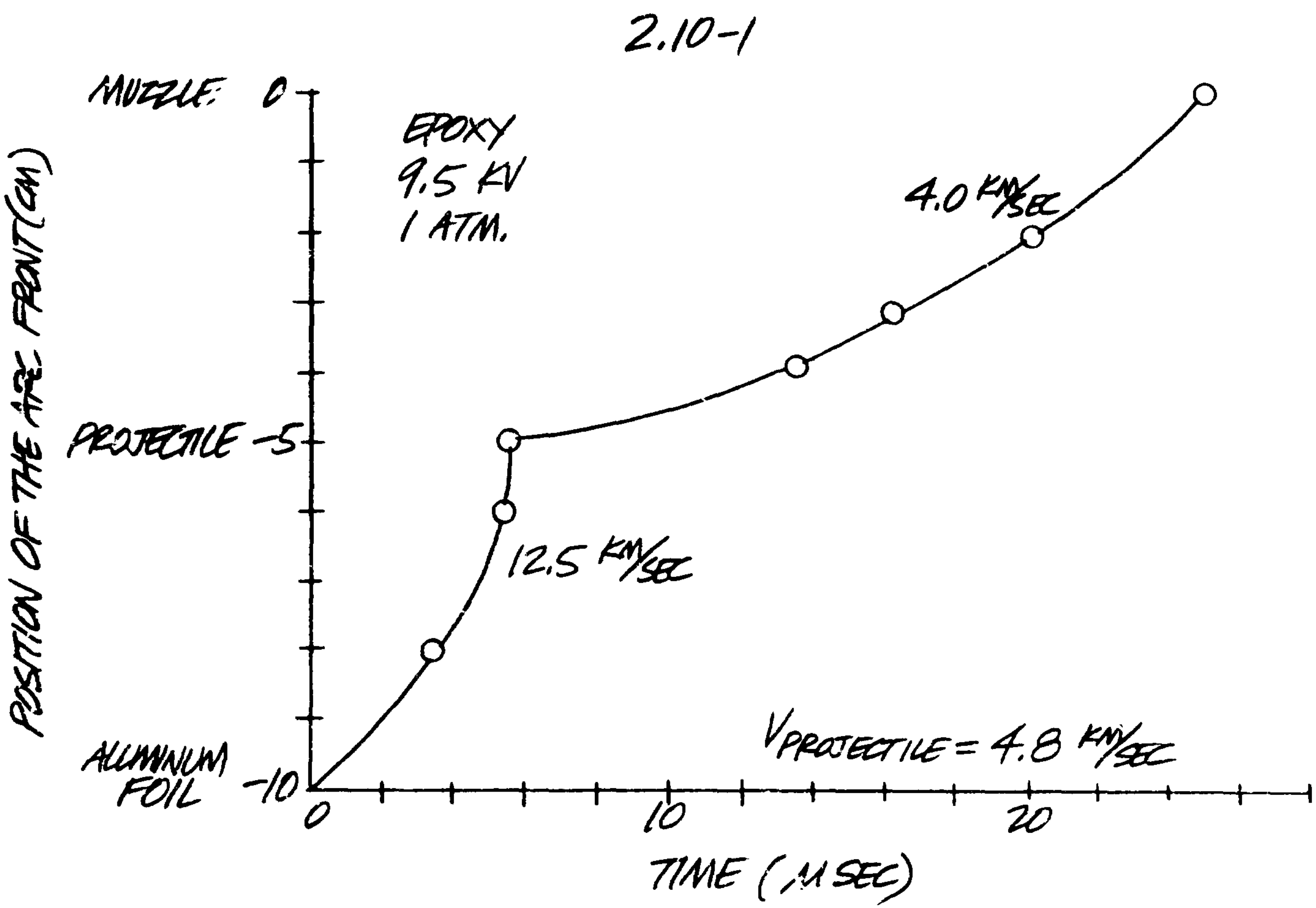

Figure 13. Position of the Arc Front versus Time
(As determined from the following magnetic flux data)

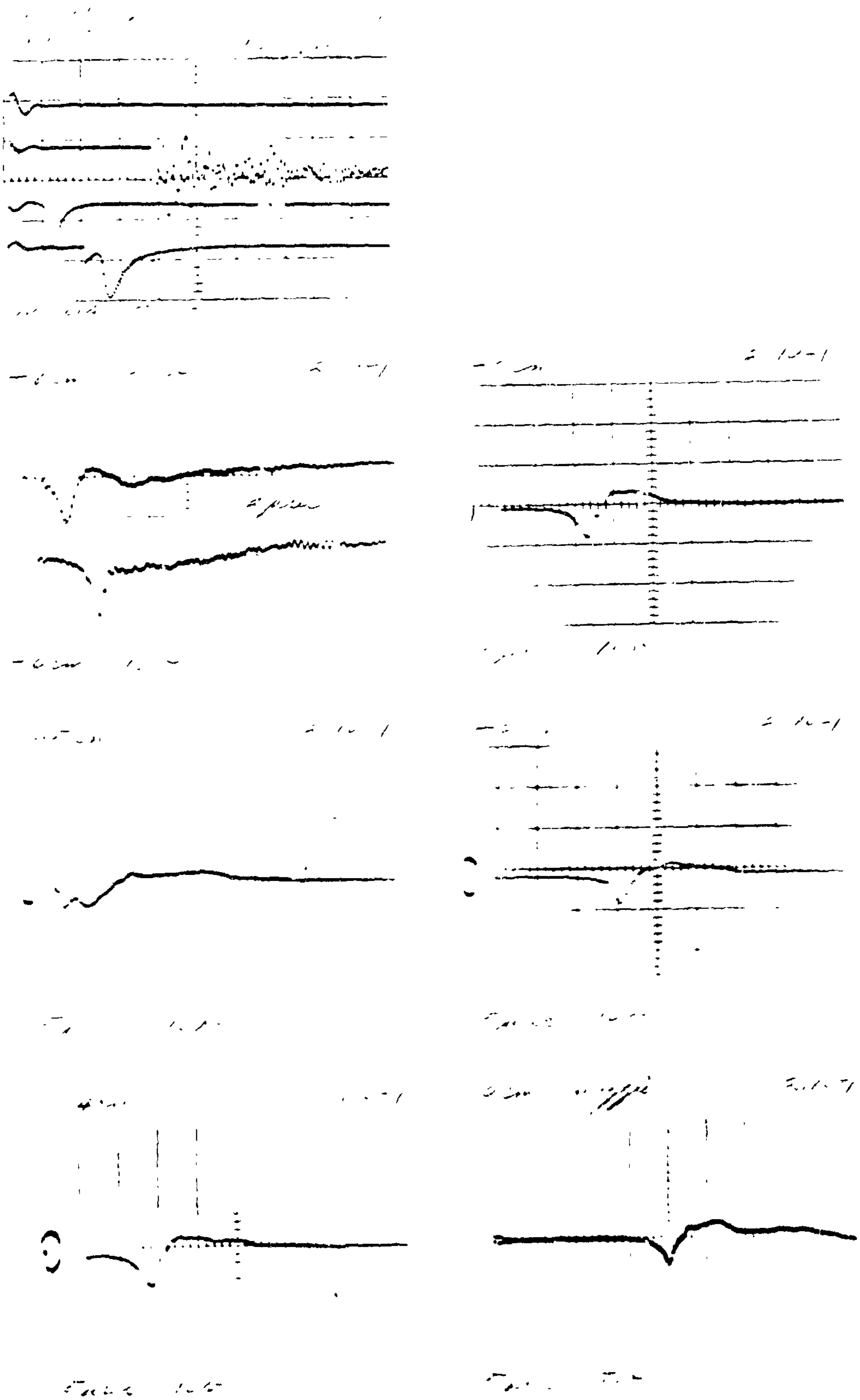

Figure 14. Magnetic Flux and Projectile Velocity Data

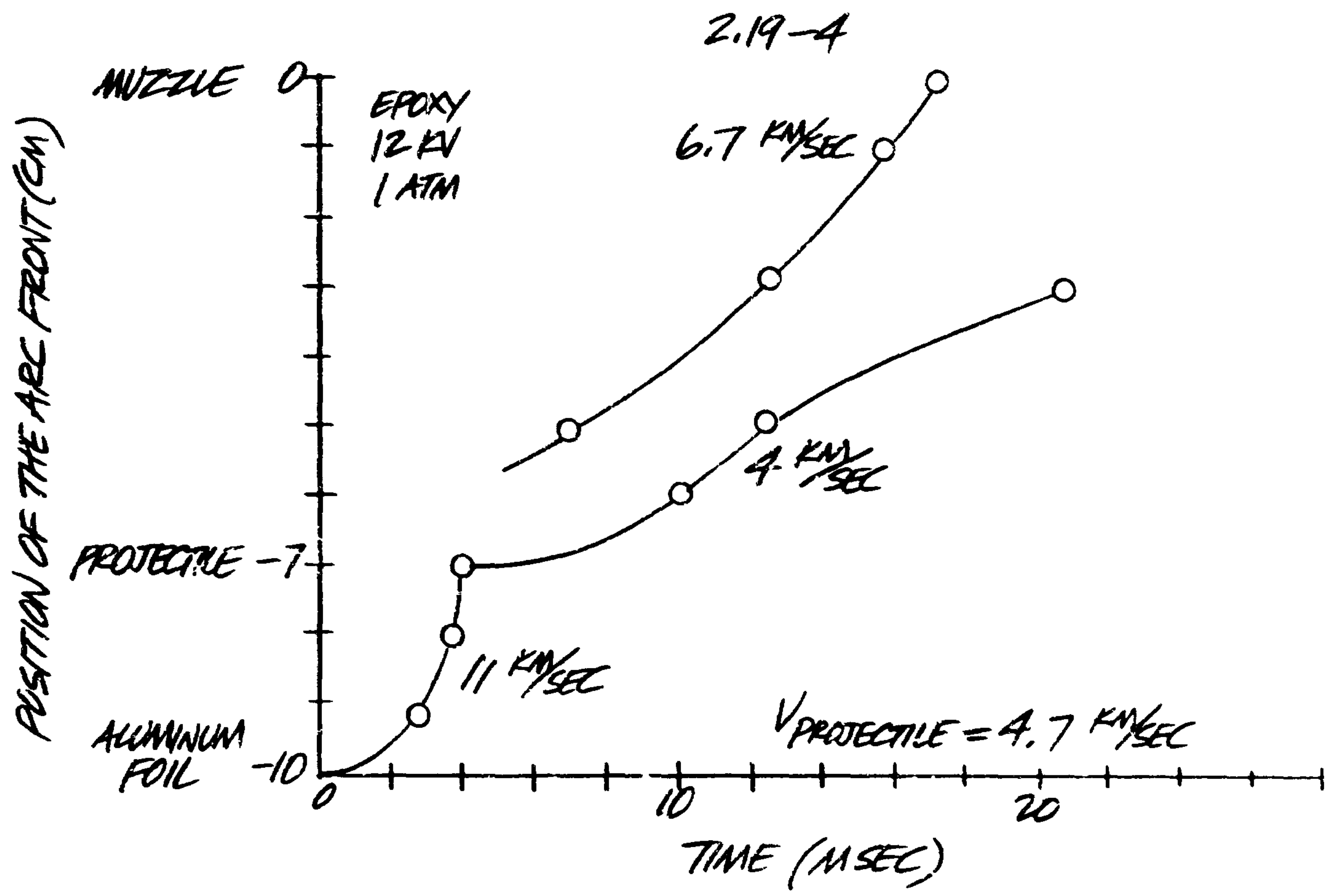

Figure 15. Position of the Arc Front versus Time
(As determined from the following magnetic flux data)

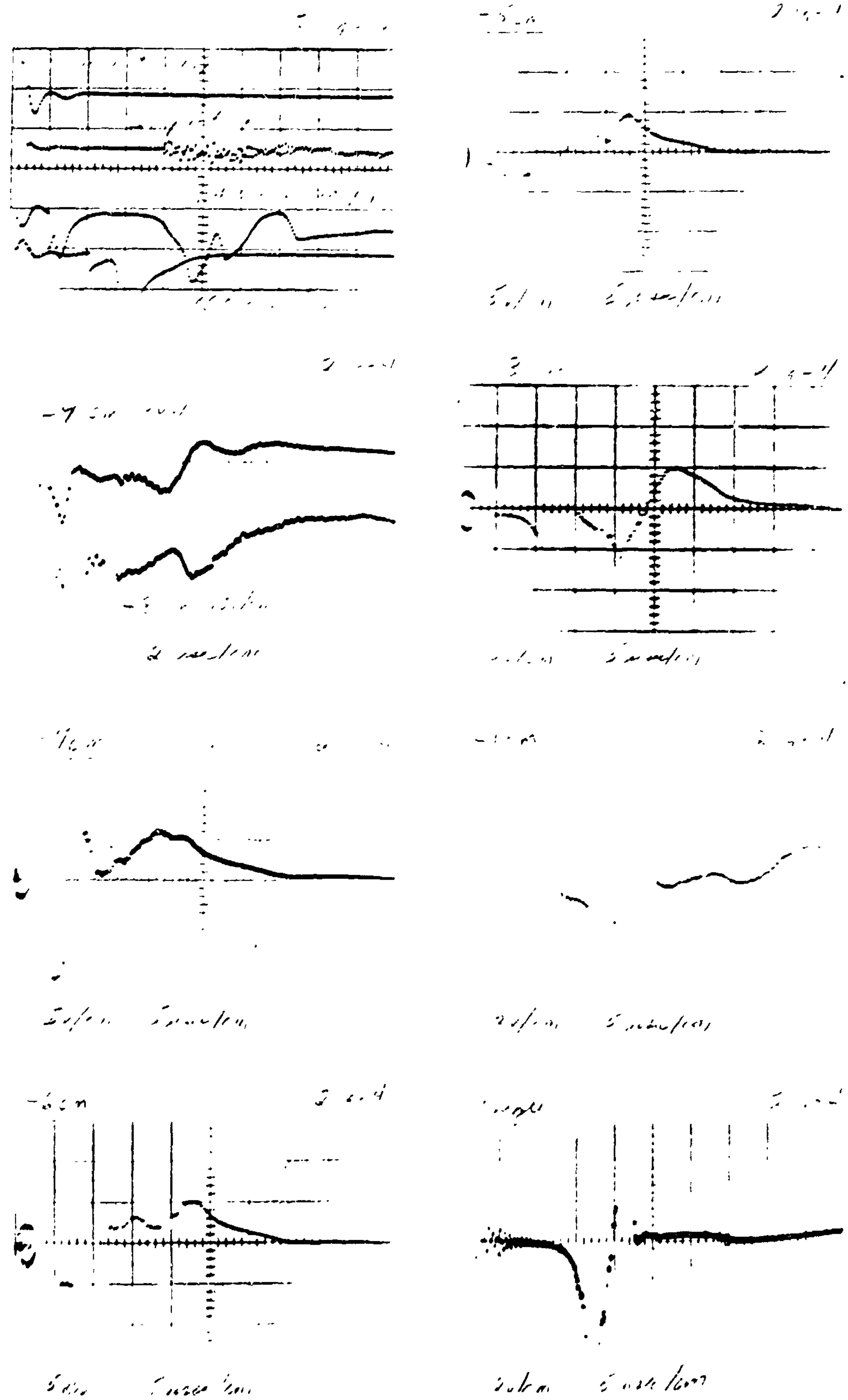

Figure 16. Magnetic Flux and Projectile Velocity Data

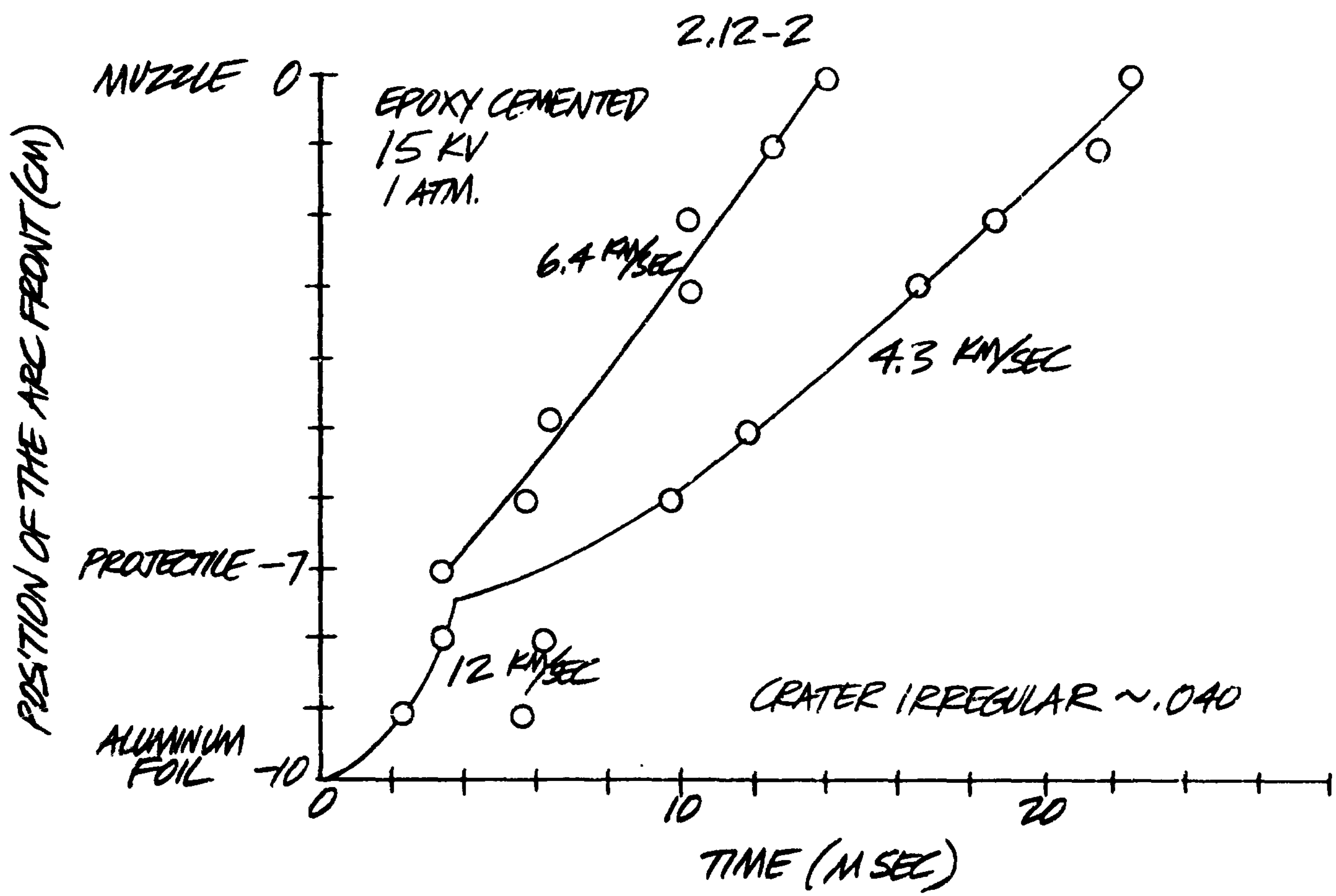

Figure 17. Position of the Arc Front versus Time
(As determined from the following magnetic flux data)

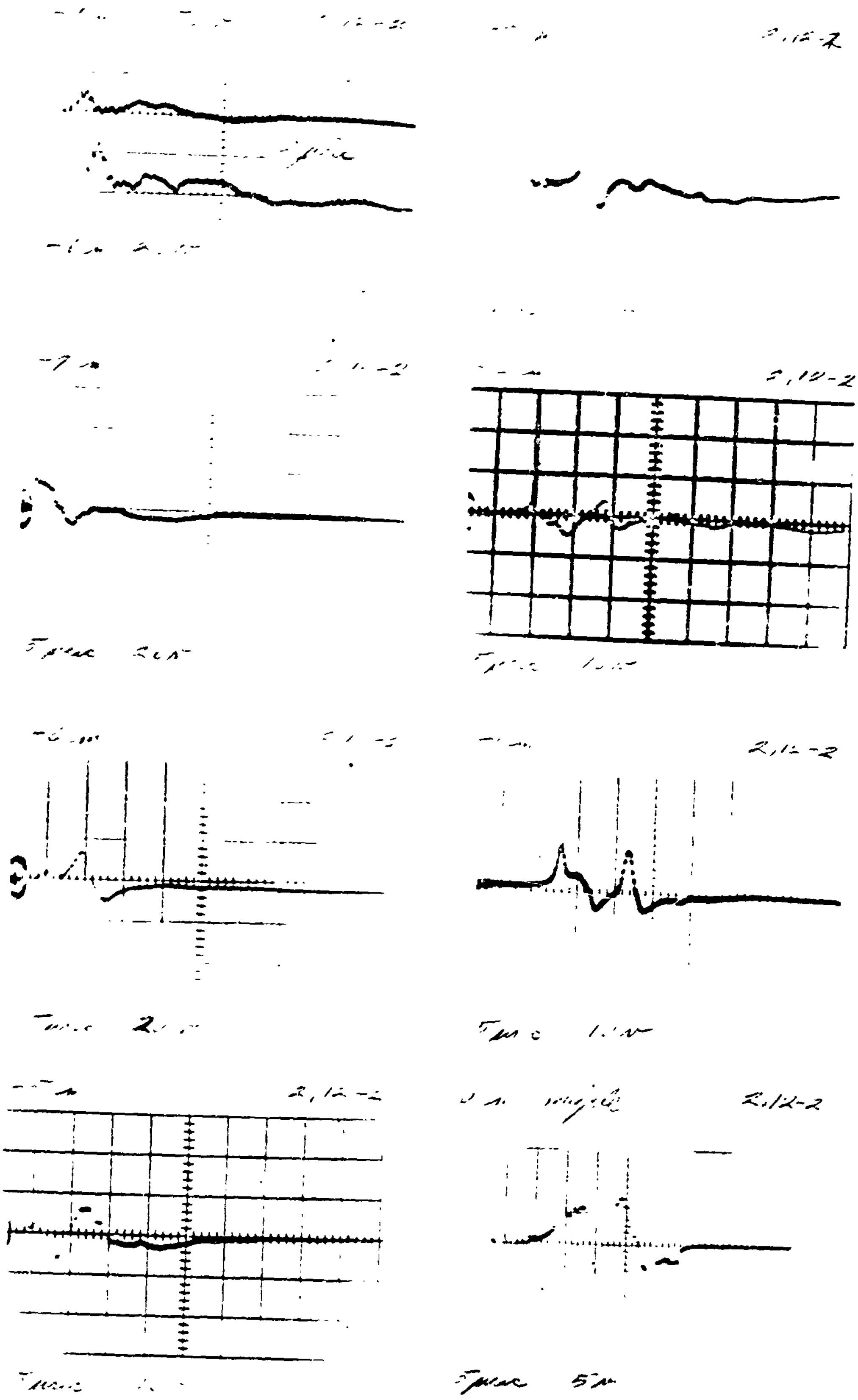

Figure 18. Magnetic Flux Data

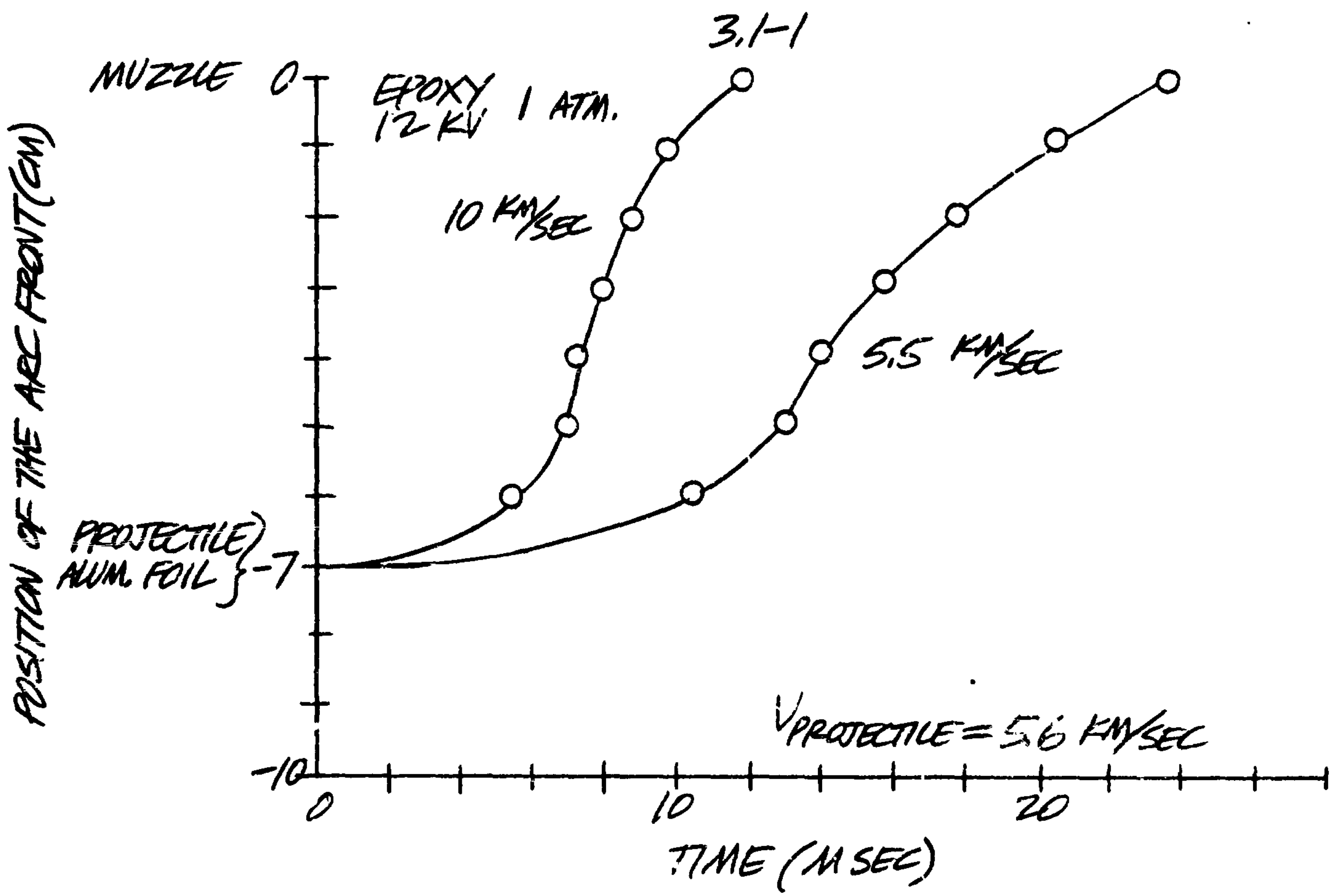

Figure 19. Position of the Arc Front versus Time
(As determined from the following magnetic flux data)

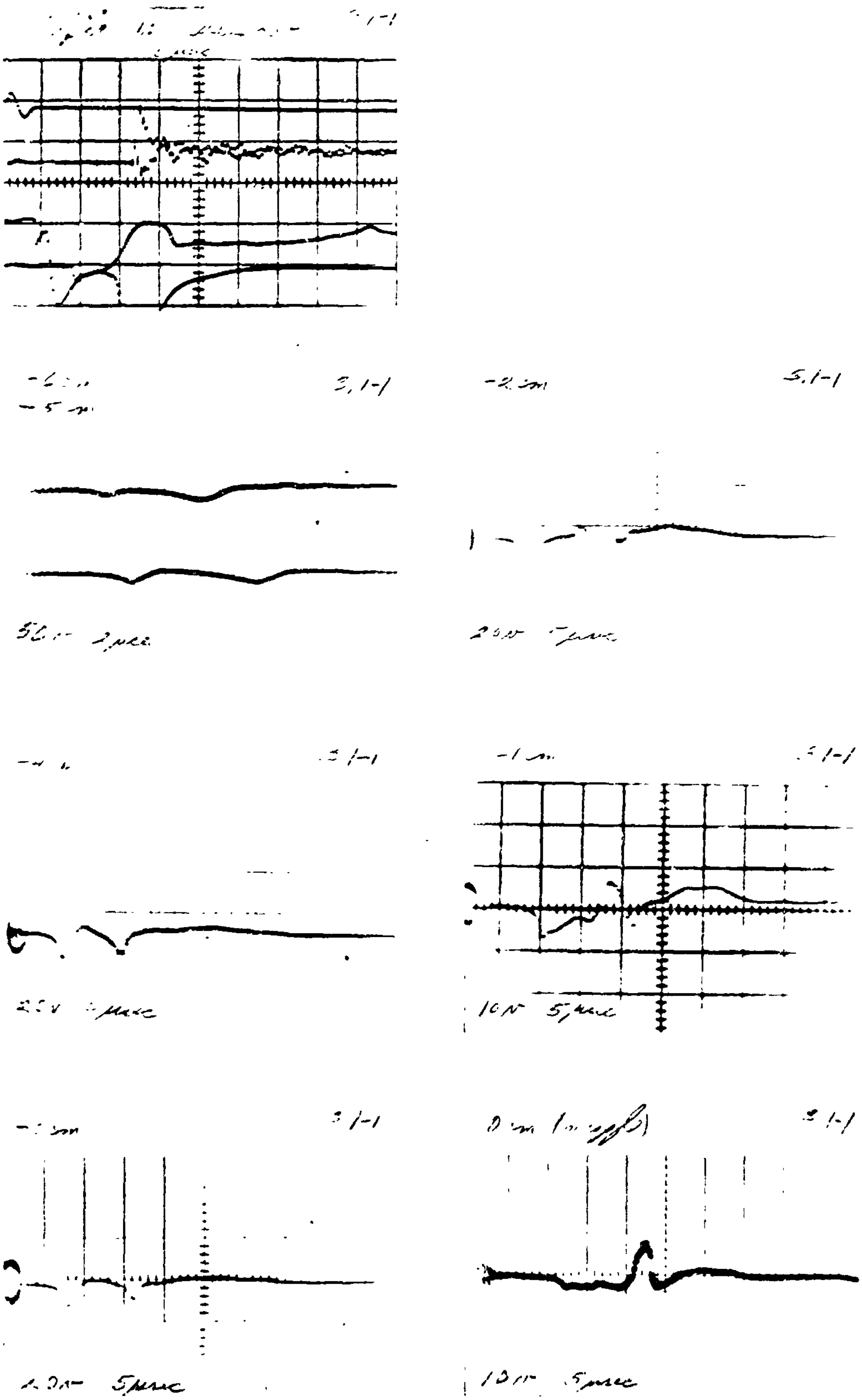

Figure 20. Magnetic Flux and Projectile Velocity Data

so that we could observe clearly any change in behavior when the arc reached the projectile.

The observed result is that, at first, a well defined front, behind which current flowed more or less uniformily over several centimeters behind the front, moved forward with a velocity of 10 or 12 km/sec just as in experiments without a projectile. When this front reached the position of the projectile, a second arc formed in front of the projectile. The velocity of the first arc dropped to zero and gradually increased to a velocity of the order of 4 km/sec. At the same time the second arc accelerated to a higher velocity, and the current in it increased from a very small fraction of the total to roughly half or more by the time it reached the muzzle. Furthermore, instead of a uniform current distribution, both arcs became rather well defined filaments of less than a centimeter in extent. The separation of the two arcs grew from less than 1 cm to between 3 and 4.5 cm. This phenomenon is especially clear in Figures 5 through 7.

The effect of this second arc is to decrease the Lorentz force on the first and hence on the projectile. The magnitude of the effect can be estimated as follows. The total force on both arcs is the same as on a single arc, namely, $\frac{1}{2}L'I^2$. If the forward arc is far enough from the other, the force on it is just $\frac{1}{2}L'I_1^2$, where I_1 is the current through the forward arc. The force on the rear arc is, therefore, $\frac{1}{2}L'(I^2-I_1^2)$ and the fraction of the force lost to the rear arc just $(I_1/I_2)^2$. For $I_1 = \frac{1}{2}I_2$ as observed, the fraction of the force lost is one-fourth.

An explanation for the inverse dependence of velocity on current in terms of this phenomenon is that before a certain critical current is reached no second arc forms and the projectile is accelerated according to the considerations of Section II.B. After this critical point, a second arc grows, and the net effect of increasing the current is to increase the predominance of the first arc over the second at the expense of velocity. Experiments 2.10-1 at 250 k amp, 2.19-4 at 310 k amp, and 2.12-2 at 390 k amp (See Figures 13-18) are consistent with this. In the experiment at 250 k amp, only one arc appears, at the high currents two.

Two kinds of explanation have been offered for the appearance of the second arc. In one, the initial conductive path in front of the projectile is provided by the ionized shock front due to the motion of the projectile or by the front surface of the projectile itself, in the other, by plasma leaking around the projectile. The evidence is ambiguous but favors the latter explanation.

In the series of experiments represented in Figure 21 various amounts of aluminum foil were used to initiate the arc, and an optimum of 7 mg was found for a given gun at a given peak current. The time required for current to diffuse from the back to front of a wad of this mass due to the finite conductivity of aluminum is of the order of 40 μsec. One can imagine that until current diffuses through the

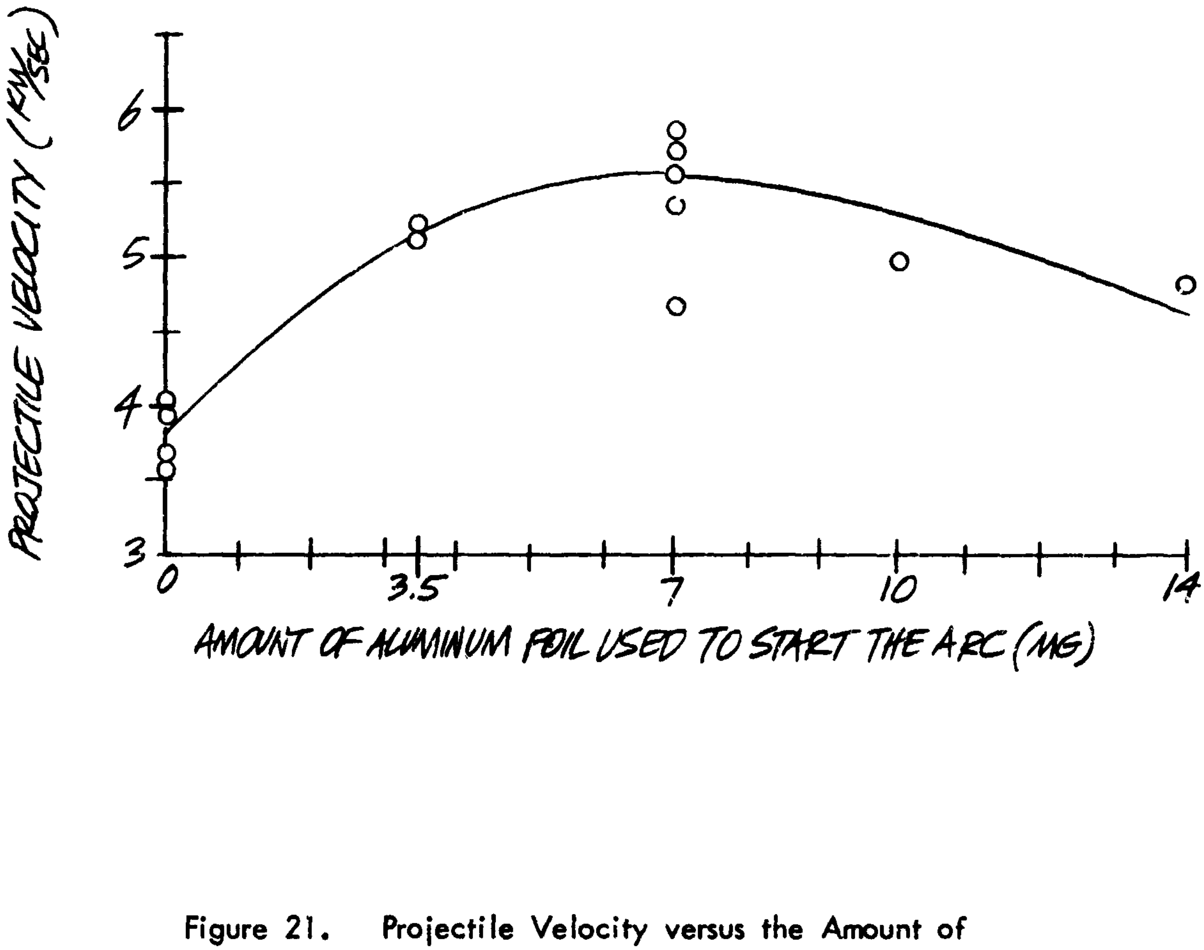

Figure 21. Projectile Velocity versus the Amount of Aluminum Used to Initiate the Arc

wad, it acts as an impermeable sabot against the arc plasma. However, beyond the optimum mass of aluminum, nothing further is gained in sealing the barrel, and any additional mass decreases the velocity by absorbing momentum.

Experiments 1.27-2 and 1.29-1 (Figures 5-8) were done with the gun of Appendix D without epoxy sealant. This left a small channel at each corner of the projectile, through which plasma could leak. Experiment 2.10-1 (Figures 13 and 14) was with the same gun except with the epoxy and, so, with the projectile completely sealing the barrel. In 1.27-2 and 1.29-1, we see two arcs, in 2.10-1, only one. Also, the projectile velocity is about 10% higher with the sealed barrel.

These two groups of experiments tend to support the plasma leakage explanation. The following experiments are less clear.

Experiments 1.29-1, 2.4-2, and 2.4-1 (Figures 7-12) were done at pressures of 760, 38 and .14 mm Hg, respectively. In all of them, two arcs appeared. The single arc before reaching the projectile and the forward arc afterwards had progressively higher velocity with decreasing pressure, in agreement with a series of experiments under the previous contract. The projectile velocities had the opposite dependence on pressure.

If the ionized shock front were providing the initial conductive path before the projectile, one would expect that the number of ions and hence the conductivity would go down with pressure, that the formation of the second arc would be inhibited, and that the projectile velocity would increase. On the other hand, it is hard to explain the decrease in velocity by the plasma leakage. Possibly the air before the projectile reduces the rate of plasma leakage.

In experiment 3.1-1 (Figures 19 and 20) the foil wad was placed directly behind the projectile as is usually done. In 2.19-4 (Figures 15 and 16), there was a space of 3 cm between projectile and foil. Neither mechanism seems to explain the difference in projectile velocity.

E. VOLTAGE ACROSS THE MUZZLE AND BREECH

The voltage differences shown in Figure 22 are related in the following way:

$$V_b = V_m + \frac{d}{dt}(LI) \qquad (9)$$

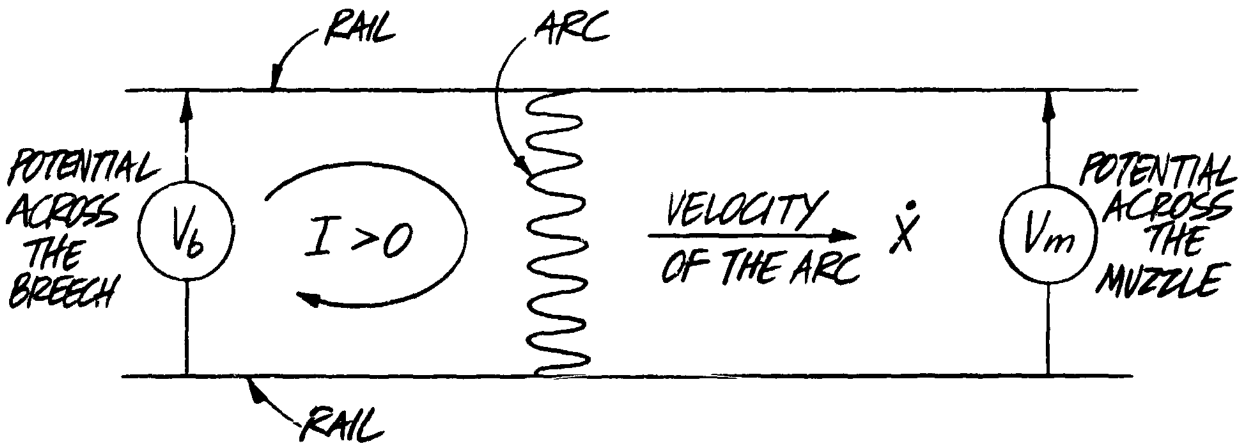

Figure 22. Voltage Measurements Across The Rails

where I is the total current through the arc and L is the inductance included between the breech and the arc. By decomposing $\frac{d}{dt}(LI)$ we have:

$$V_b = V_m + L'\dot{x} + L\dot{I} \tag{10}$$

where L' is the inductance per unit length of the rails. (V_m, which is the voltage across the arc, may be measured anywhere across the rails in front of the arc.)

The following actual measurement of I, L', V_b, V_m, and $\dot{x}$ taken at peak current ($\dot{I} = 0$) were consistent with Equation 10:

$$I = 290 \text{ k amp}$$

$$L' = .28\,\mu\text{h/m}$$

$$\dot{x} = 3.2 \text{ km/sec}$$

$$V_b = 700 \text{ v}$$

$$V_m = 440 \text{ v}$$

The total electric power into the gun is $V_b I$. Of this, $V_m I$ is irretrievably dissipated in the arc, $L\dot{I}I$ goes into increasing the magnetic field in the region between the breech and the arc, $\frac{1}{2}L'I^2\dot{x}$ into creating field in the region being uncovered by the motion of the arc, and $\frac{1}{2}L'I^2\dot{x}$ into the kinetic energy of the arc-projectile system. The fraction V_m/V_b is, therefore, a minimum measure of the energy inefficiency of the gun.

In experiments with no projectile, V_m/V_b appeared to be greater than 90% indicating a very poor energy efficiency of the gun. When the experiment was repeated with a projectile (a 1/8 inch nylon cube), V_m/V_b was found to be roughly 60% during almost the entire acceleration. Since the magnetic field energy is always at least as great as the projectile kinetic energy, the net energy efficiency must be less than half the complement of 60%, i.e., less than 20%. The gross energy efficiency computed from the projectile mass and velocity and the condenser bank capacity and voltage was 2.0% - less than the 20% upper limit on the gun's efficiency, as it must be.

F. ADDITIONAL EXPERIMENTS

1. Measurement of the Mass Removed from the Rails During a Shot

The appearance of the rails shows that several mils of metal are removed from the face of the rails forming the barrel during the shot. Some of this is found redeposited as a very fine film on the side faces of the rails and the adjacent insulator as well as upon all exposed surfaces in front of the gun. The theory of Section II.B. requires that the total amount be of the order of 20 milligrams. We have four estimates of the mass which are consistent with this: the apparent amount removed from the rail, the amount deposited on the insulator, the amount deposited on a ballistic pendulum, and the momentum delivered to the pendulum together with the known velocity of the arc.

The film deposited on the insulators appears as streaks running away from the barrel. In the region near where the arc first strikes, the streaks are nearly straight and perpendicular to the barrel. Further down the barrel, they slant more and more towards the muzzle, eventually making angles of say, 15°, and curve away from the barrel. This suggests that the metal vapor leaves the barrel at first with only lateral momentum and, further down the barrel, with more and more forward momentum, so that in the region of high arc velocity the forward components becomes of the order of four times greater than the lateral.

2. Tests with Various Rail Metals

Experiments with rails of various metals gave the following results:

Rail Metal	Projectile Velocity (km/sec)
Brass	2.0
Soft aluminum	2.1
Mild steel	3.1
Untempered tool steel	3.2
Copper	3.7
Aluminum 7075	3.7
Magnesium	3.9
1/6" copper strip silver soldered to mild steel	4.7
.008" cold rolled annealed copper sheath on untempered tool steel	5.2
	Arc Velocity
Copper	13
2% thoriated tungsten rod silver soldered to untempered tool steel	10

These experiments, especially the last two, seem to show that sputtering yield and heat content are not so important as electrical conductivity and strength (See Table 1). The dependence on electrical conductivity is in agreement with the conclusions of Section II.A.

3. Tests with Various Insulating Linings

Experiments with guns of identical construction except for the thin insulating liner next to the rails were done at a relatively low current to minimize mechanical effects. The results were as follows:

Insulator	Projectile Velocity (km/sec)
Glass	3.8
Melamine-fiberglass laminate	3.8
Epoxy-fiberglass laminate	2.0

The glass and melamine showed much less erosion compared with the epoxy.

4. Auxiliary Field Guns

Two kinds of auxiliary-field guns have been used by us. In one kind, the auxiliary-field turns are in series with the rails. The net effect of this arrangement is to increase the effective inductance per unit length[4]. Experiments using a series auxiliary-field gave an arc-front velocity of 4 km/sec. The same gun using no auxiliary-field gave 2.3 km/sec.

A projectile gun based on this principle was built (See Figure 23) and gave an immeasurably low velocity. On the conjecture that this was due to increased ohmic skin heating (See Section I., B.2), a gun with independent auxiliary-field turns (See Figure 24) and a separate condenser-bank-transformer system was built (See Appendices C, D and E). The results were that, with the auxiliary-field, the gun gave 4.3 km/sec and, without, 4.5 km/sec. This is understandable under the considerations of Section II.C.2, in which, after a critical current, or, in the case, a critical magnetic pressure has been reached, the velocity decreases.

Two experiments were performed in which the auxiliary-field was reversed to oppose the field due to the rails. The result was, in both cases, very low velocities, less than 0.4 km/sec. Both projectiles were recovered hardly damaged. The important conclusion to be drawn from this is that the exploding foil effect is relatively unimportant in accelerating the projectile compared to the Lorentz force.

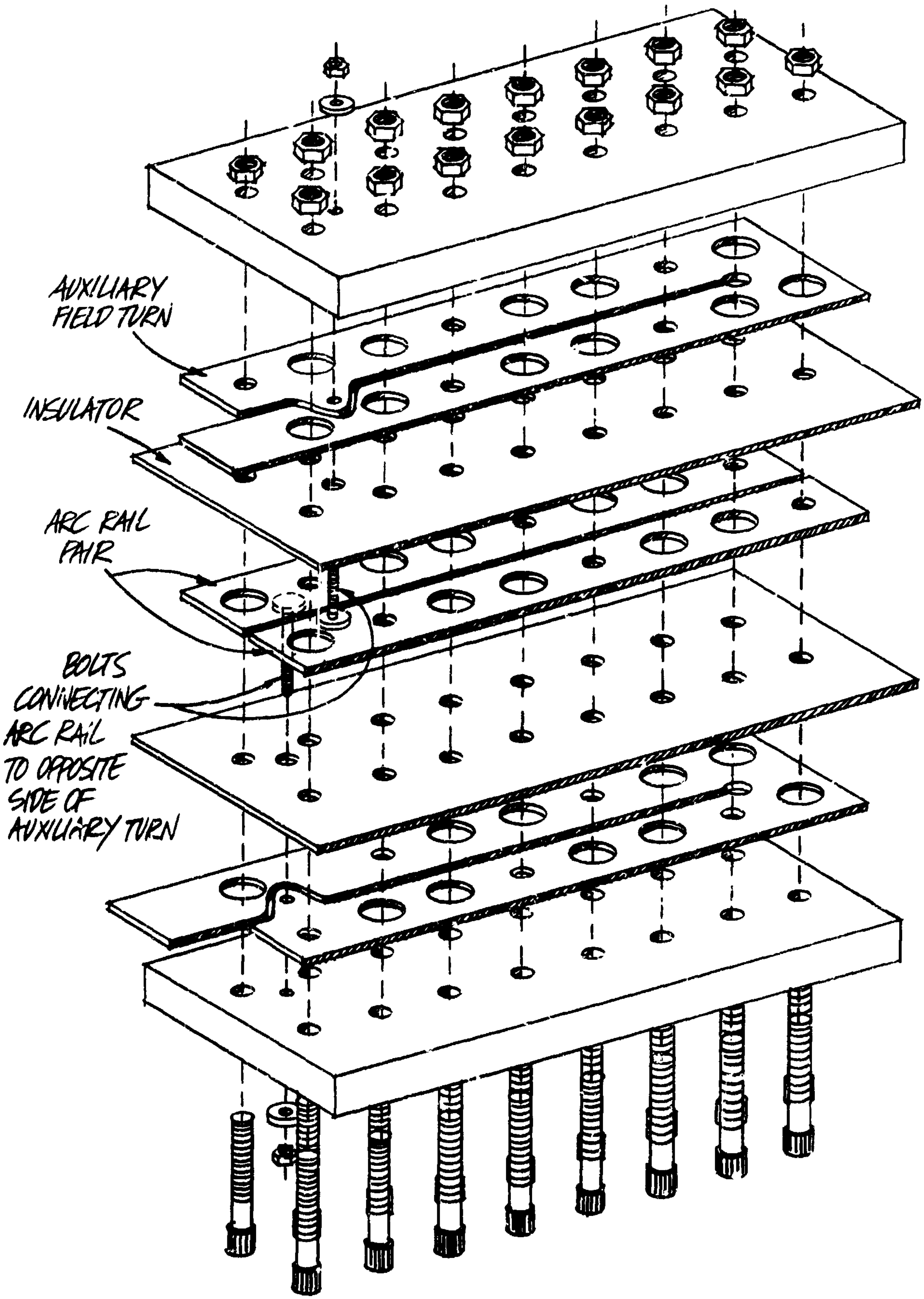

Figure 23. Exploded View of Series Type Auxiliary Field Gun

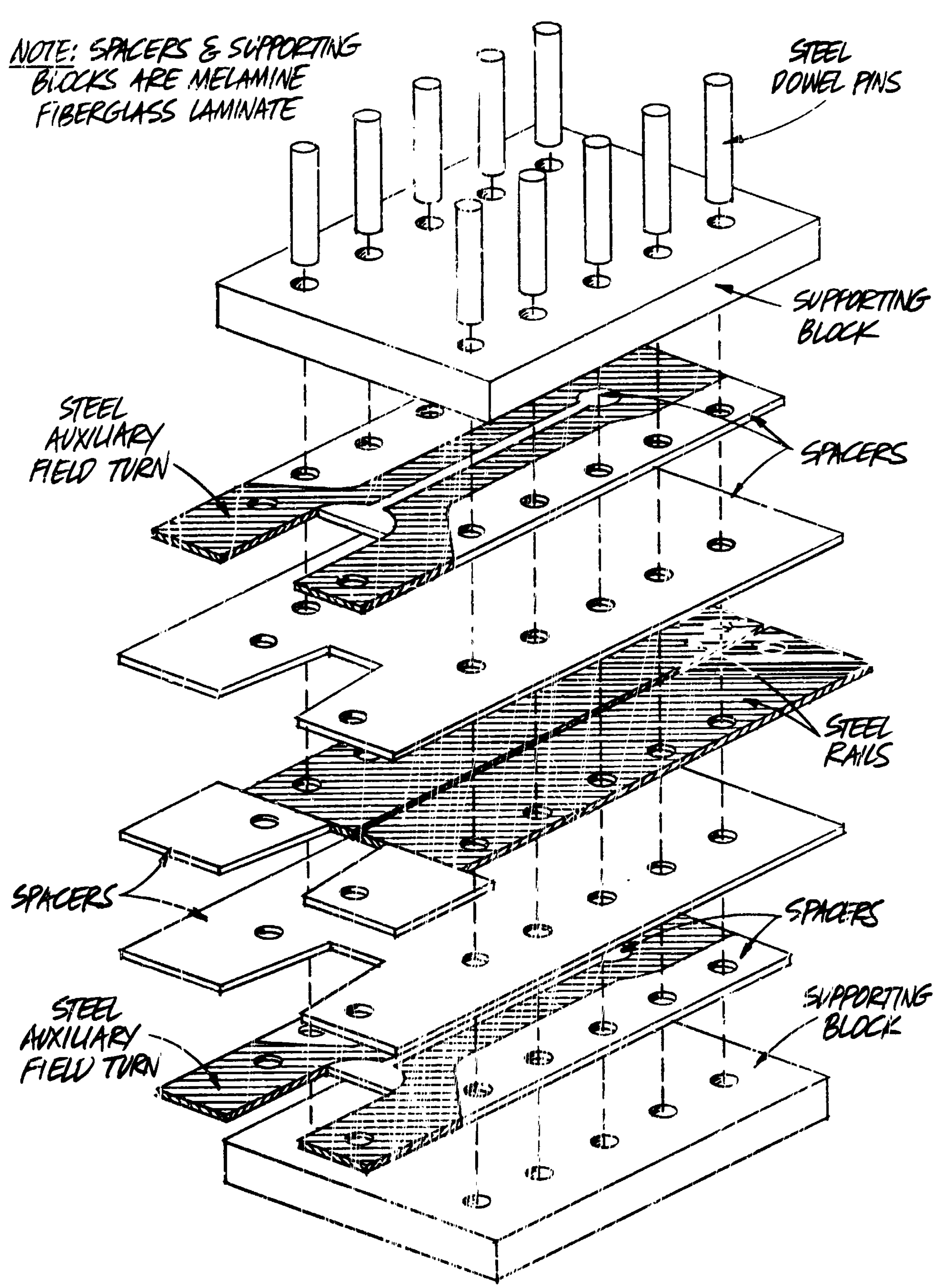

Figure 24. Exploded View of the Rail-Gun with Separate Auxiliary-Field Turns

51

III. THE DRAG APPROACH

The drag approach assumes that the diameter of the projectile is smaller than the bore of the rail gun. The projectile is accelerated by the drag force of the plasma. This approach does not have the velocity limitations found in other approaches, although it is inefficient from an energy standpoint.

A. MODEL OF THE ARC IN A RAIL GUN AT VERY HIGH CURRENTS

Most of the reported work on plasma rail guns uses relatively low density plasma ($<<1$ milligram/cc). For the purpose of accelerating a projectile; a high density (>1 milligram/cc), high velocity plasma is desirable. This can be achieved with small rail spacings and high current densities.

The theoretical results discussed in Section II. B. gave the arc velocity as proportional to the peak current in the gun. This result was based upon the assumption that the skin friction was negligible. However, it has been found that as the peak current is increased a point is reached where the arc velocity no longer increases as rapidly. Including the skin friction in the equation for the arc velocity gives an equation which more nearly explains the experimental data. The equation for the arc in a rail gun becomes

$$\frac{d}{dt}(mv) + \frac{2C_f}{D}(mv^2) = F$$

where

m is the mass of the arc

D is the diameter of the channel

C_f is the skin friction coefficient

F is the force on the arc = $1/2\ L'\ I^2$ where L' is the rate of change of inductance with unit length

We will assume the velocity is essentially constant particularly in the region of peak current, i.e., where

$$\frac{2 C_f m}{D} v^2 + \dot{m} v - F = 0$$

$$\dot{m} = m' I \qquad m = m' Q$$

$$\frac{2 C_f m' Q}{D} v^2 + m' I v - \frac{1}{2} L' I^2 = 0$$

Let $\frac{DI}{2 C_f Q} = \alpha$ and $\frac{1}{4} \frac{L' D I^2}{m' C_f Q} = \beta$

$$v = \frac{1}{2} (-\alpha \pm \sqrt{\alpha^2 + 4\beta}$$

$$= \frac{1}{2} \alpha (-1 \pm \sqrt{1 + 4\beta/\alpha^2})$$

$$= \frac{DI}{4 C_f Q} (-1 \pm \sqrt{1 + \frac{4 L' Q C}{m' D}}$$

For $t = \frac{\pi}{2}$

$$Q = I_p \int_0^{\pi/2} \sin \omega t \, dt = \frac{I_p}{\omega}$$

so

$$v = \frac{D\omega}{4 C_f} \left[\sqrt{1 + \frac{4 L' I_p C_f}{m' D \omega}} - 1 \right]$$

Assuming the following

$$L' = 0.3\ \mu h/m$$

$$I_p/\omega = 5 \times 10^5 \text{ amps} \times \frac{20\mu \text{sec}}{\pi} = 3.2 \text{ coulombs}$$

$$m' = 6 \text{ atoms}/e \times \frac{e}{1.6 \times 10^{-19} \text{ coul}} \times \frac{0.0635 \text{ Kg/mole}}{6 \times 10^{23} \text{ atom/m}}$$

$$= 4 \times 10^{-6} \text{ Kg/coul.}$$

$$C_f = 0.0044 \quad \text{ie} \quad C_f = \frac{0.074}{Re^{1/5}} \text{ and } Re = 10^7$$

Then

$$\frac{4L' \frac{I_p}{\omega} C_f}{m'D} = \frac{4 \times 0.3\ \mu h/m \times 3.2 \text{ coul} \times 0.0044}{4 \text{ Kg/coul} \times 0.0063}$$

$$= 0.75$$

$$\frac{D\omega}{4C_f} = \frac{0.0063}{4 \times 0.0044} \times \frac{\pi}{20} = 56 \text{ Km/sec}$$

$$V = (\sqrt{1.75} - 1)\, 56 = 18 \text{ Km/sec.}$$

For 1/8 inch channel the result is 16 km/sec and for the 1/16 inch channel the velocity is 14 km/sec. The velocity would increase approximately as the square root of the peak current for large currents. The arc velocity according to this equation increases inversely as the square root of the rise time, thus short rise times are desirable, from the standpoint of arc velocity although the density of the plasma is lower under these conditions.

B. UNIFORM DENSITY - UNIFORM VELOCITY PLASMA STREAM

The equation for the drag on a projectile is given by

$$\frac{dV}{dt} = \frac{C_D \rho A}{2 g m} \left(V_{pl} - V \right)^2$$

where

C_D	=	the drag coefficient $\sim$ 0.9 for a sphere at Mach 7
ρ	=	density of the stream of gas or plasma
A	=	the projected area of the projectile
V_{pl}	=	velocity of the plasma
V	=	velocity of the projectile

The solution of the above equation for a uniform density uniform velocity plasma stream is

$$V = V_o \left[1 - \exp\left(- \frac{x}{\ell} - \frac{V}{V_o - V} \right) \right]$$

where x is the distance the projectile moves in the gun and

$$\ell = \frac{2\, m_{proj}}{C_D \rho_{pl} A} \quad \text{or} \quad \frac{8}{3} \frac{\rho_B\, r}{\rho_{pl}\, C_D}$$

This curve is plotted as Figure 25.

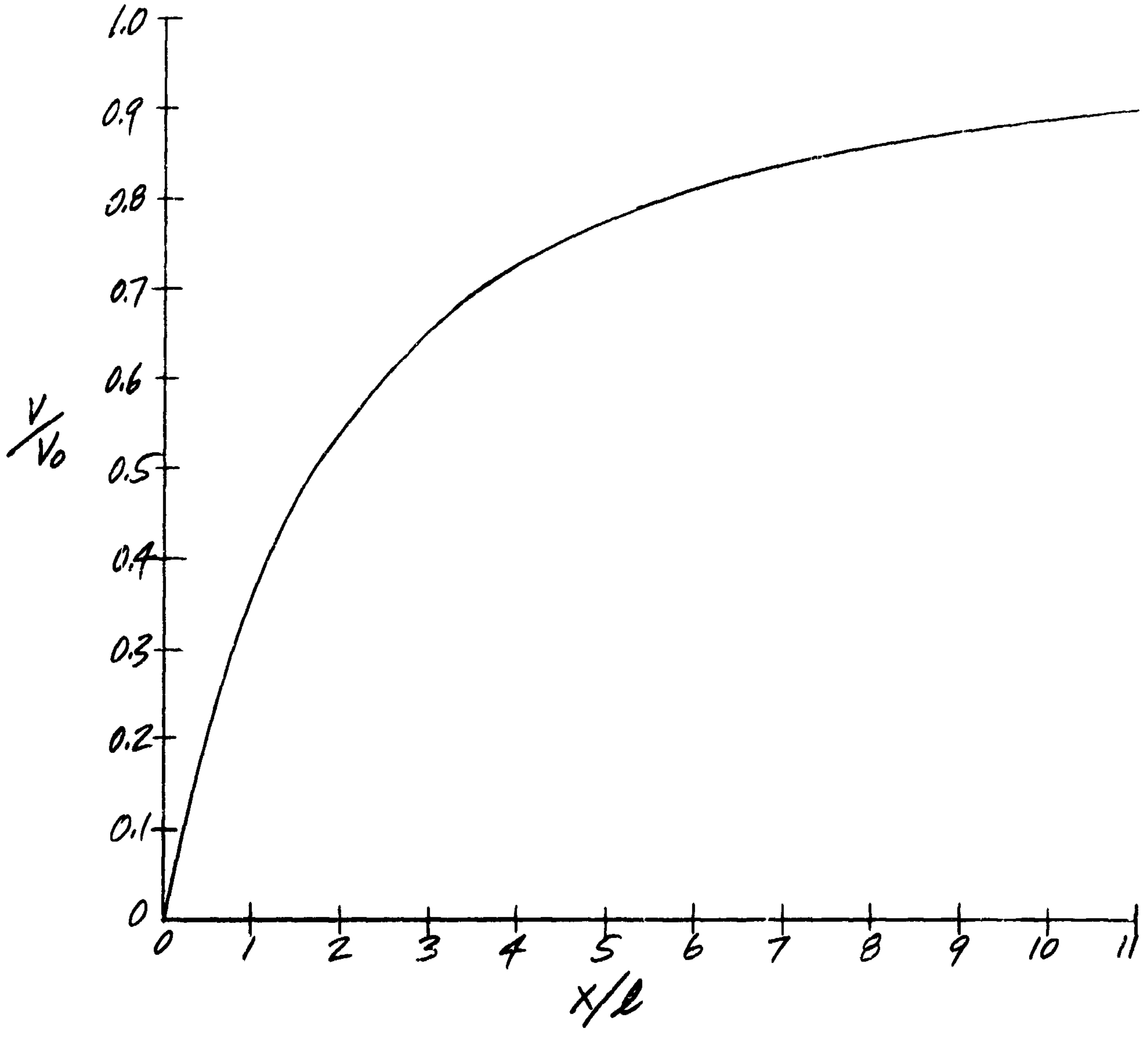

V = pellet velocity
V_o = plasma velocity
$\ell = \frac{2\,m}{C_D \rho A}$
X = distance the projectile moves in the gun

Figure 25. Pellet Velocity as a Function of Relaxation Lengths in the Gun

A typical example would be for a 10 mil diameter nylon projectile with a average plasma density of 2 mg/cm^3

$$\ell = \frac{8}{3} \frac{\rho_B}{\rho_{Pl}} \frac{\Omega}{C_D}$$

$$= \frac{8}{3 \times 0.9} \times \frac{1.1 \times 1/2 \times 10^{-2} \text{ inches}}{2 \times 10^{-3}} = 8.1 \text{ inches}$$

With a 1/4 inch square cross section channel at 20 km/sec the total mass ejected in 30 μsec is

$$= 2 \times 1 \text{ mg/cc} \times (2.54/4)^2 \times 20{,}000 \times 30\,\mu\text{sec}$$

$$= 0.5 \text{ milligrams}$$

The actual quantity of material ejected appears to be about 50 times this. The initial density of the first plasma to emerge from the gun is probably about the above value. The density would be expected to increase and velocity decrease with time. By using a nozzle on the end of the gun the pellet would see more nearly constant density and constant velocity along its path in the gun. This is because as the pellet moves into the nozzle section, a later more dense part of the plasma column would have reached the nozzle and would expand and increase in velocity.

C. DISPERSION MEASUREMENTS

Several of the two stage experiments resulted in no projectile emerging from the second stage so measurements of the dispersion of the projectile on the target were made under a number of different conditions. This data is shown as Table 2. Use of the dispersion concept assumes the distribution about the point of aim is a circular normal distribution. The data obtained is insufficient to give a accurate measurement of dispersion but it does indicate that the dispersion is about 150 milliradians. It would appear that the smaller the initial loading of foil the lower the dispersion.

Dispersion is probably not a highly accurate way of looking at the probability of a projectile emerging from a long channel without striking the walls. However, it should give a first approximation to the results if it is recognized that the value used for the dispersion is somewhat sensitive to the length of the channel, the velocity and density of the plasma, etc. The probability of a projectile emerging from the channel becomes

$$P = 1 - \exp -\left[\frac{N}{2\sigma^2}\left(\frac{\Omega}{L}\right)^2\right]$$

where

σ	is the dispersion
r	is the radius of the channel
L	is the length of the channel
N	is the number of projectiles

For a 90% probability

$$\frac{N}{2\sigma^2}\left(\frac{r}{L}\right)^2 = 2.3$$

For 1/8 inch radius channel and 150 milliradians dispersion

$$N = 2.3 \times 2 \times 0.15^2 \times 4 \left(\frac{L}{D}\right)^2$$

$$= 0.41 \left(\frac{L}{D}\right)^2$$

Thus for a L/D of 20 (1/4 inch diameter channel 5 inches long) about 160 projectiles would be required for a 90% probability of one emerging.

To use a single pellet, a taper in the channel of 150 milliradians ($\sim 8°$) would be required to give a reasonable probability of one pellet emerging.

D. ABLATION OF THE PROJECTILE

The ablation problem is very similar to the reentry heating problem. The technique used for calculating the thickness ablated is to estimate the heating rate and make a heat balance, or

$$q \Delta t = h_A \rho_m x$$

where

t	=	length of time the projectile is in the stream
x	=	thickness ablated
h_A	=	effective heat of ablation
q	=	heating rate
ρ_m	=	material density

One of the equations commonly used for convective heat flux at the stagnation point is

$$q_0 = 865 \left(\frac{V}{10^4}\right)^{3.15} \sqrt{\frac{\rho}{\rho_a}} \sqrt{\frac{1}{R}}$$

(See Reference (13))

where

v	=	velocity ft/sec
ρ	=	density
ρ_a	=	atmospheric density
R	=	radius, ft

Assuming a 5 mil radius particle, atmospheric density, and 10 km/sec relative velocity between the stream and particle, $q_o = 1.8 \times 10^6$ Btu/ft^{2}sec. The heat transfer along the side of the body is given from

$$\text{Stanton \#} = \frac{q}{\rho V h} = \frac{1}{P_r^{2/3}} \frac{C_f}{2}$$

where

ρ	=	density
h	=	$\frac{v^2}{2g}$
C_f	$\cong$	0.003
$P_r^{2/3}$	$\cong$	1

or

$$q = 3700 \left(\frac{v^3}{10^4}\right)$$

which is about 1/10 the above result. There is almost no heat transfer to the rear surface of the pellet. The pellet will tumble in the stream, so all surfaces would be ablated similarly, although corners would ablate first. On the basis of the above

Table 2

DISPERSION MEASUREMENTS
Distance Measured From Muzzle

Test	Bail Position	Gun	Foil Weight	Foil Position	Crater Position x mm	Crater Position y mm	Crater Plate Distance	Velocity (km/sec)	Remarks
A-1	7 cm	19 cm 1/4"	20 mg	19 cm					No crater
A-2	2 cm	"	20 mg		+7	-1	10 cm	3.7	Crater measurement
A-3	4 cm	"	20 mg						No crater
A-4	0 cm	"	20 mg						No crater
A-5	2 cm	"	20 mg						No crater
A-6	1 cm	"	20 mg		+1	+14	20 cm	1.4	
A-7	1.5 cm	"	20 mg		+16	-37	20 cm	1.4	
A-8	1.5 cm	"	100 mg		-20	+28	20 cm	1.4	
B-1	2 cm	12 cm 1/4"	20 mg						Ball broke up
B-2	1.5 cm	"	20 mg						Ball broke up
B-3	1.5 cm	"	10 mg		-24	-6	20 cm	1.6	
B-4	2 cm	"	5 mg		+27	+8	20 cm	~2	
B-5	3 cm	"	2.3 mg		-30	-16	20 cm	1.6	
B-6	1.5 cm	"	3 mg	12 cm	-28	+22	20 cm	1.1	Nylon backed foam sabot
C-1	1.5 cm	12 cm 1/4" 5 cm after-section	5 mg	12 cm	15	3	20 cm	1.7	
C-2	3 cm	"	5 mg	12 cm	-38	+27	20 cm	1.7	
C-3	5 cm	"	5 mg	12 cm					No impact on plate
C-4	5 cm	"	5 mg	12 cm	+18	0	20 cm	1.5	Very small impact
C-5	5 cm	"	5 mg	12 cm	-13	-18	20 cm	1.16	
C-6	5 cm	"	5 mg	12 cm	-4	-4	20 cm	1.2	Nylon backed foam sabot - Backing broke
C-7	5 cm	"	5 mg	5 cm			20 cm	1.2	Broke up
C-8	5 cm	"	5 mg	5 cm			20 cm	1.6	Broke up

arguments, the average heating will be assumed to be 20% of the stagnation point heating rate.

The effect of the high temperature of the plasma stream can be neglected in the calculation of convective heat transfer to the projectile since the kinetic energy of the stream is high compared to the thermal energy (assuming the thermal temperature is 5 ev), i.e.,

$$\frac{v^2}{2g} = \frac{(10 \times 3.3 \times 10^3)^2}{2 \times 32.2 \times 778} = 21{,}000 \text{ Btu/\#}$$

$$E_{th} = \frac{5 \text{ ev} \times 1.6 \times 10^{-12} \times 6.02 \times 10^{23} \times 453.6 \text{ g/lb}}{63 \text{ g/mole} \times 10^7 \times 1054 \text{ joules/Btu}} = 3{,}200 \text{ Btu/\#}$$

The effective heat of ablation is dependent upon the enthalpy of the stream. For these heat rates an estimate of 5000 Btu/lb has been used.

The ablation is found from the heat balance

$$x = \frac{q \Delta t}{h \rho} = \frac{0.2 \times 1.8 \times 10^6 \times 20 \times 10^{-6} \times 12 \text{ inches/ft}}{5000 \text{ Btu/lb} \times 1.2 \times 62.4 \text{ lb/ft}^3}$$

$$= 0.23 \text{ mil}$$

The stagnation point radiative heat transfer, if the plasma is assumed to be similar to air, is negligible -- just as it is in the earth reentry case. This is because of the low emissivities. The equation shown below assumes atmospheric density

$$\frac{q_{rad}}{R} = 100 \left(\frac{v}{10^4}\right)^{8.5}$$

$$= 100 \left(\frac{3.3 \times 10^4}{10^4}\right)^{8.5}$$

$$= 100 \times 21{,}000 \times 0.0004 \text{ ft}$$

$$= 840 \text{ Btu/ft}^2 \text{ sec}$$

From these calculations the ablation loss would appear to be negligible for 10 mil diameter projectiles with an average relative velocity of 10 km/sec. With densities greater than atmospheric, and with relative velocites of 20 km/sec, an ablation loss of as much a 1 mil could be expected.

E. EXPERIMENTAL RESULTS

Table 3 shows the experimental results obtained using the experimental configuration shown in Figure 26. The time of flight is measured by the time at which an 8 mil aluminum sheet is perforated by the pellet. It is necessary to correct the time of flight by the length of time it takes the arc to reach the pellet and for the fact that the pellet does not immediately reach full velocity. Two velocities are quoted for each of the experiments. One velocity is calculated on the following basis

$$V_{av} = \frac{\text{Distance from pellet to impact plate}}{\text{time of impact} - 9\ \mu\text{sec}}$$

The nine microsecond correction allows fo the time for the arc to reach the pellet. Thus this velocity is in reality the average velocity of the pellet over its total path length. This should be corrected for the time required to accelerate the pellet to velocity. The second velocity shown corrects for the time to accelerate to full velocity by assuming that the average velocity over the gun length is 2/3 of the final velocity. Thus

$$V = \frac{\text{Distance from pellet to impact plate}}{\text{time of impact} - 9\ \mu\text{sec} - \left[\frac{\ell}{\frac{2}{3}V} - \frac{\ell}{V}\right]} \quad \text{where } \ell = \text{gun length}$$

$$= \frac{\text{Distance from pellet to impact plate} + 0.5\ell}{t - 9}$$

The relatively small increase in velocity which resulted when the peak current was increased is expected because the rise time also increased and the plasma velocity should be proportional to $\sqrt{\frac{I_p}{t_r}}$. The increase that did result is due to the increased plasma density.

These measurements were made with nylon particles which varied between 0.004 and 0.010 inch in diameter. Inspection under a optical comparator showed few particles outside this size range. The gun which was used is shown as Figure 27

F. IMPROVED DESIGN

Figure 28 and Table 4 show the characteristics of an improved design which should give an improved velocity. The ratio of $\sqrt{\frac{I_p}{t_r}}$ has been increased by 40%. In addition the increase in I_p should double the density of the plasma. The increase in average density will increase the value of x/λ (gun length/relaxation length) by a factor of 2. The combination of increased plasma density and velocity should give a velocity of 20 km/sec for a 7 mil diameter cylinder and 15 km/sec for a 15 mil diameter cylinder.

Table 3

RESULTS WITH DRAG TEST

Test No.	Current (Megamps)	Rise Time (μsec)	Foil Weight (mg)	Sabot & Pellet Weight (mg)	Sabot* Position (cm)	Foil* Position (cm)	** V_{av} (km/sec)	Pellet Velocity (km/sec)
3.23-1	0.52	20	50	20	3	6	3.7	3.9
3.24-1	0.52	20	20	18	4	14	6.4	6.9
3.24-2	0.52	20	10	29	6	14	7.2	8.0
3.25-2	0.52	20	10	28	8	14	4.8	5.3
3.25-3	0.52	20	20	20	6	14	8.0	8.8
3.25-4	0.52	20	50	23	6	14	7.2	8.0
3.27-1***	0.52	20	20	24	6	14	7.5	8.2
3.27-2***	0.52	20	20	14.5	6	14	8.5	9.4
3.27-3***	0.7	25	20	19	6	14	9.9	10.3

* Distances measured from muzzle end of rails

** Velocity computed as average over total flight path

*** Gun had 15 cm total nozzle length

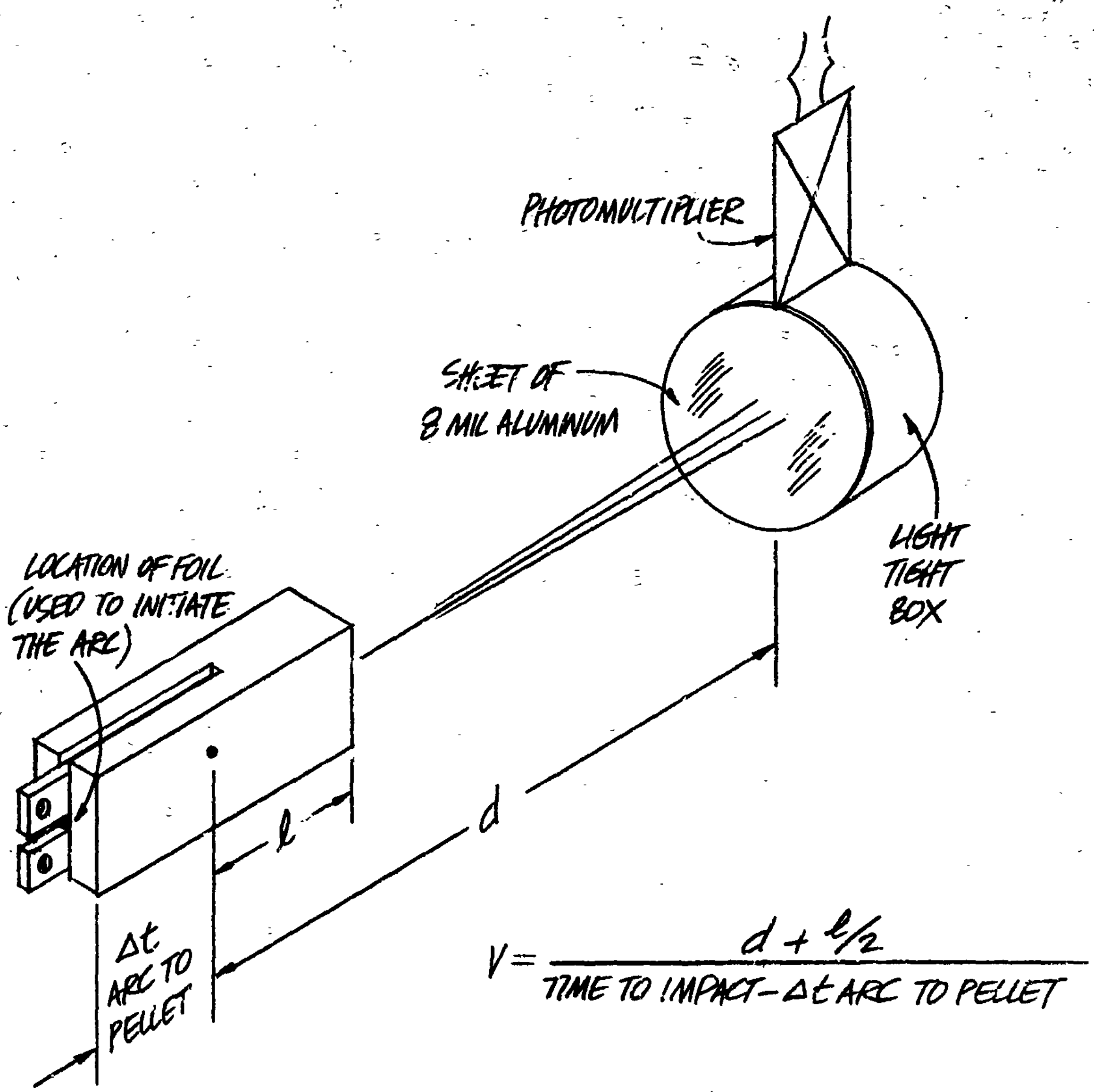

Figure 26. Experimental Configuration for Drag Tests

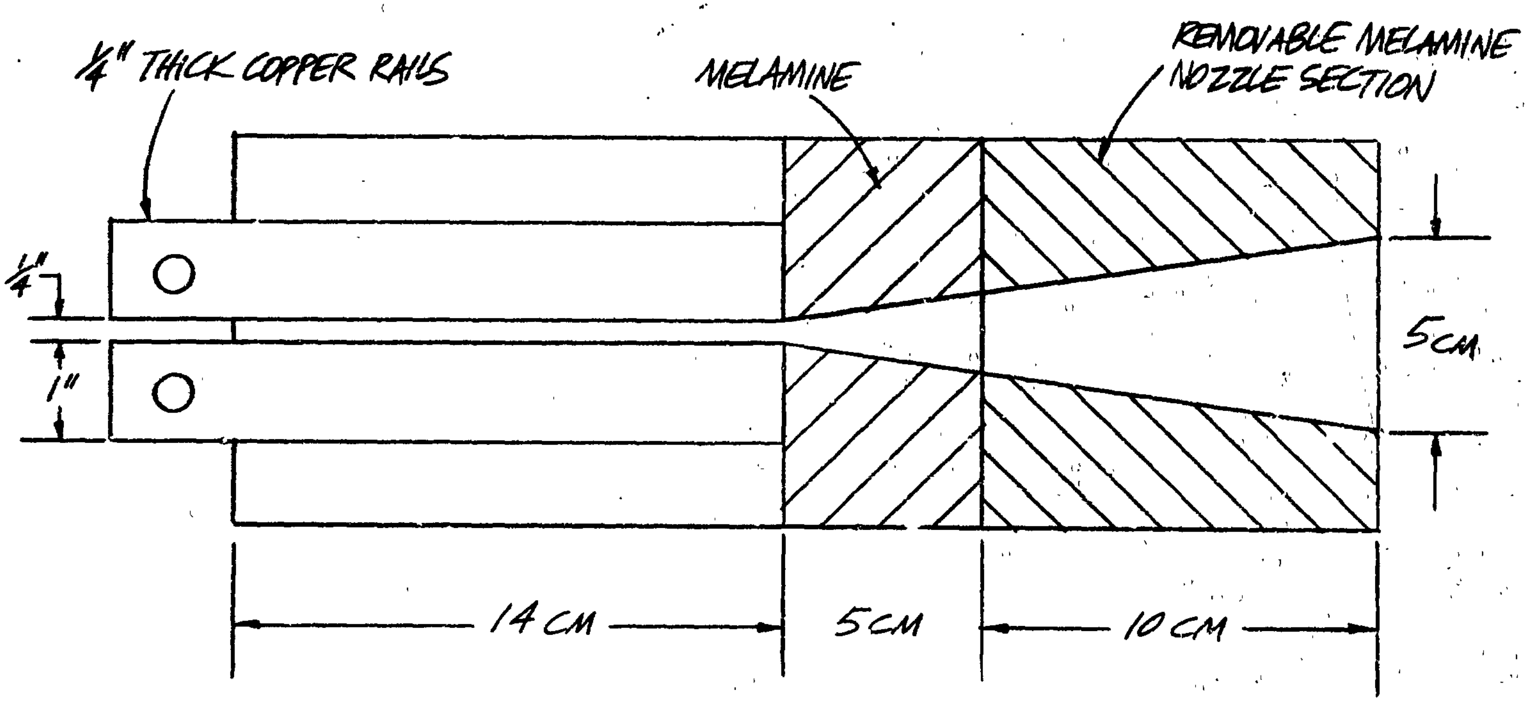

Figure 27. Standard Gun Used for Drag Experiments

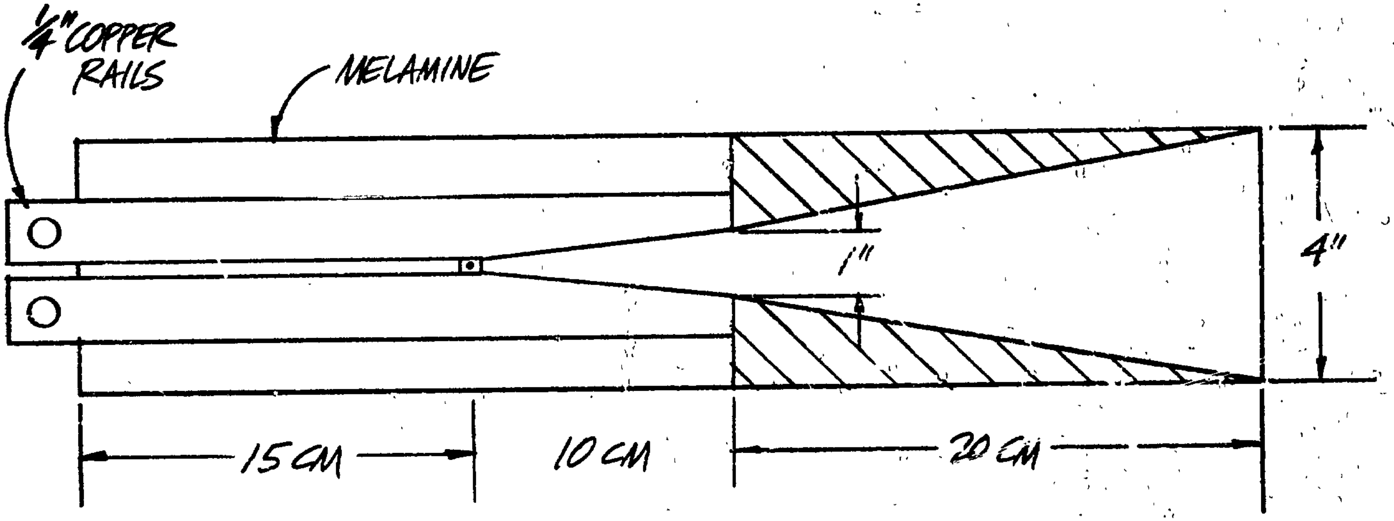

Figure 28. Improved Gun Design

Table 4

PROPOSED DESIGN CHARACTERISTICS

	Test 3/27/2	Test 3/27/3	Design A
Rail Spacing (inches)	0.25	0.25	0.25
Energy of Bank (kj)	25	53	100
Current (Megamps)	0.52	0.7	1.5
Rise Time (μsec)	20	25	30
Plasma Velocity (km/sec)	20	20	30
Gun Length (cm)	22	22	30
Velocity (km/sec)	9.4	10.3	20
V/V_p	0.45	0.5	.7
x/ℓ	1.5	1.7	3.5
Average Plasma Density (mg/cc)	1.7	2	4
$\frac{1}{2} m_p V_p^2 = \rho \frac{AV^3}{2} \Delta t$ (assuming A = 1 in x 1 in)	1.7	2.5	17
Velocity with 15 mils diameter projectile			
x/ℓ			1.7
V/V_o			0.5
V km/sec			15

IV. REFERENCES

1. J. Marshall, Phys. Fluids 3, (1960)

2. P. J. Hart, Phys. Fluids 5, 38 (1962)

3. W.W. Salisbury, Proc. of Ist Symp. on Hypervelocity Impact

4. K.W. Miller and R.M. Bergslien, Proc. 2nd Hypervelocity and Impact Effects Symp., Vol. 1, USNRL, Washington (1957) p. 127

5. C. Mannal and Y.A. Yoler, Proc. 2nd Hypervelocity and Impact Effects Symp., p. 169

6. D.L. Wennersten, Proc. 3rd Symp. on Hypervelocity Impact, Vol. 1, US Army, Chicago (1958) p. 475

7. R.L. Chapman, D.E. Harms, and G.P. Sorenson, Proc. 6th Symp. on Hypervelocity Impact, Vol. 1, US Army, Cleveland (1963) p. 317

8. J.J. Baruch, etal., High Velocity Electric Accelerator Systems, WADD 60-468, USAF (1960)

9. L. Leibing, Phys. Fluids 6, 1035 (1963)

10. "Sputtering Yield Data in the 100 - 600 ev Energy Range", General Mills Report No. 2309, July 15, 1962, Minneapolis

11. G.K. Wehner, Advances in Electronics and Electron Physics, Vol. 7, Academic Press, New York (1955) pp. 292-296

12. K. Thom, J. Norwood, and N. Jalufka, Phys. Fluids 7, 567 (1964)

13. R.W. Detra and H. Hidalgo, "Generalized Heat Transfer Formulae and Graphs", AVCO Everett Research Laboratory, Everett, Mass., March 1960, AD 233702.

APPENDIX A

DIAGNOSTICS

1. Velocity Measurements

Figures A-1 and A-2 show the system used to measure the projectile velocity and to observe the motion of the arc. The puncturing of the two light tight boxes and the impact provide three independent measures of the velocity of the projectile. Figure A-3 is a set of typical traces from this system. Figure A-4 shows the construction of the mylar window assembly through which the projectile passes.

In the drag techniques of acceleration the entire gun assembly is placed within the vacuum tank and one photomultiplier is used to record the time of penetration of the 8 mil aluminum sheet which covers the light tight box. This was shown previously on Figure 26.

2. Magnetic Flux Loops

With the high currents achieved with the transformers built under this contract and the resulting high pressure along the barrel (See Section II.C.a), we found that flux loops of the old design placed between the expendable liner and the supporting blocks (See Figure B-1) were destroyed during the shot and had to be rebuilt for each shot. In order to avoid this problem, we designed and built the flux loop assembly shown in Figures A-5 and A-6. Its position in the gun is shown in Figure B-1.

The chief virtues of this device is that, except for the small regions occupied by the coils themselves, that part of the structure exposed to the pressure of the arc is of high impact melamine fiberglass laminate. Since the epoxy resin combines with the melamine, the structure has little tendency to delaminate. Repeated use of this device has shown only little more damage than solid pieces of melamine-fiberglass.

Figure A-7 shows a typical trace from one of these loops, the same signal integrated, and the trace of rail current for the same shot. The integrated trace represents total flux through the loop, and, since the arc is traveling with nearly constant velocity over the duration of the pulse, the integrated trace represents approximately the current distribution in the arc. The long overshoot following the spike in the integrated trace is probably due to a slight disorientation of the loop, which causes it to couple with the current in the rails. At a velocity of 5 km/sec a current distribution like the one shown has a length of about one centimeter.

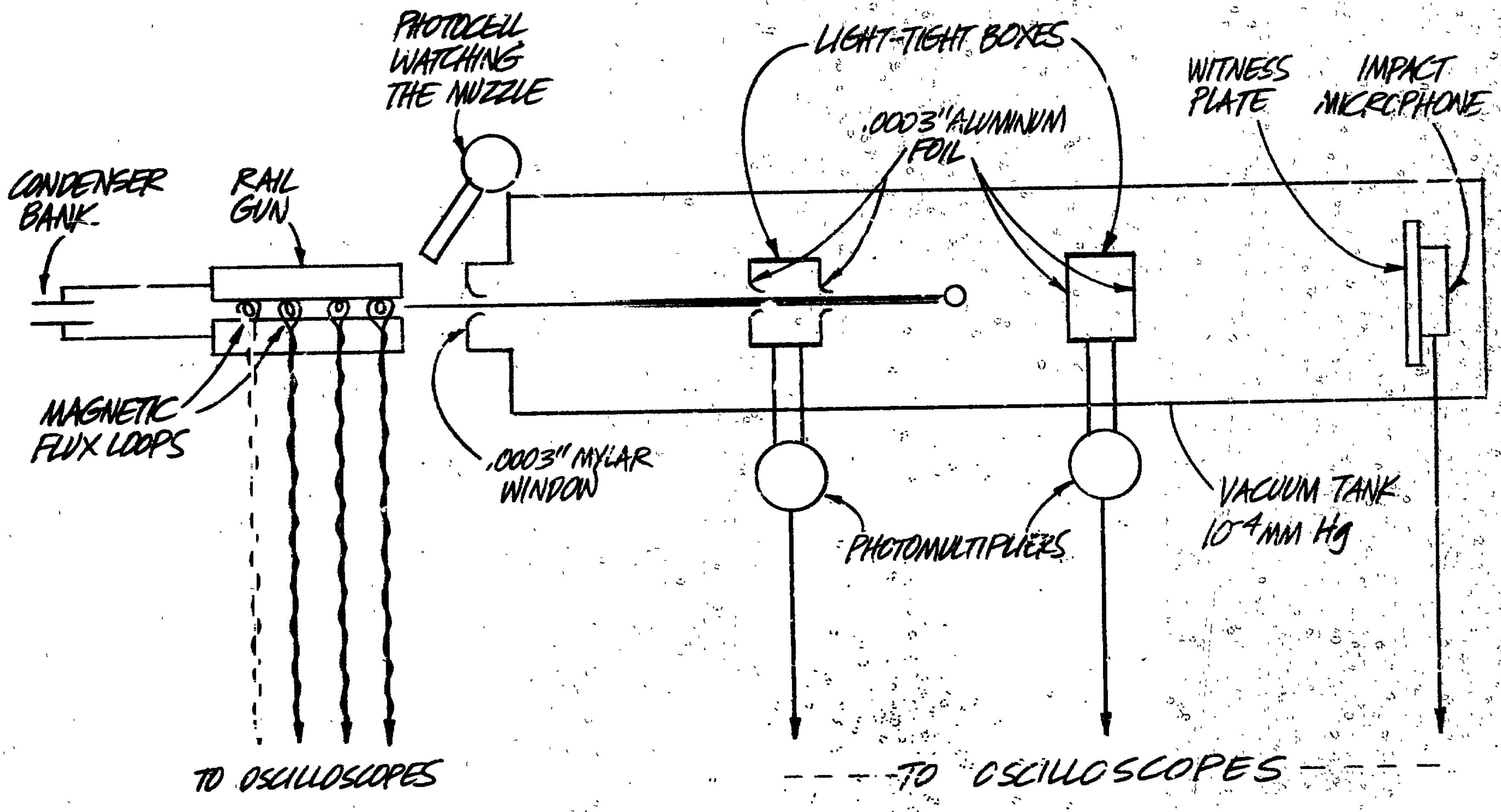

Figure A-1. Schematic of Diagnostics System

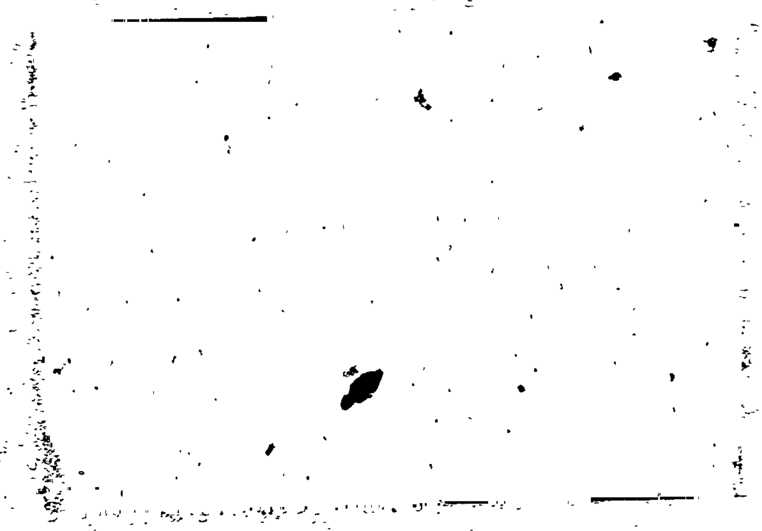

Figure A-2. Photograph of Diagnostics System

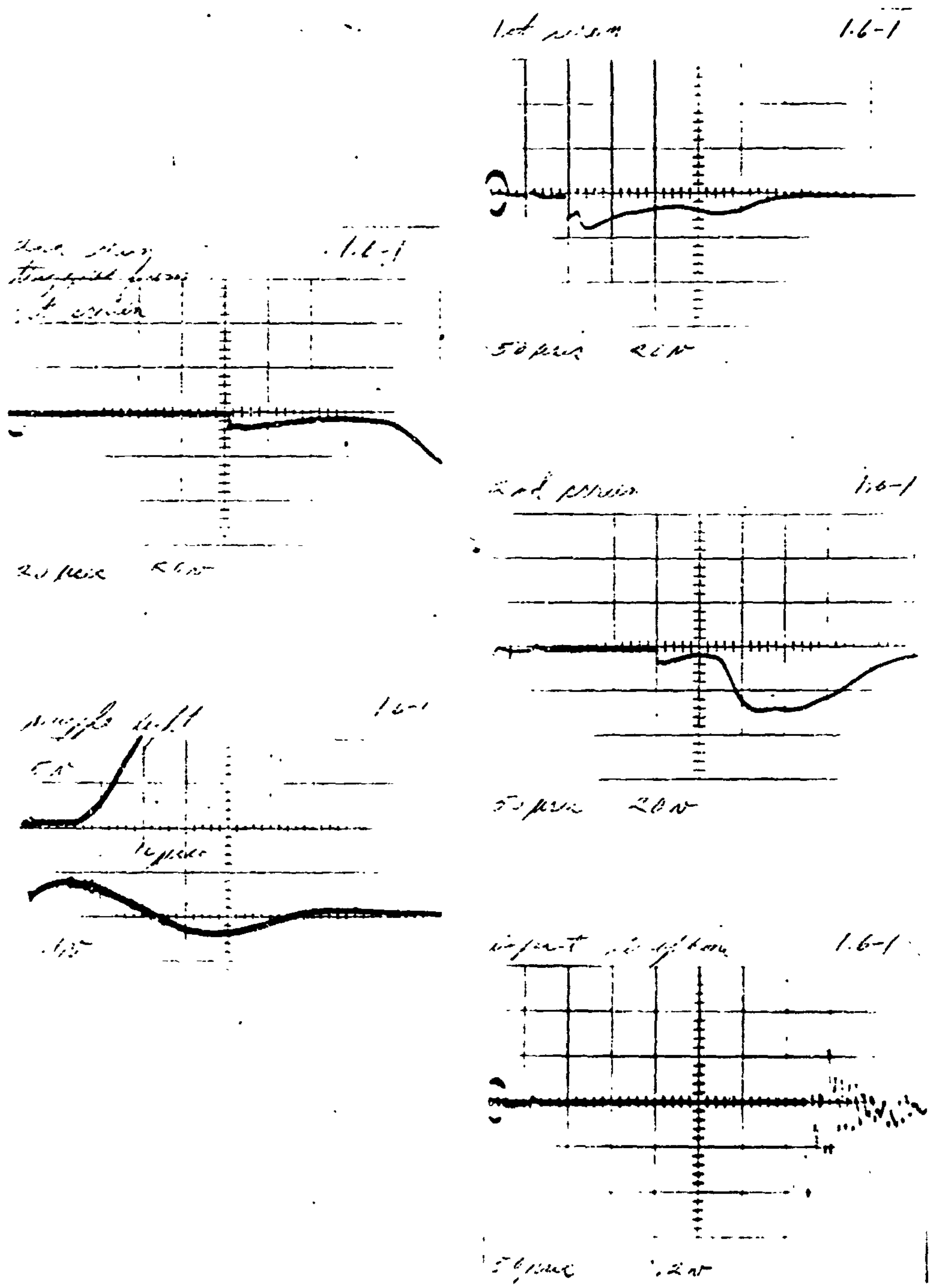

Figure A-3. Typical Velocity Data

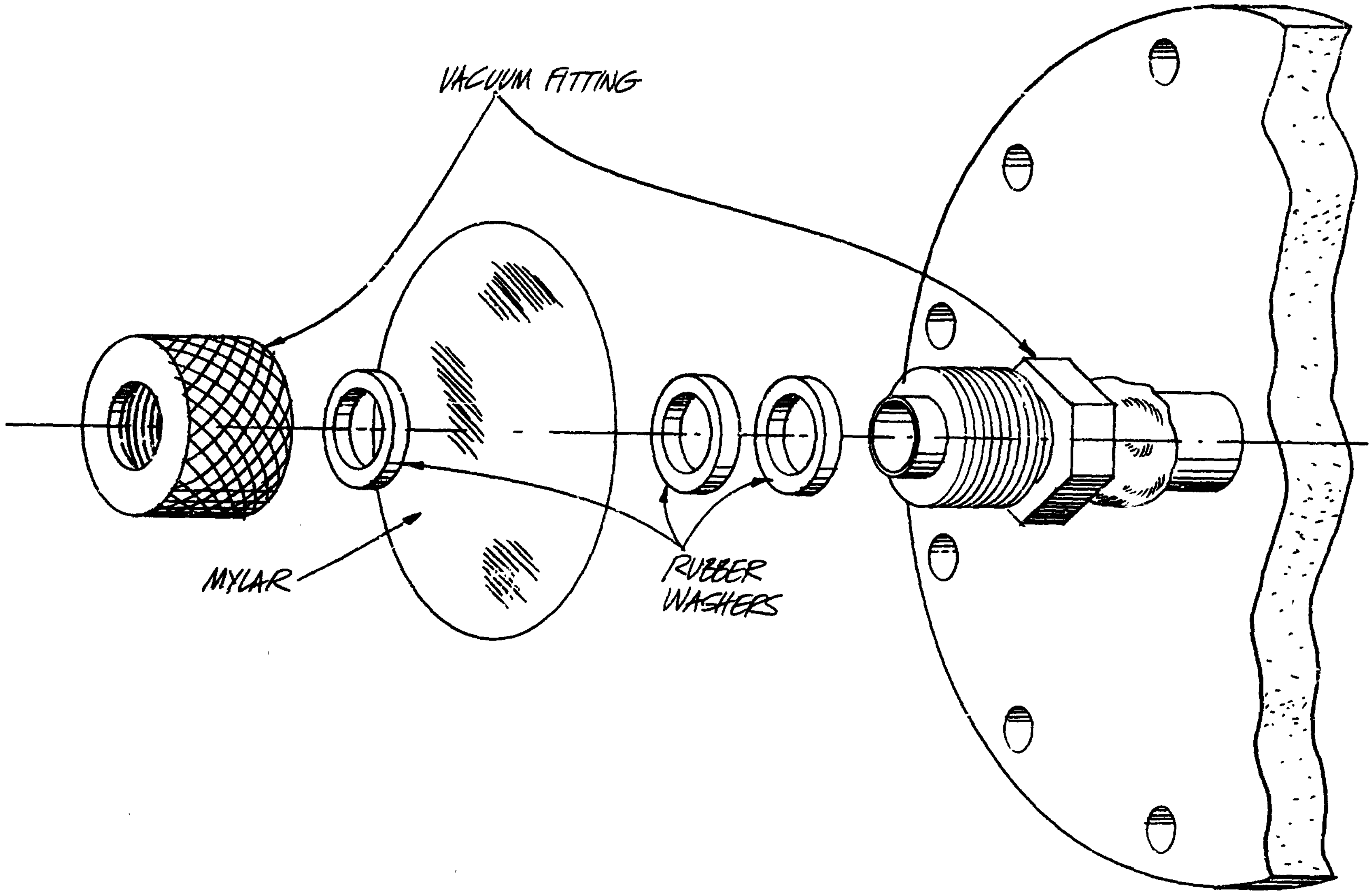

Figure A-4. Construction of Mylar Window

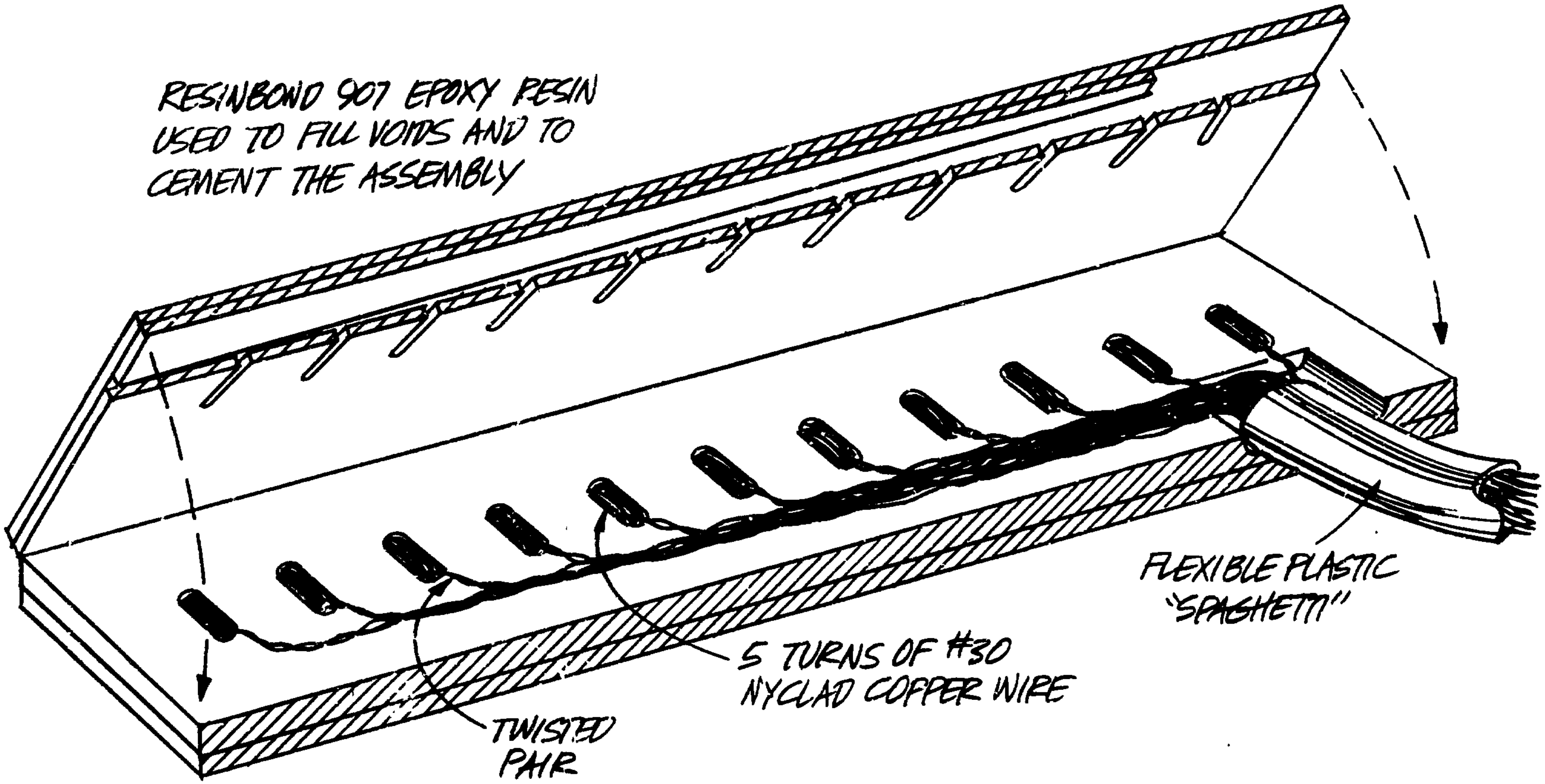

Figure A-6. Flux Loop Sandwich Before Cementing

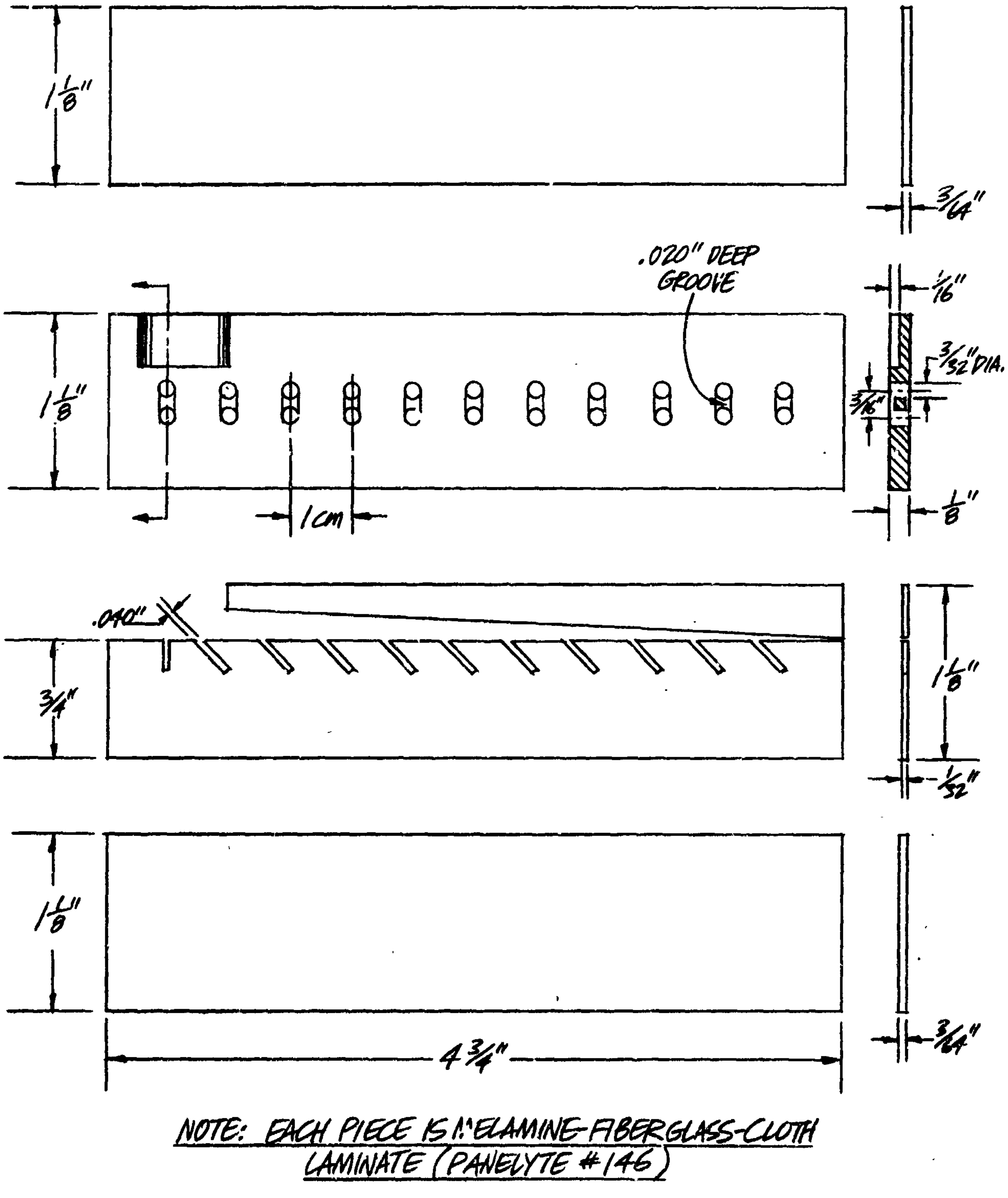

Figure A-6. Component Layers of the Flux Loop Sandwich

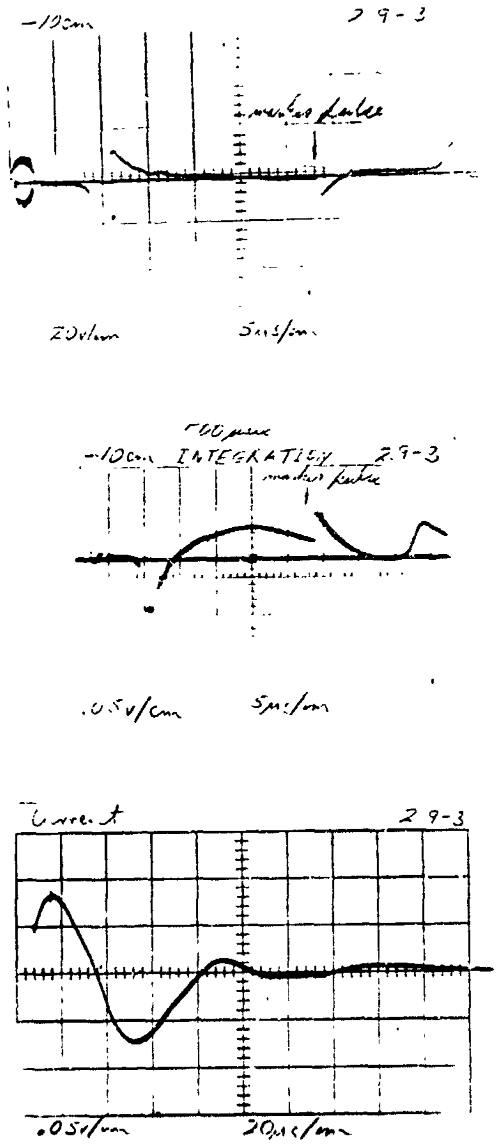

Figure A-7. Typical Flux Loop and Current Traces

APPENDIX B

DEMOUNTABLE GUN

Figures B-1 and B-2 show the construction details of the most recent and most successful demountable gun. This design enables one to use rail cores and insulators of any arbitrary material available in slabs, and rail sheaths of any malleable material available in thin sheets.

The melamine-fiberglass laminate (Panelyte #146) was chosen for the supporting blocks and clamps because of its hardness, density, and high impact strength. It was also chosen for the expendable insulating lining because of its resistance to erosion by the arc (See Section II.F.3).

The epoxy resin used to cement the barrel assembly actually combines with the melamine as well as bonds with the rail sheath to give additional strength in the plane of the rails. By using a mandrel of the appropriate cross section, either a square or a circular barrel can be fabricated with the epoxy.

The reason for not using steel for the clamp is that, for times of the order of 20 μsec, magnetic fields due to eddy currents in the clamp would tend to cancel the fields due to the rail current. This was also the reason for placing the large bolts of the clamp far from the rails.

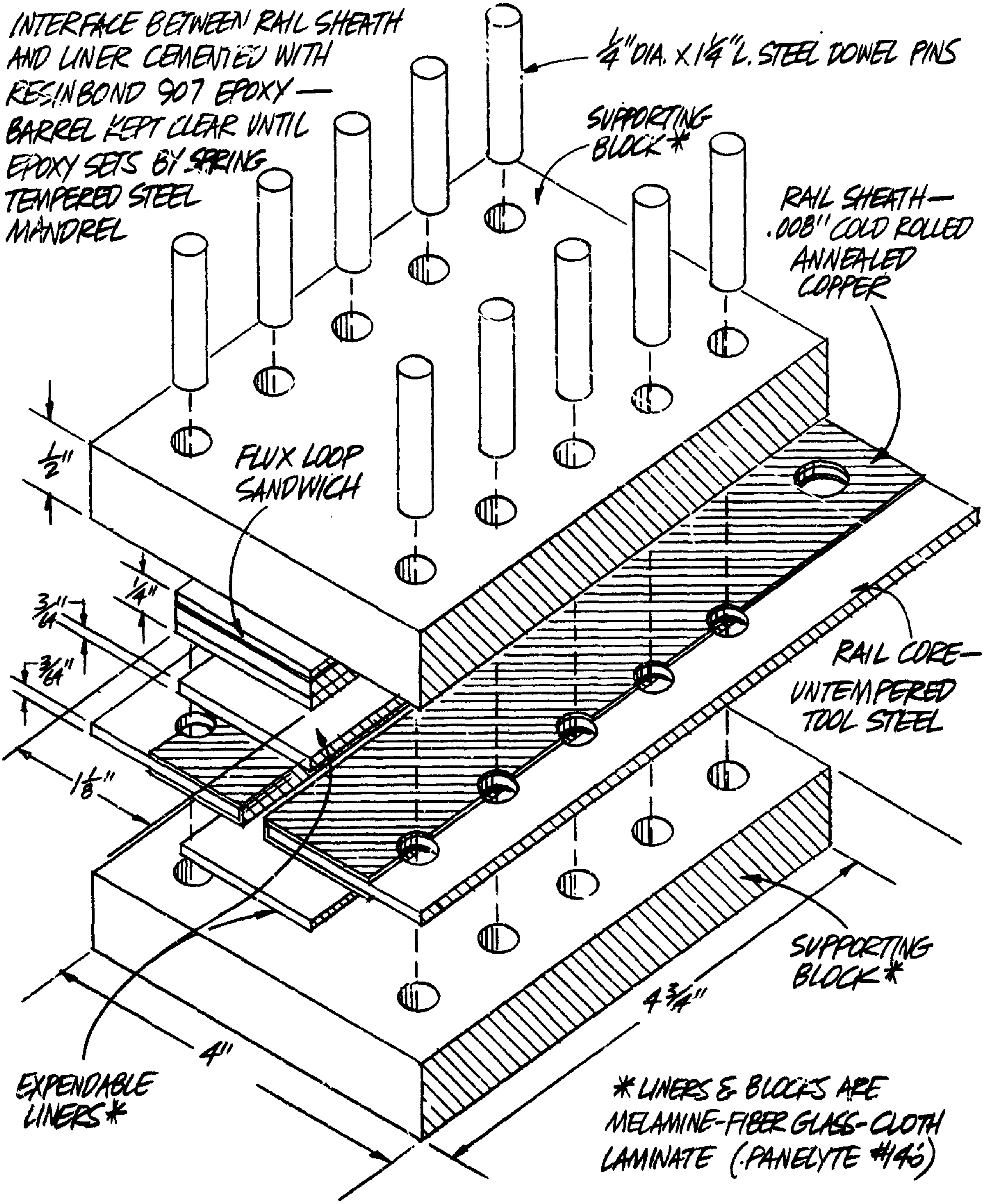

Figure B-1. Exploded View of Demountable Rail Gun

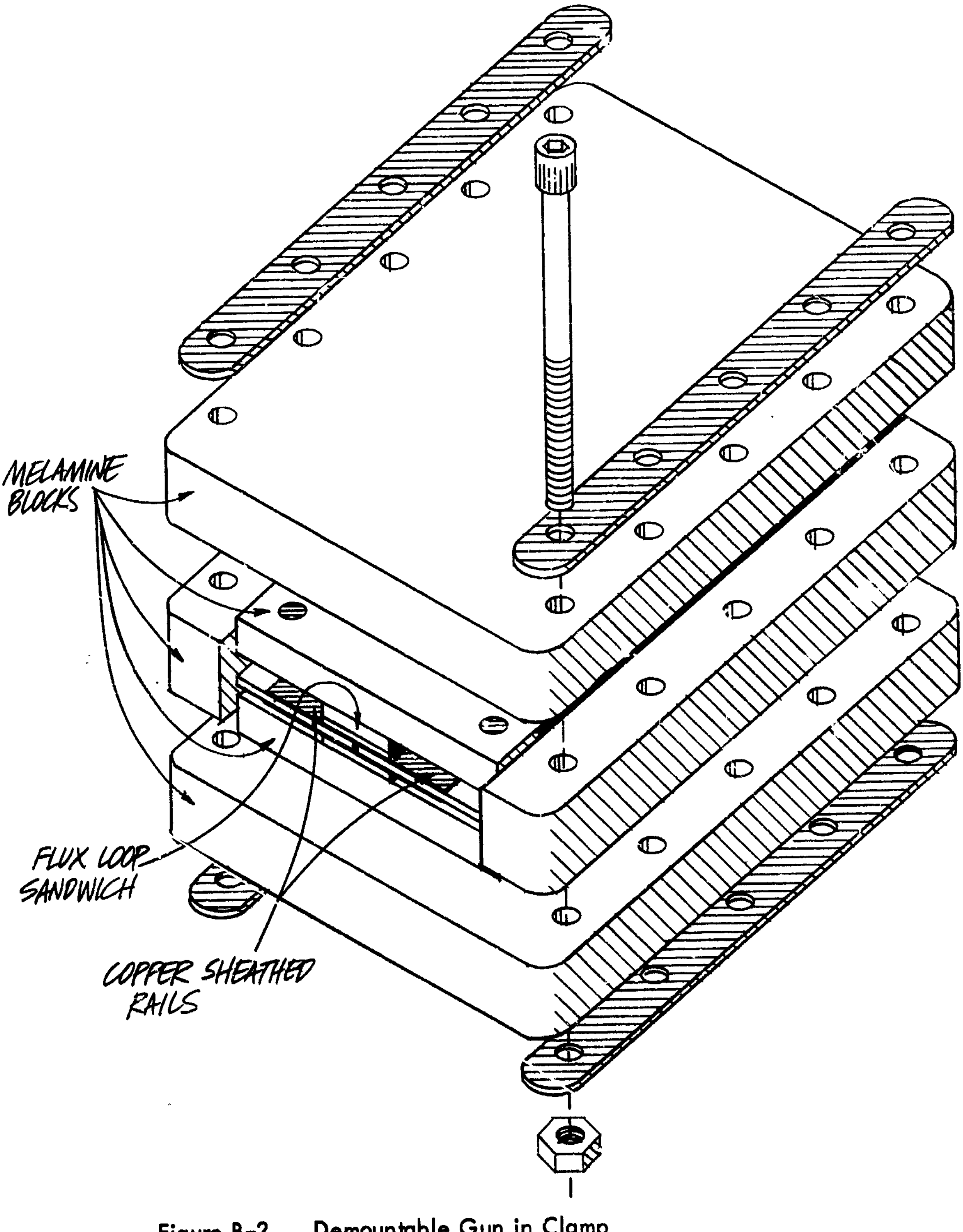

Figure B-2. Demountable Gun in Clamp

APPENDIX C

TRANSFORMERS

Two air-core transformers with low leakage inductance were built to bring the condenser bank voltage (up to 20 kv) closer to the breech voltage of the gun or the voltage of the auxiliary field turns (about 1 kv) and, thereby, increase the current. Figures C-1, C-2 and C-3 and Table C-1 give the performance and construction specifications of the transformers as well as the construction of the leads used to connect the secondary side to various equipment.

Table C-1

Pulse Transformer Specifications

Number of Primary Turns	4.6	10.6
Dimension A	26"	32"
B	13-3/4"	12"
C	6"	3"
D	30"	36"
E	10"	7"
Secondary Induction	.13 μh	.087 μh
Effective admittance*	26 mho	36 mho
Ringing period with typical load	60 μsec	200 μsec

* The ratio of peak secondary current to the peak voltage of the 142 fd condenser bank with a typical load on the secondary.

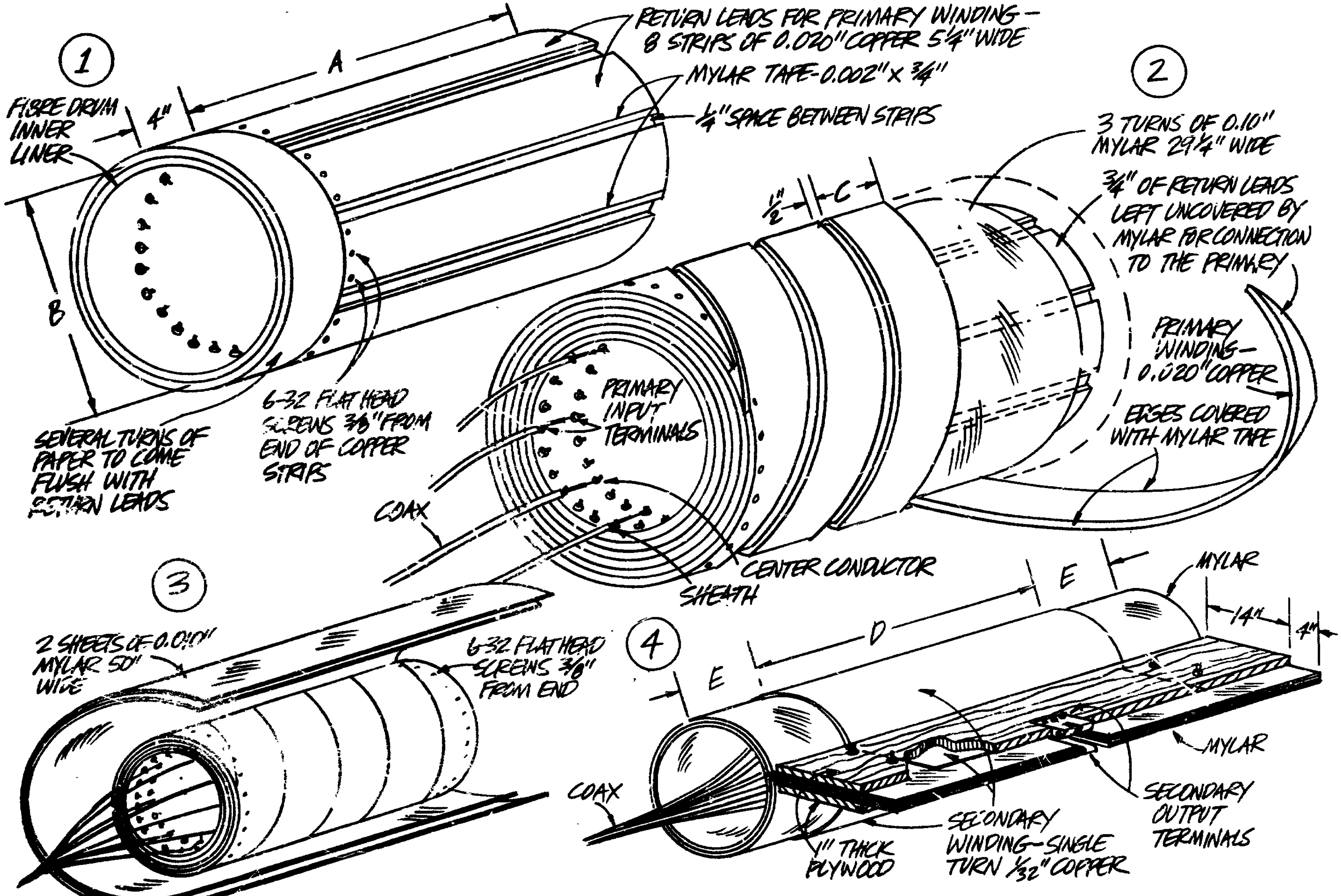

Figure C-1. Construction Details of Pulse Transformers

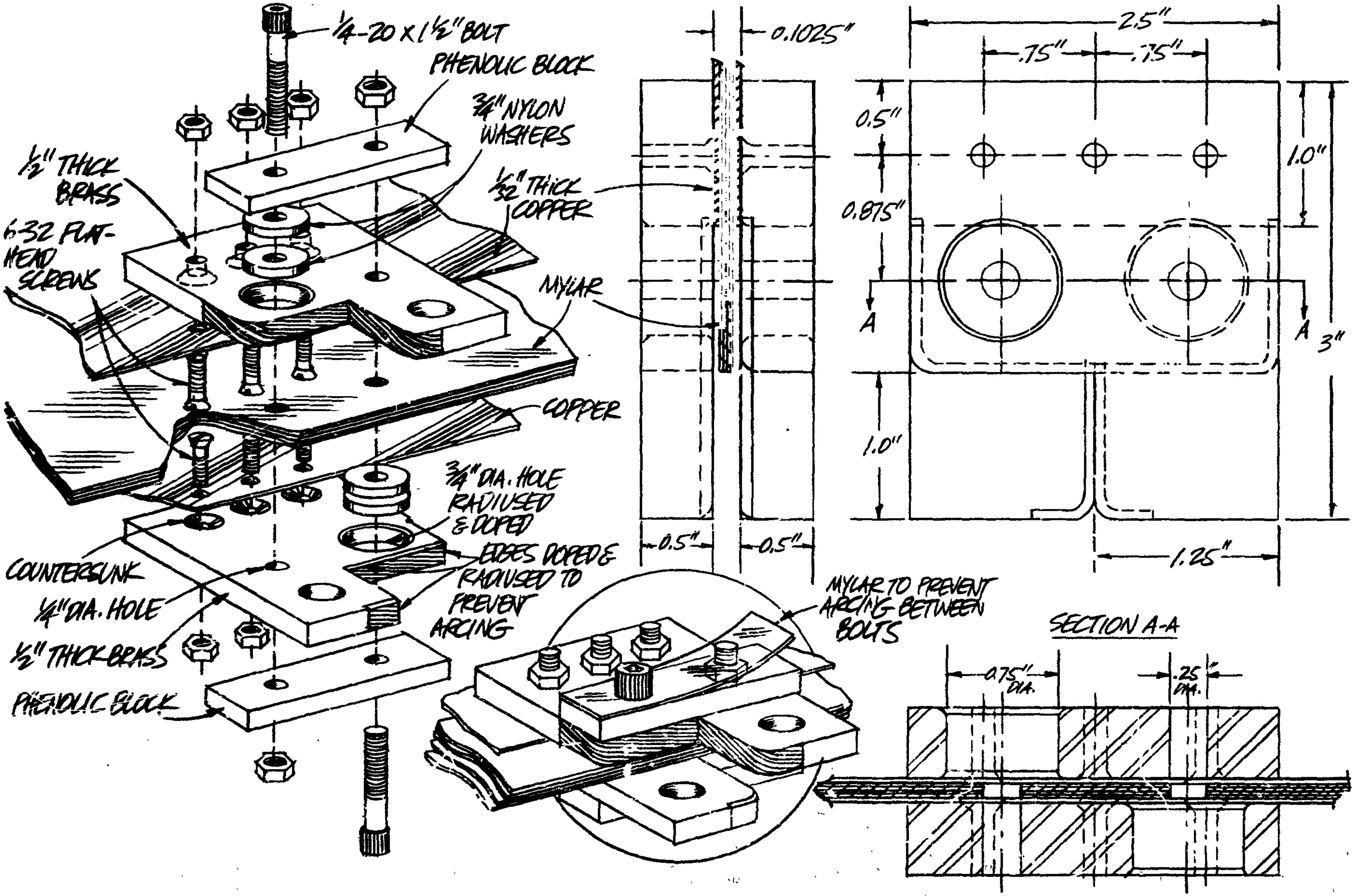

Figure C-2. Construction of Secondary Output Terminals of Pulse Transformer

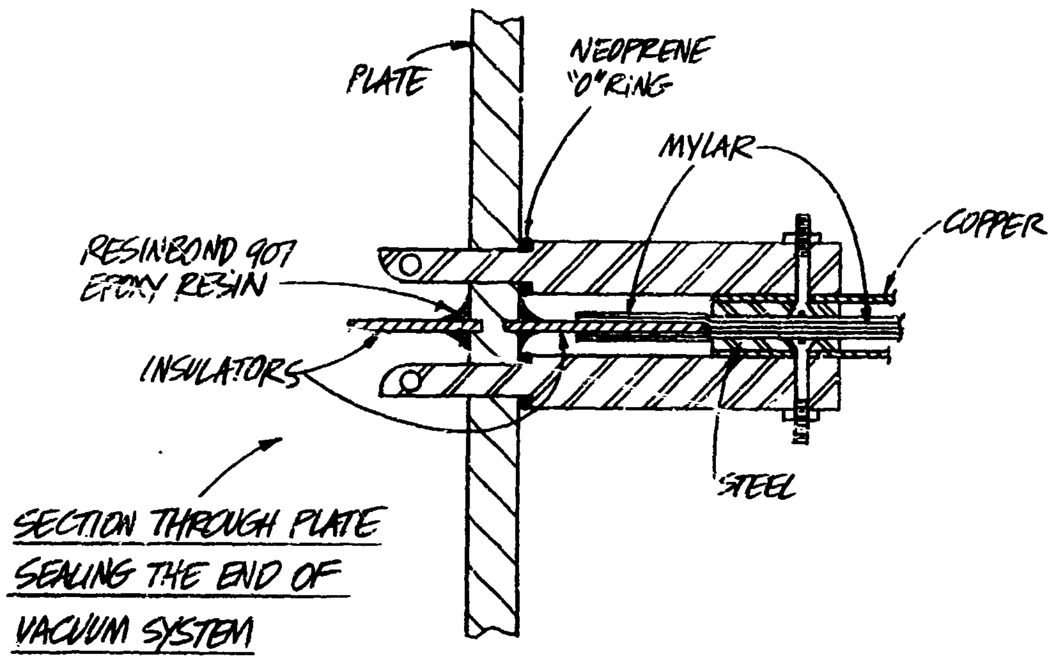

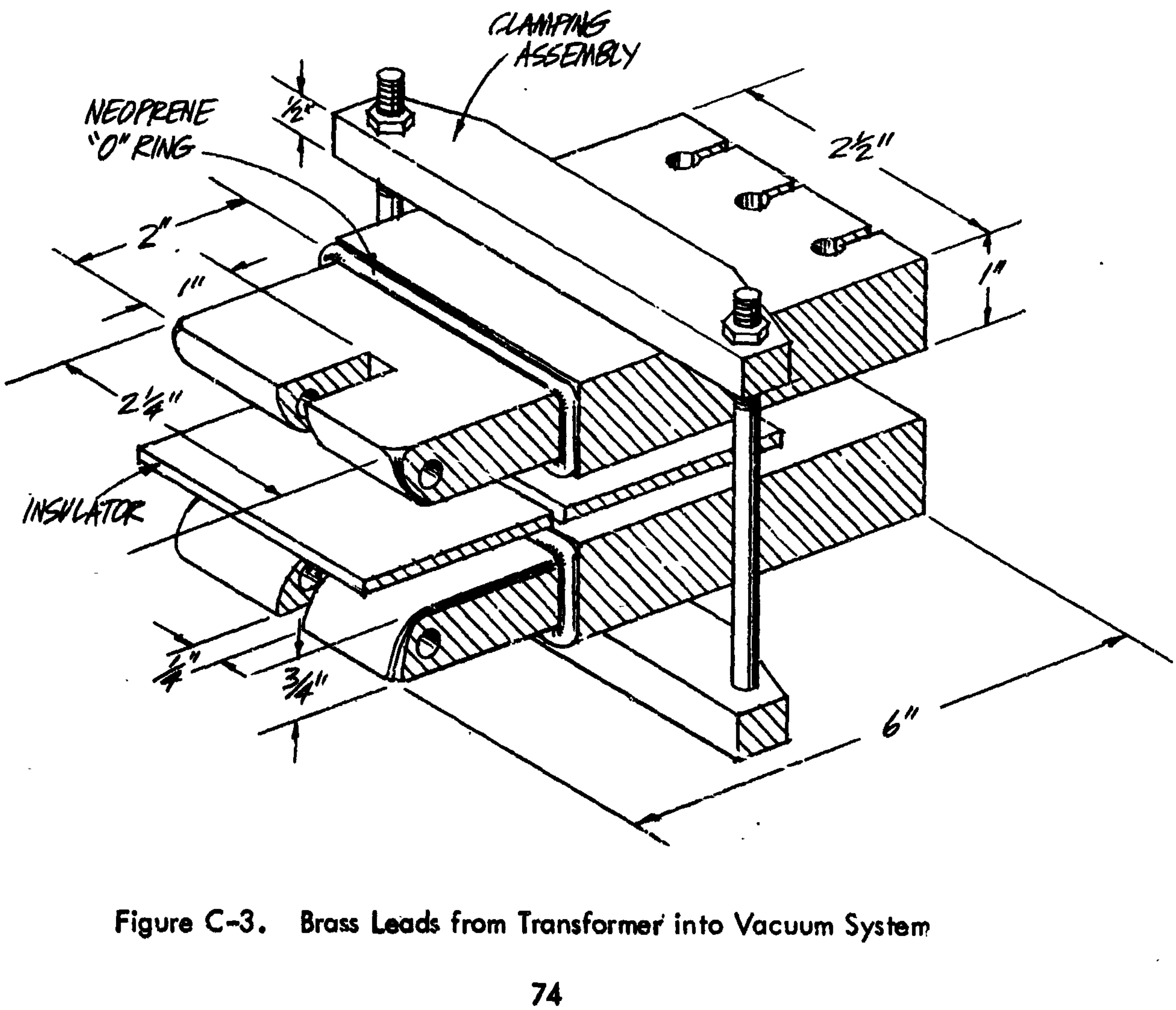

Figure C-3. Brass Leads from Transformer into Vacuum System

APPENDIX D

AUXILIARY FIELD AND TWO-STAGE SYSTEMS

In order to perform experiments with auxiliary-field turns and with a two-stage gun the system shown in Figures D-1, D-2 and D-3 was built. Figure D-4 shows the two-stage gun.

The new condenser bank consists of ten μfd, 20 kv capacitors of the same type as used in the old bank (Sangamo, type EDC, Class B). (In addition to these, an eleventh capacitors were bought to replace a damaged one in the old bank.) These ten capacitors were strapped together in pairs and each pair placed on a separate, four wheel dolly. Each capacitor is connected to the spark gap switch by separate coaxial cables. (See Figure D-5). This bank was used with the old bank in experiments with auxiliary-field turns and with two-stage guns.

A remote control charging and automatic crowbar mechanism was attached to the new bank. The charging leads are connected to the same power supply as the old bank so that both banks may be charged in parallel, each being disconnected from the charging supply as it reaches the desired voltage. The banks are discharged through their respective spark gaps in a controlled time sequence provided by an Abtronix delay chassis. Figure D-6 shows the construction of the triggered spark gap.

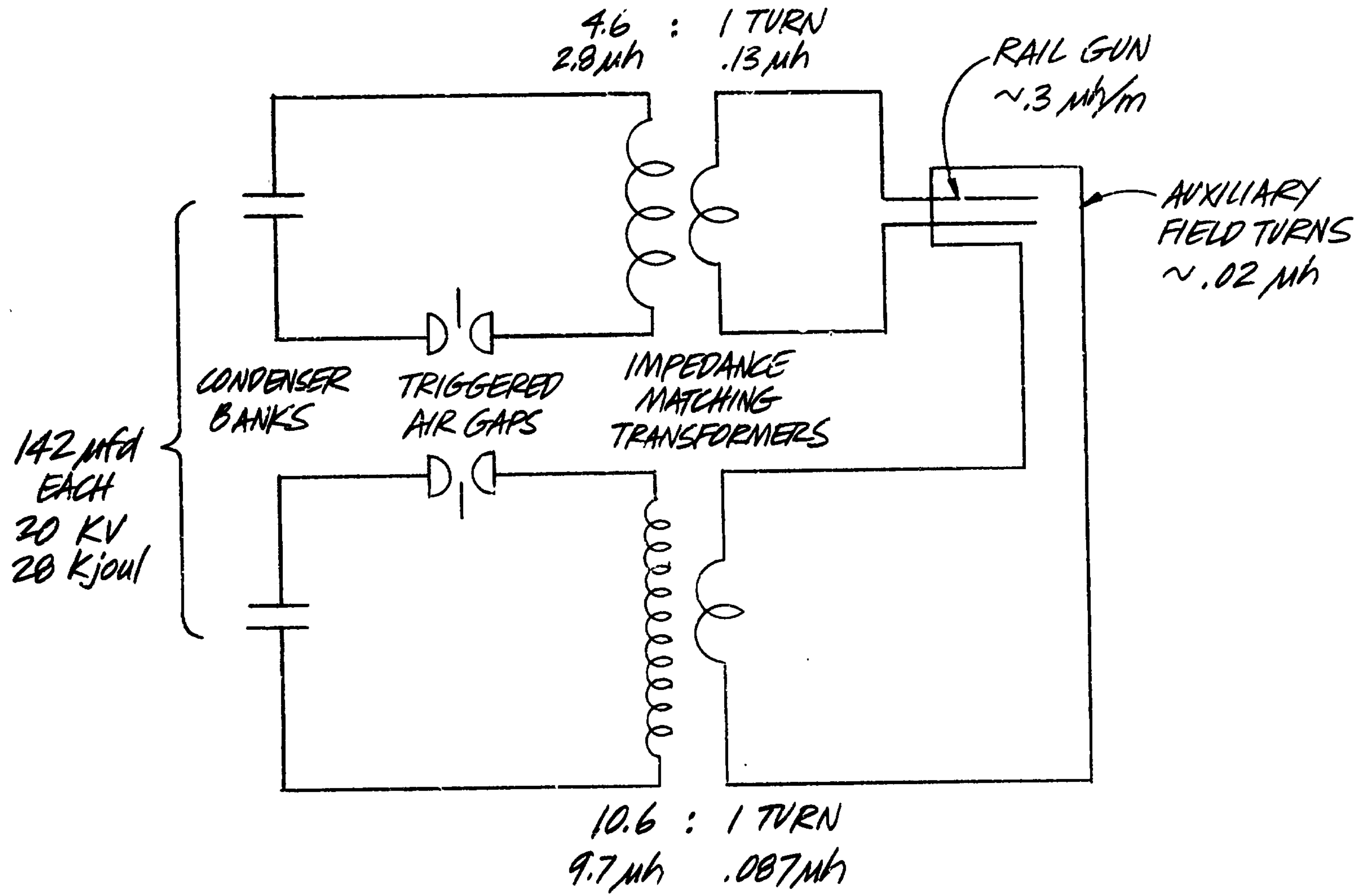

Figure D-1. Auxiliary-Field Rail-Gun System

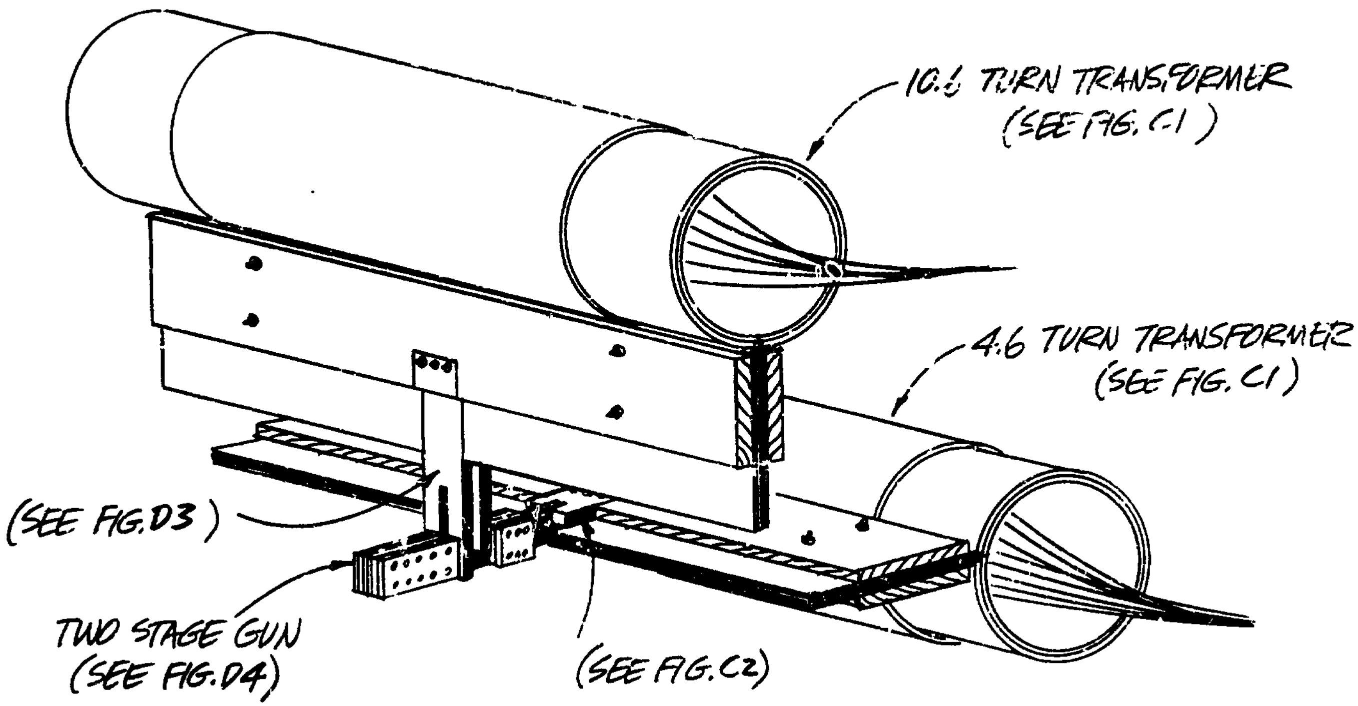

Figure D-2. Two-Stage Gun System

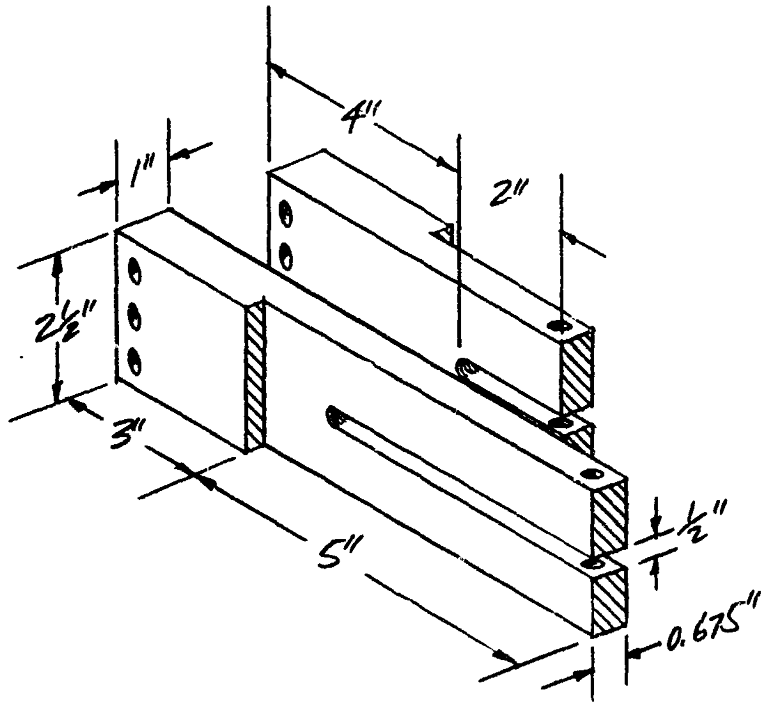

Figure D-3. Brass Leads from Transformers to Second Stage of Two-Stage Gun or to Auxiliary Field Turns

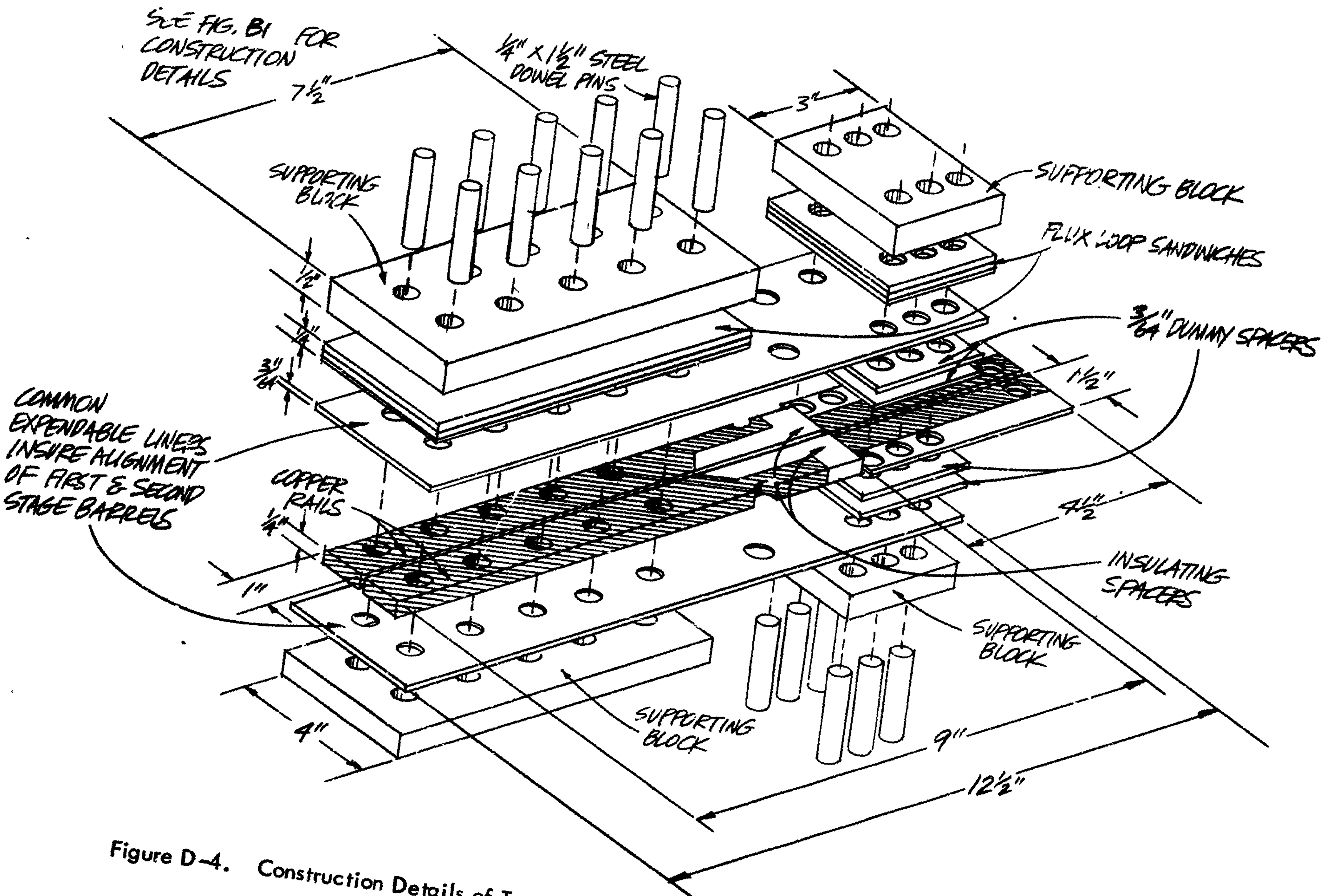

Figure D-4. Construction Details of Two-Stage Gun

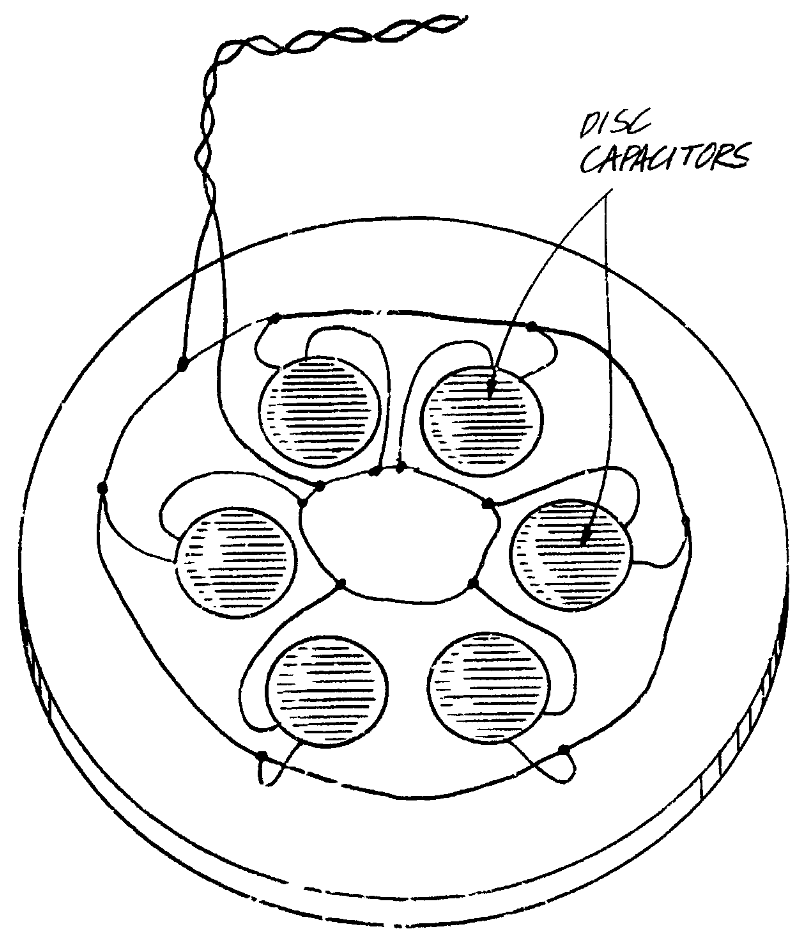

Figure D-5. Construction of Witness Plate and Impact Microphone

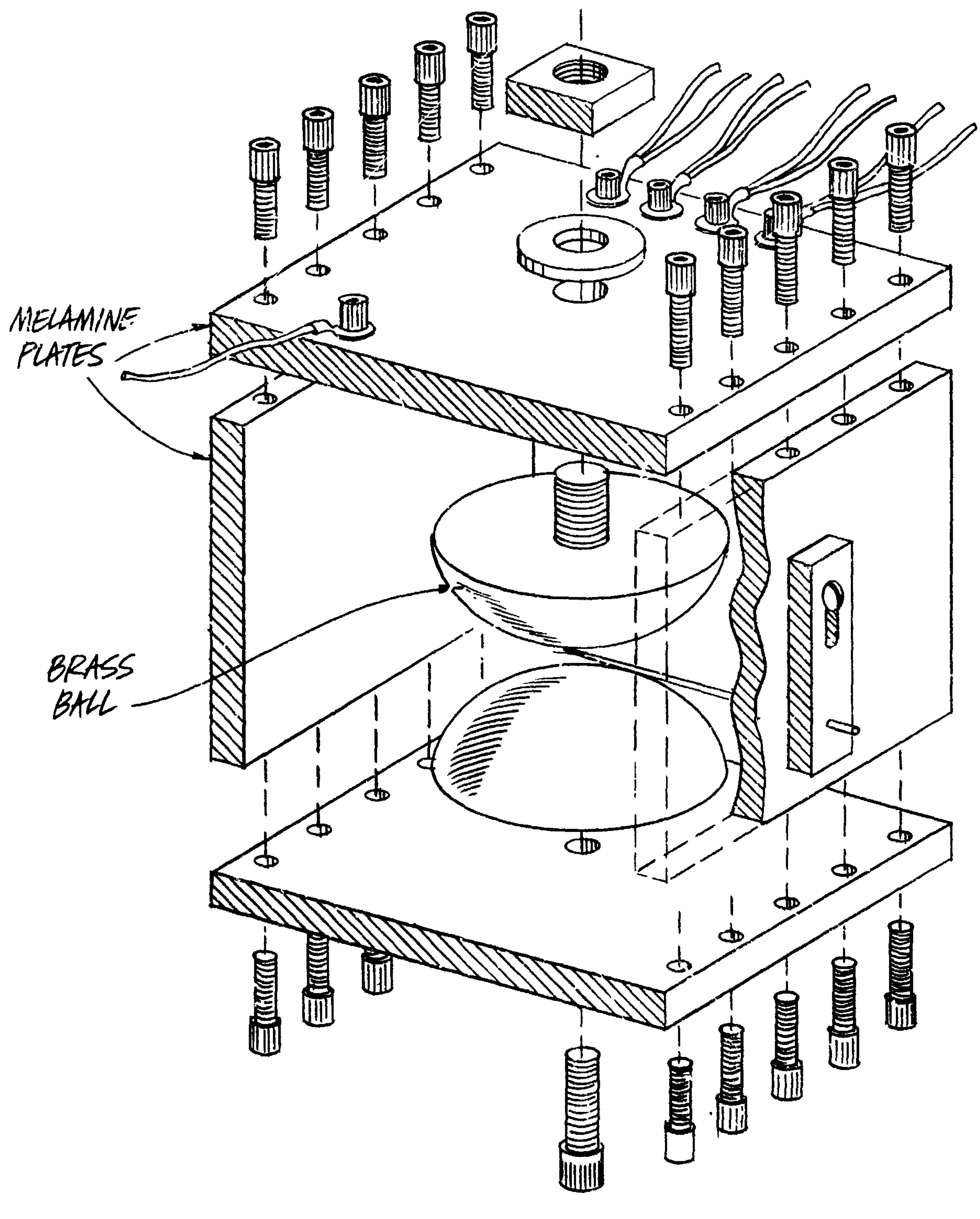

Figure D-6. Construction Details of Spark Gap